Available online at www.sciencedirect.com
ScienceDirect
Journal of Power Sources 163 (2007) 1003–1039
JOURNAL OF POWER SOURCES
www.elsevier.com/locate/jpowsour

Review

Nano- and bulk-silicon-based insertion anodes for lithium-ion secondary cells

Uday Kasavajjula [a], Chunsheng Wang [a,**], A. John Appleby [b,*]

[a] *Department of Chemical Engineering, Center for Manufacturing Research, Tennessee Technological University, Cookeville, TN 38505, USA*
[b] *Center for Electrochemical Systems and Hydrogen Research, Texas A&M University, College Station, TX 77843-3402, USA*

Received 14 July 2006; received in revised form 28 September 2006; accepted 29 September 2006
Available online 9 November 2006

Abstract

The increase in energy density and power density requirements for lithium-ion secondary cells for commercial applications has led to a search for higher capacity electrode materials than those available today. Silicon would seem to be a possible alternative for the graphite or carbon anode because its intercalation capacity is the highest known. However, the large capacity fade observed during initial cycling has prevented the silicon anode from being commercialized. Here we present a review of methodologies adopted for reducing the capacity fade observed in silicon-based anodes, discuss the challenges that remain in using silicon and silicon-based anodes, and propose possible approaches for overcoming them.

Keywords: Silicon anode; Lithium-ion batteries; Volume changes; Cycle life

Contents

* Corresponding author. Tel.: +1 979 845 2033; fax: +1 979 845 8281.
** Corresponding author. Tel: +1 931 372 3678; fax: +1 931 372 6345.
E-mail addresses: ajappleby@gmail.com (A.J. Appleby), cswang@tntech.edu (C. Wang).

0378-7753/$ – see front matter © 2006 Elsevier B.V. All rights reserved.
doi:10.1016/j.jpowsour.2006.09.084

1. Introduction

Lithium-ion (Li-ion) cells are now the most widely used secondary battery systems for portable electronic devices. Compared to conventional aqueous rechargeable cells, such as nickel–cadmium and nickel metal hydride, Li-ion cells have higher energy density, higher operating voltages, lower self-discharge, and lower maintenance requirements [1]. These properties have made Li-ion cells the highest-performing available secondary battery chemistry. However, due to miniaturization and other advances presently occurring in the portable device industry, and to use their advantages for aerospace, military, and automobile applications, their mass capacities (Wh kg^{-1}), and energy densities (Wh l^{-1}) require a further increase. This can be carried out by replacing the widely-used lithium cobalt oxide cathodes and carbonaceous anodes with higher performance electrode materials. In general, the total mAh g^{-1} capacity of Li-ion cells may be expressed in terms of anode and cathode capacity as follows:

$$\text{Total cell (mAh g}^{-1}) = \frac{1}{(1/C_A) + (1/C_c) + (1/Q_M)} = \frac{C_A C_C Q_M}{C_A Q_M + C_C Q_M + C_A C_C}$$

where C_A and C_C are the theoretical specific capacities of the cathode and anode materials, respectively, and $1/Q_M$ is the specific mass of other cell components (electrolyte, separator, current collectors, case, etc.) in g mAh^{-1}. $1/Q_M$ will vary with cell geometry and dimensions, and will include any failure to obtain the theoretical capacity values and any other excess required, e.g., to provide excess cathode material for formation of the surface electrolyte interphase (SEI) film at the anode. For carbon, C_A is 372 mAh g^{-1}, and for $LiCoO_2$, C_C is 135 mAh g^{-1}. For the Sony 18650G8 cell (2550 mAh, 46 g), Q_M may be calculated to be 130.4 mAh g^{-1}. A similar calculation may be performed in terms of mAh cm^{-3}.

So far, specific capacities between 160 and 200 mAh g^{-1} may be obtained with new cathode systems such as $LiMn_{1-x}Mi_xO_2$ [2], $Li[Ni_xCo_{(1-2x)}Mn_x]O_2$ [3], defective Li–Mn–O spinels [4], olivine $LiFePO_4$ [5,6], and related materials. These correspond to a 9–18% increase in total mAh g^{-1} capacity over today's cells, which is insufficient to satisfy requirements. Since finding suitable cathode materials with higher capacities has been a difficult issue, higher performance Li-ion cells will require anode materials with considerably higher specific capacities than those of carbons or graphites.

The total cell capacity as a function of C_A is shown in Fig. 1 for C_C values of 140 and 200 mAh g^{-1} and for Q_M = 130.4 mAh g^{-1}. A slow increase in total capacity is observed until C_A reaches 1200 mAh g^{-1}, after which improvement becomes negligible. At this C_A value, total cell capacities will be 63.9 and 74.1 mAh g^{-1} for C_C equal to 140 and 200 mAh g^{-1}, respectively. However, if anode porosity can also be reduced, allowing reduction in the total amount of electrolyte (e.g., for Q_M increased by one-third to 173.9 mAh g^{-1}), the corresponding total cell capacities will be 72.9 and 86.3 mAh g^{-1}.

This makes it clear that to obtain a noticeable improvement in the specific capacity of Li-ion cells, it is essential to replace carbonaceous anodes with anodes having capacity on the order of 1000–1200 mAh g^{-1} [7]. Experimental work on anodes using chemical elements which form alloys with lithium was started in early 1960s. In 1971, Dey [8] found that lithium can be electrochemically alloyed with a number of metals at room temperature, including Sn, Pb, Al, Au, Pt, Zn, Cd, Ag, and Mg. However, the alloying process resulted in complete disintegration of the electrodes and loss of electronic contact. Similarly, Sharma and Seefurth [9] reported the formation of Li–Si alloys in high temperature cells operating in the 400–500 °C range. It was reported that the alloying process in silicon anodes results in formation of $Li_{12}Si_7$, $Li_{14}Si_6$, $Li_{13}Si_4$, and $Li_{22}Si_5$ alloys [10]. Study of the Li–Si binary system [9–11] indicated that each silicon atom can accommodate 4.4 lithium atoms leading to formation of $Li_{22}Si_5$ alloy, i.e., a specific insertion capacity of 4200 mAh g^{-1}, the highest among the above alloying elements. In addition to

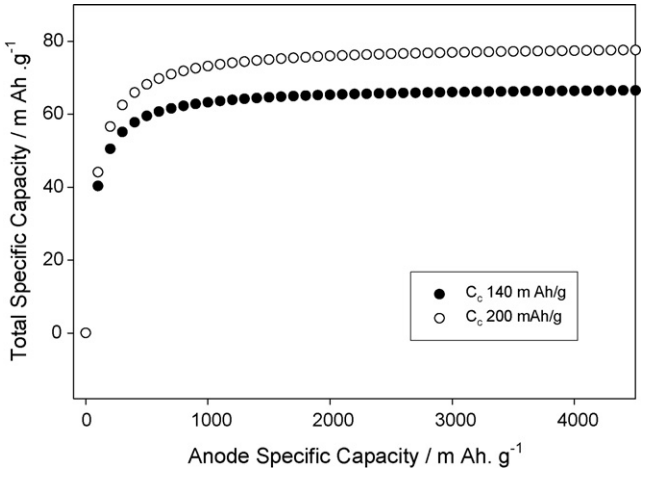

Fig. 1. Total capacity of 18650 Li-ion cell as a function of anode capacity (C_A), including masses of other required internal components and case. Capacities of cathodes considered were 140 and 200 mAh g^{-1}.

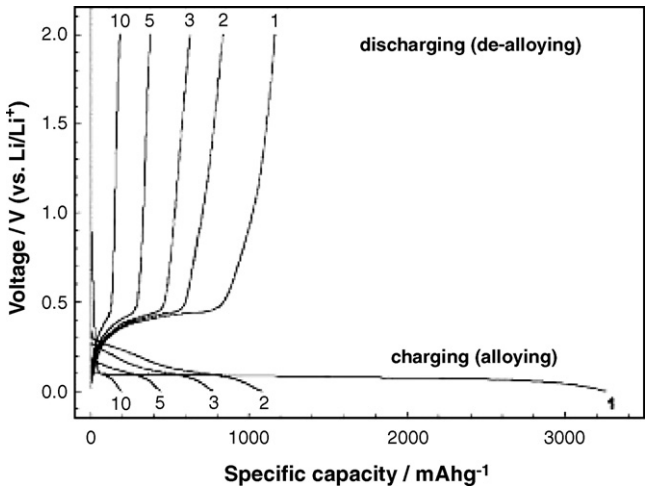

Fig. 2. Galvanostatic charge–discharge profiles for micro-Si (10 μm) anode [15].

its outstanding capacity, silicon is the second most abundant element on earth. Because of these attributes, a great deal of attention has been given to using silicon as Li-ion cell anode material. However, the alloying process of Li with Si was found to be less reversible at room temperature [12–14]. As Fig. 2 shows, during the initial cycle a bulk-silicon anode showed a charge capacity above 3260 mAh g^{-1} and a discharge capacity close to 1170 mAh g^{-1}, corresponding to a coulombic efficiency of only 35% [15]. During Li insertion into Si in the first cycle, the voltage initially dropped quickly to 0.2 V versus Li/Li^+ in the liquid organic electrolyte used,* and then a slow decrease took place as seen in the long potential plateau in Fig. 2. This plateau is due to formation of Li–Si alloys, which co-exist with Si as two-phase regions. During the discharge process, a rapid increase in voltage was observed, followed by a plateau between 0.3 and 0.4 V. From the initial charge–discharge profile, it was evident that silicon anodes operate in a narrow potential range between 0.0 and 0.4 V (Fig. 2), which would be suitable for use in Li-ion cells. During further cycling, rapid capacity fade was observed, which resulted in a reversible capacity lower than 500 mAh g^{-1} by the 5th cycle. Li insertion in Si results in the formation of successive Li–Si alloys, each of which result in progressively larger volume expansions of the parent lattice. Table 1 [10] shows the data for crystal structure, unit cell volume, and volume per silicon atom for each alloy formed during the alloying process. It shows that the volume per silicon atom for $Li_{22}Si_5$ alloy is four times higher than that of the parent silicon atom, i.e., a 400% volume expansion of the silicon lattice occurs. This results in cracking and disintegration of the electrode, with active material loss via reduced electronic contact, giving severe capacity fade. Although it was initially thought that the low coulombic efficiency of the bulk Si anode was due to low electrochemical reactivity of Li with Si at room temperature, results showed that poor electronic contact between Si particles resulting from the large volume expansion in Si during Li insertion is the real reason for capacity loss.

Table 1
Crystal structure, unit cell volume and volume per Si atom for the Li–Si system [10]

Compound and crystal structure	Unit cell volume (Å^3)	Volume per silicon atom (Å^3)
Silicon cubic	160.2	20.0
$Li_{12}Si_7$, ($Li_{1.71}Si$) orthorhombic	243.6	58.0
$Li_{14}Si_6$, ($Li_{1.71}Si$) rhombohedral	308.9	51.5
$Li_{13}Si_4$, ($Li_{3.25}Si$) orthorhombic	538.4	67.3
$Li_{22}Si_5$, ($Li_{4.4}Si$) cubic	659.2	82.4

The effect of Si anode volume change on cell capacity can be estimated in a similar way to that in terms of cell capacity per unit mass. The $LiCoO_2$ unit cell volume of 95.963 Å^3 [16] corresponds to a density of 5.07 g cm^{-3} [17], giving a cathode volume capacity $C_{C(V)}$ of 659.0 mAh cm^{-3}. For a graphite anode, $C_{A(V)}$ is 837.5 mAh cm^{-3}. The corresponding Q_V value for the 1.8 diameter, 6.5 cm high 154.2 mAh cm^{-3} Sony 18650 cell is 265.0 mAh cm^{-3}. Assuming a silicon anode with the maximum insertion capacity of $Li_{4.4}Si$ (see the following paragraph), a volume expansion corresponding to 400% at this capacity, and an approximately linear relationship between degree of insertion and expansion, the $C_{A(V)}$ values for the LiSi (0.954 mAh g^{-1}) and $Li_{4.4}Si$ (4199 mAh g^{-1}) compositions are 1322 and 2446 mAh cm^{-3}, respectively. Assuming a cathode with a $C_{C(V)}$ 54% higher than $LiCoO_2$, a graphite anode, and the same Q_V as that given above would result in a cell giving 168 mAh cm^{-3}. With a silicon anode, with charge limited to LiSi with the above assumptions, the cell would give 181 mAh cm^{-3}, while charging to $Li_{4.4}Si$ would give 193 mAh cm^{-2}. As before, if Q_V can be increased by one-third, the corresponding cell capacities per unit volume would be 219 and 237 mAh cm^{-2}. In each case, the increase in capacity per unit volume on going from LiSi to $Li_{4.4}Si$ is not dramatic. It is in fact less than the improvement in capacity per unit mass, due to the effect of the volume expansion of Si.

To overcome the large volume change and thus obtain better capacity retention and cycle life for Si anodes, various approaches have been used. In this review, we have classified the various approaches to silicon anodes reported in literature into five types, as follows:

1. Pure Si micro- and nano-scale powder anodes.
2. Si dispersed in an inactive matrix.
3. Si dispersed in an active matrix.
4. Si anodes with different binders.
5. Si thin films.

In this review, we will discuss the current status of approaches to Si- or Si-based anodes and summarize their typical electrochemical performance in tables. We will also describe the challenges that remain to using silicon anodes and give possible approaches to overcome them. The emphasis of the review was initially on the scientific journal literature, which has been covered extensively. However, the experiments described in this literature often occur under conditions differing in certain respects from those in real secondary cells. The major difference is that anodes are generally cycled in the laboratory in a large excess of electrolyte in contact with inert gas at atmospheric pressure,

while while secondary cell components are in contact with a minimum of electrolyte in a sealed container at essentially constant volume. Because lithium insertion anodes show volume changes on cycling, it is apparent that cycling under these differing conditions may give contrasting results, particularly in regard to cycle life. It will be seen that laboratory results usually show rapid capacity fade. During the review process, it was suggested that some of the recent patent literature might throw some light on how to reduce fade under practical conditions. As a result, the review was extended to the recent US patent literature, including published patent applications. The patent review has been selective, rather than exhaustive.

High-surface-area electrodes mentioned throughout this review, excluding those in Sections 4 and 5, were made using polyvinylidene fluoride (PVDF, poly-1,1-difluoroethene) binder unless otherwise stated. Readers can find detailed information in the articles cited.

Finally, a word of warning to readers. For over 50 years, electrochemists have used the word "discharge" to mean "losing positive electronic charge by combination with an electron." So, "the hydrogen ion or proton is discharged to become a hydrogen atom." For some reason, if the ion is negatively charged, as is, say, Cl^-, the loss of an electron is not normally called "discharge." In contrast, for almost 150 years, addition of electrical energy to a secondary cell or battery has been called "electrical charging." So, battery electrochemists have considered the application of a reductive, i.e., cathodic, reaction, to a secondary cell electrode acting as an anode in the opposite direction (when it produces, rather than takes up, electricity) as "charging the anode." Thus, to take the familiar example of a metal hydride (e.g., palladium hydride) in acid media, "the proton is discharged to become a hydrogen atom, which diffuses into the palladium insertion matrix, charging it." The same would be true of the corresponding first step for metal hydride insertion compounds in alkaline media, in which $H_2O + e^-$ becomes $OH^- + H$. If one is an electrochemist studying the first step, one would call it hydrogen ion discharge, especially if this step is rate-determining. If one is a battery electrochemist who is more interested in the second step of intercalating hydrogen atoms into the substrate, which is much more likely to be rate-determining in reality, one would call the process "charging." This dichotomy of nomenclature can become confusing when a sub-set of electrochemists or materials scientists examining lithium insertion half-cells have called the overall cathodic reaction at the anode $Li^+ + e^- \rightarrow Li_{substrate}$ "the discharge reaction." The substrate is thereby gaining negative Gibbs energy as it is being electrically charged. After considerable deliberation, we have decided to retain the word "charging" for this process, the main reason being that our interest is in the ability of the substrate to take up lithium atoms, and to release them reversibly, rather than the ability of Li^+ to combine with an electron at the surface *per se*. This convention is used in the text, tables, and figure captions. However, this review has used figures from the original references which could not be easily revised, in which "charging the substrate" is called "discharge," i.e., that of Li^+ ion, and vice versa. In these, the figures internally contain the word "discharge" meaning Li atom intercalation, and "charge" meaning dealloying. So a "charge–discharge curve" to a battery electrochemist becomes a "discharge–charge curve." Those in question are Figs. 5, 7, 8, 13, 15, 17 and 18. The captions of these figures are marked§§.

The authors believe that this review is as complete as might be achieved up to a journal literature cut-off date of June 15, 2006. They would be grateful if readers would point out any omissions.

2. Pure Si powder anodes

This Section discusses the electrochemical performance of anodes made from pure Si powders. The methodology for reducing Si particle size to that required to reduce volume expansion is discussed. When particle size was reduced to micrometers, no particular improvement in electrochemical performance was observed. As for bulk Si anodes, those fabricated from micro-Si powder also showed a large irreversible capacity and poor capacity retention.

2.1. Explanation of the high irreversible capacity and poor cycle life of micro-Si anodes

To understand the reasons for the poor cycling stability of micro-Si anodes, their internal electrochemical resistance was measured during charge–discharge cycling by the galvanostatic intermittent titration technique (GITT) [15]. In this, a current pulse of $100\,mA\,g^{-1}$ was applied for 10 min to measure the closed-circuit voltage (CCV) for the composition that had been previously obtained galvanostatically. The current was then turned off for 20 min to obtain the quasi-open-circuit voltage (QOCV) for this composition. Transient voltage profiles obtained from such GITT measurement are shown in Fig. 3(a). From these, the internal reaction resistance was obtained by calculating the difference between the CCV and QOCV for each voltage transient [15]. Its variation during the charge–discharge process is shown in Fig. 3(b). This shows that during the alloying process the internal reaction resistance decreases, since Li–Si alloys have a higher electronic conductivity than that of pure silicon. During de-alloying, the resistance increases, since volume contraction takes place, giving less effective electronic contact between particles with an increase in contact resistance and charge transfer resistance. As a result, complete de-alloying cannot take place because of trapping of Li^+ ion inside the anode host particles. This was confirmed by imposing pressure during de-alloying, which considerably increased the charge capacity by improving electronic contact between the active particles and the current collector. These results suggested that de-alloying is more detrimental to Si anode cycle life than alloying. The poor cycling performance of silicon anodes was due to breakdown of the electronically conductive network, which resulted from the large Si volume expansion. It should be noted that the internal reaction resistances calculated from the difference between the CCV and QOCV within each voltage transient or local composition are only approximate, and their accuracy decreases with increasing reaction overpotential. A more accurate *in-situ* method to directly measure the internal contact

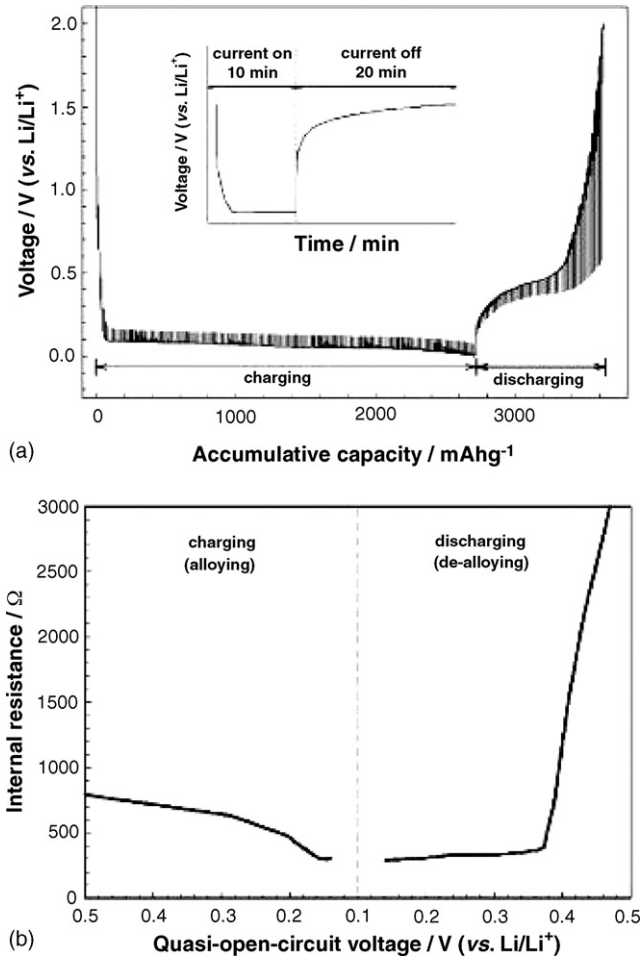

Fig. 3. (a) Transient voltage profiles for micro-Si anode obtained using the galvanostatic intermittent titration technique (GITT). *Inset*: A typical voltage transient obtained in one current pulse cycle. (b) Internal resistance of micro-Si anode calculated from transient voltage profiles [15].

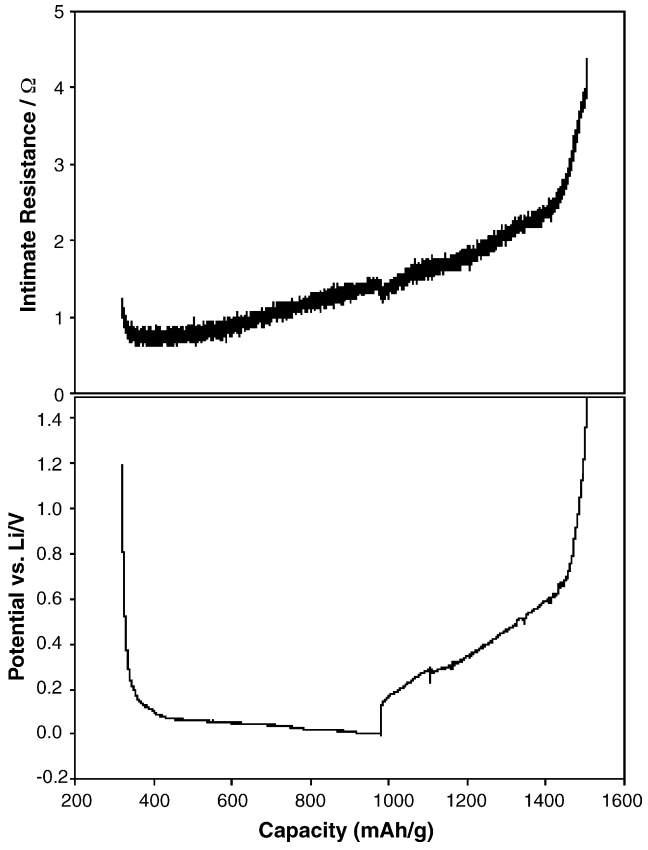

Fig. 4. Potential and intrinsic resistance of anode with 60 wt% Timcal KS-15 graphite, 20 wt% nano-Si, 10 wt% carbon black, 10 wt% polyvinylidene fluoride (PVDF) during first cycle at 5 mA g^{-1} charge, 10 mA g^{-1} discharge. Current for intrinsic resistance measurement: 5 mA [19].

and reaction resistances of the electrode during insertion and extraction was developed by us using two potentiostats [18], which allowed these resistances to be measured successfully for graphite anodes [18]. The same technique was used to measure the contact resistance of graphite–silicon composite anodes during charge–discharge, as shown in Fig. 4 [19]. In contrast to a graphite (G) electrode, the internal contact resistance of G–Si composite electrode increased continuously during both Li-insertion and extraction. This effect results from pulverization of Si during Li-insertion and its shrinkage during extraction. These results suggest that both Li-insertion and extraction are detrimental during Si anode cycling.

2.2. Technologies to improve the performance of Si anodes

One way to improve electronic contact between particles during insertion and extraction is by mixing conductive additives (CA) such as graphite flakes and/or nano-scale carbon black into micro-Si anodes [20]. Increasing CA content dramatically increased the cycle life and irreversible capacity of silicon anodes due to the increased interparticle electronic contact, which gave improved Li de-alloying kinetics and also prevented the agglomeration of Si particles. The buffering action of soft CA particles also suppressed the large Si volume change on some degree, relieving mechanical stresses inside the anode. A second way to improve Si anode performance is to decrease Li insertion/extraction levels by narrowing the cycling voltage window [20]. A third and most widely studied method is to reduce the Si particle size to nano-scale [21,22] using laser-induced silane gas reaction [21]. Fig. 5 shows voltage versus capacity curves for nano-Si anode. It shows that a charge capacity of 2775 mAh g^{-1} and a discharge capacity close to 2097 mAh g^{-1} could be obtained for a nano-Si anode during the first cycle, giving 76% coulombic efficiency. Its reversible capacity on the 10th cycle was 1729 mAh g^{-1}, i.e., the capacity fade was much lower than that of a bulk Si because of smaller volume expansion due to reduced particle size. While particle size reduction can reduce volume change to a certain degree, it cannot completely eliminate capacity fade.

3. Si-inactive material composites

Another method used to suppress Si volume expansion has been to create a composite structure consisting of an inactive host matrix in which silicon is finely dispersed. An inactive matrix used in the anode acts as a cushion and accommodates the volume change in the Si active material, thereby preventing

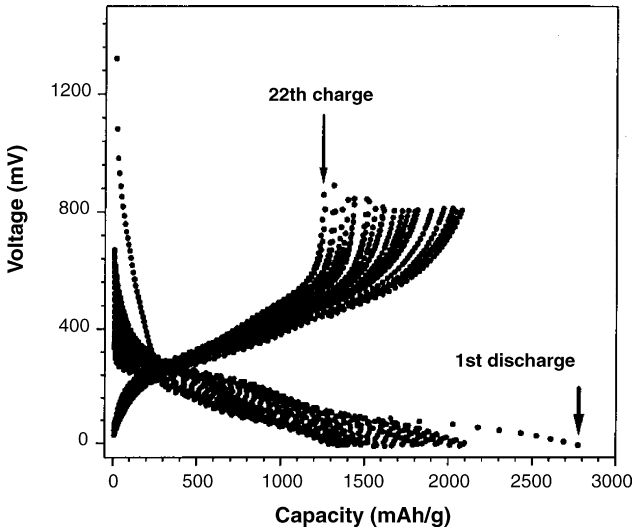

Fig. 5. §§Charge–discharge curves between 0.0 and 0.8 V at 0.1 mA cm^{-2} for nano-Si anode with 4:4:2 weight ratio of nano-Si, carbon black and PVDF binder. Electrolyte: 1 M $LiPF_6$ in ethylene carbonate (EC)–diethyl carbonate (DEC) (1:1) [22].

pulverization of the anode. This inactive matrix must have a high mechanical strength to withstand the volume change of Si on cycling. Ideally, it should also have high electronic conductivity to allow charge transfer reactions to take place. Metallic compounds such as TiN [23], TiB_2 [24], SiC [25], and TiC [26,27] have been examined for this purpose as inactive host matrices. These were mixed homogenously with Si by ball milling to obtain a powder to prepare anodes. X-ray diffraction (XRD) results for ball-milled samples showed that the Si in these was amorphous, while the inactive material was nano-crystalline or amorphous. When cycled between 0.02 and 1.2 V, such anodes showed stable reversible capacities of 300–400 mAh g^{-1} for 15 cycles. These capacities were low compared to their theoretical values of 700–900 mAh g^{-1}. With a reduced ball milling time, they showed higher reversible capacities, but with poor cycle life. When the inactive phase was pre-milled and then again milled with Si, anodes made from the powder thus obtained showed better capacity retention than anodes containing a non-milled inactive phase [27]. This was due to the smaller particle size of the inactive matrix, which increased buffering action, giving uniform distribution of stress throughout the electrode. Scanning electron microscopy (SEM) analysis showed that their surfaces remained crack-free after galvanostatic cycling, indicating their good structural stability. However, their reversible capacities were still low, perhaps due to poor Li^+ ion diffusivity in the inactive matrix, which limited reaction of Li with Si. To improve the electrochemical performance of Si–TiN or Si–TiB_2 composite anodes, a carbon coating technique was examined [28,29]. This was conducted by pyrolyzing a mixture of ball milled Si–TiN or Si–TiB_2 composite powders with coal tar and polyvinyl chloride (PVC) in 3:7 weight ratio at 900 °C for 1 h. Independent of the matrix, all Si anodes prepared by this method showed similar charge–discharge characteristics and trends in potential. Compared to Si–TiM, where M is the N/B ratio, carbon coated Si–M anodes showed higher cycling stability [28]. Their improved cycling performance was attributed to carbon coating from pyrolyzed PVC, which acted as an elastic binder network, resulting in an increase of anode electronic conductivity and mechanical integrity. Finally the encapsulation of Si in a carbon-M composite structure led to better accommodation of the volume change with nano-Si active material. Similarly, Si–M–C electrodes were prepared by two pyrolysis reactions with one intermittent high-energy mechanical milling (HEMM) of the same precursors in similar ratios [29]. In the cycling voltage range 0.05–1.5 V, this anode showed an initial reversible capacity of 800 mAh g^{-1}, and in the 35th cycle it showed a capacity retention ability of 90% of that of the second cycle (600 mAh g^{-1}). A lower reversible capacity of this anode compared with one prepared by pyrolysis appeared to be due to the smaller percentage of Si present in the latter. As well as good capacity retention, anodes prepared by two pyrolysis steps and one HEMM step showed high rate capability. This was due to high electronic conductivity of the anode resulting from the presence of the inactive metallic matrix and the high carbon content obtained from the two pyrolysis reactions. Other than metal nitrides and metal carbides, metal oxides such as TiO_2 and ZrO_2 have also been examined by sol–gel coating onto Si particles in the patent application literature [30]. Within an operating voltage window of 0.0–1.2 V, these were claimed to have stable reversible capacities between 800 and 900 mAh g^{-1} for 16 cycles.

Several other Si compounds containing inactive host matrices (M), such as SiB_3, $CaSi_2$, $CoSi_2$, $FeSi_2$, and $NiSi_2$ were investigated as Li-ion anodes by Netz et al. [31]. Initial discharge capacity, Li extraction ratio, and molar weight for these anodes are listed in Table 2. Among them, $CaSi_2$ and $NiSi_2$ showed the highest reversible capacities, equal to 1.15 and 0.85 Li mol^{-1}, while $CoSi_2$ and $FeSi_2$ had the lowest at 0.25 Li mol^{-1}.

The high initial reversible capacity of the $CaSi_2$ anode merited further investigation [32]. Based on the predicted Ca–Si–Li room temperature phase diagram, the following reaction was proposed for the Li insertion reaction in a $CaSi_2$ anode.

$$10.8Li + CaSi_2 \rightarrow Li_2Ca + 2Li_{4.4}Si$$

It is evident that metallic Li alloys with Si in this compound, forming the range of Li–Si alloys. When charged–discharged between 0.005 and 1.5, it exhibited a charge capacity above 1500 mAh g^{-1}, which was reduced to 310 mAh g^{-1} after 10 cycles. Beyond pulverization during Li insertion/extraction, another reason for its poor cycle life was explained by the mechanical properties of the alloy matrix, particularly its melt-

Table 2
Specific capacity data for several materials [31]

Precursor	Molar weight	First delithiation (Li mol^{-1})	Delithiation capacity (mAh g^{-1})
$CoSi_2$	115.11	0.25	58
$FeSi_2$	112.03	0.25	6
$NiSi_2$	114.87	0.85	198
$CaSi_2$	96.26	1.15	320
SiB_3	60.52	1	443
SiO	44.09	1.1	669
α-Silicon	28.09	1.05	1002

ing point, elastic modulus, and ductility. It is known that elastic modulus and ductility are directly and inversely proportional to melting point, respectively. Generally Ca–Si alloy matrices have lower melting temperatures, and high ductility and elastic modulus. This means that they cannot sustain large volume changes, and so have severe capacity fade during initial cycling. The results obtained suggested that Si dispersed in a matrix with a high elastic modulus and low ductility might relieve tensile stresses during the reaction of Li with Si, making it an excellent candidate for a Li-ion cell. Thus Si_3N_4 [33], whose hardness is employed in tools, and $Si_{3-x}Fe_xN_4$ [34] were also investigated as anodes. When charged to 0.01 V, Si_3N_4 [33] showed a capacity of only 83 mAh g^{-1}, considerably less than that of graphite, suggesting that hardness results in low Li insertion ability. To increase reversible capacity, Fe was added to Si_3N_4, which was then ground and calcined to form the composition $Si_{3-x}Fe_xN_4$ [34]. XRD results showed that it consisted of solid solution of Si_3N_4 and Fe. When used as an anode, this compound showed an improved specific capacity compared with that of an Si_3N_4 anode, which was explained by the presence of vacant Fe sites acting as Li intercalation/deinteracalation centers. Although $Si_{3-x}Fe_xN_4$ had a reversible intercalation capacity four times higher than that of Si_3N_4, it was still too low for commercial application.

Apart from hard metallic compounds such as TiN, medium-strength metals with high electronic conductivity such as Ni [35,36], Fe [36], and Cu [12] were also selected as a matrix to form alloy anodes by mechanical milling. With Ni, the resulting anode was found to have a homogenous NiSi phase, while with Fe, it contained FeSi and Si phases, the latter having a large particle size. Based on the active and inactive elements present in the alloy anodes, the following reaction mechanisms were proposed for Li insertion and extraction.

$$x\mathrm{Li}^+ + x\mathrm{e}^- + \mathrm{NiSi} \rightarrow \mathrm{Li}_x\mathrm{Si} + \mathrm{Ni} \rightarrow \mathrm{Ni} + \mathrm{Si} + x\mathrm{Li}^+ + x\mathrm{e}^-$$

$$x\mathrm{Li}^+ + x\mathrm{e}^- + \mathrm{FeSi} \rightarrow \mathrm{Li}_x\mathrm{Si} + \mathrm{Fe} \rightarrow \mathrm{Fe} + \mathrm{Si} + x\mathrm{Li}^+ + x\mathrm{e}^-$$

In the proposed mechanisms, the theoretical value for NiSi is 1360 mAh g^{-1} if all the Si reacts with Li to form $Li_{4.4}Si$. Ni and Fe are present in the elemental state after the first charge and discharge process. It was thought that the elemental Ni and Fe formed during initial charge would act as buffering matrix to suppress the Si volume change. Though both of these anodes have shown similar initial reversible capacities, NiSi showed better capacity retention than FeSi [36]. The poor cycle life of FeSi was due to the large particle size of unalloyed Si, which resulted in a large overall anode volume change.

To improve the cycling stability of FeSi alloy, an alloy was prepared by annealing Fe and Si powders at 1000 °C, followed by milling. Annealing was performed to increase the binding strength between Fe and Si [37]. The powder obtained from ball-milling was mixed with graphite to improve buffering action in the anode and the composite was again ball-milled. From XRD analysis, FeSi alloys prepared by annealing were found to contain α-$FeSi_2$ and β-$FeSi_2$. It was thought that Si particles were embedded in the $FeSi_2$ compounds, which would act as buffering matrix. However, such FeSi alloys showed low reversibility and poor cycle life. Poor cycling performance was attributed to the small amount of $FeSi_2$ phase present in the anode, which could not completely cover all the Si particles. When graphite was added to the alloy powders, it resulted in a first charge capacity of 800 mAh g^{-1}. After 25 cycles, it showed a charge capacity of 550 mAh g^{-1}, so addition of graphite resulted in increased reversible capacity and improved cycling performance. While the Fe–Si/graphite anode showed better electrochemical performance, it also had 100% irreversible capacity, which is a potential disadvantage. Similar results were also reported for Fe–Si/G composite anodes prepared from ball milling of commercially available Fe–Si alloy and graphite [38]. X-ray photoemission spectroscopy (XPS) showed that the Fe–Si/G anode has a composite structure, with graphite as an outer shell, and with FeSi alloy containing dispersed Si particles as a middle shell. Li insertion into Fe–Si/G was predicted to be:

$$\mathrm{FeSi_2} + \mathrm{Si} + \mathrm{G} + y\mathrm{Li}^+ + y\mathrm{e}^- \rightarrow \mathrm{Li}_{y-z}\mathrm{Si} + \mathrm{Li}_z\mathrm{G} + \mathrm{FeSi_2}$$

The improved cycling performance of Fe–Si/graphite was attributed to its "sandwich" structure, which suppressed the Si volume change. To further improve the cycling stability of Fe–Si–graphite, Ba was added to this alloy by ball milling [39]. XRD patterns of a Ba–Fe–Si/G anode before charging and discharging consisted of peaks identified as $BaSi_2$ and $FeSi_2$ alloys. Based on XRD and XPS results, the following Li insertion mechanism was proposed for Ba–Fe–Si/G:

$$\mathrm{Ba–Fe–Si/C} + x\mathrm{Li}^+ + x\mathrm{e}^- \rightarrow \mathrm{Li}_y\mathrm{Si} + \mathrm{Li}_{x-y}\mathrm{C} + \mathrm{BaSi_2} + \mathrm{FeSi_2}$$

Compared to pure Si anodes, Ba–Fe–Si anodes showed better cycling performance. The reason for improvement was considered to be due to the presence of $BaSi_2$ and $FeSi_2$ alloys which acted as inactive buffering matrix to offset the Si volume change. However, after 15 cycles, the Ba–Fe–Si anode showed a reversible capacity less than 400 mAh g^{-1}. When graphite was mixed with this alloy powder, it resulted in a reversible capacity of 420 mAh g^{-1} after 15 cycles. The improvement was attributed to graphite preventing aggregation of alloy particles. However, the capacity retention ability of such anodes was less than that of Fe–Si/G. The reason for their poor capacity retention was unknown.

Ni–Si/G composite was also synthesized by arc-melting followed by HEMM. It showed improved cycling stability [40] (Fig. 6). Improved cycling stability was attributed to better accommodation of the volume change, which resulted from the presence of NiSi, $NiSi_2$ phases, and disordered graphite layers.

Further efforts were made by Lee et al. [41] to improve the cycling performance of Ni–Si/G anodes by carbon coating. Initially $Ni_{20}Si_{80}$ alloys were prepared by milling Ni and Si powders. The $Ni_{20}Si_{80}$ alloy powders thus obtained were milled with graphite to form $Ni_{20}Si_{80}$ graphite composite. Carbon was coated onto this composite by mixing it with coal tar pitch, then pyrolyzing at 900 °C for 1 h. XRD patterns of carbon-coated composite indicated crystalline $NiSi_2$ and Si phases. Compared to untreated Ni–Si/C anodes, those coated with carbon showed better capacity retention due to the enhanced conductive contact

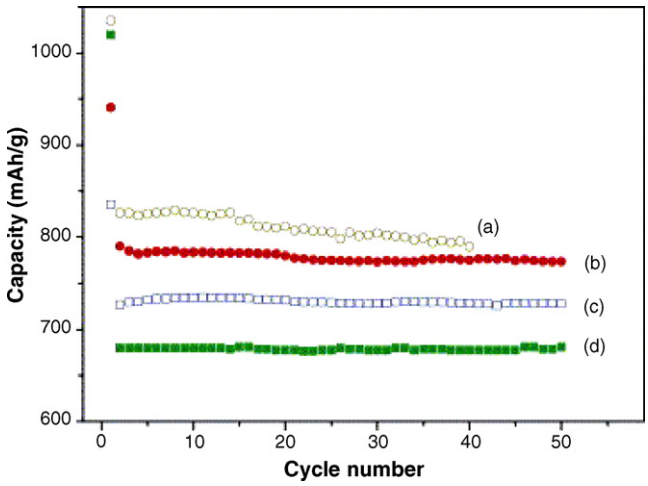

Fig. 6. (a–c) Cycle performance of Si/Ni alloy/graphite composites with different alloy to graphite weight ratios: (a) 7:3, (b) 6:4, (c) 5:5, and (d) Si/carbon (5:5) composite [40].

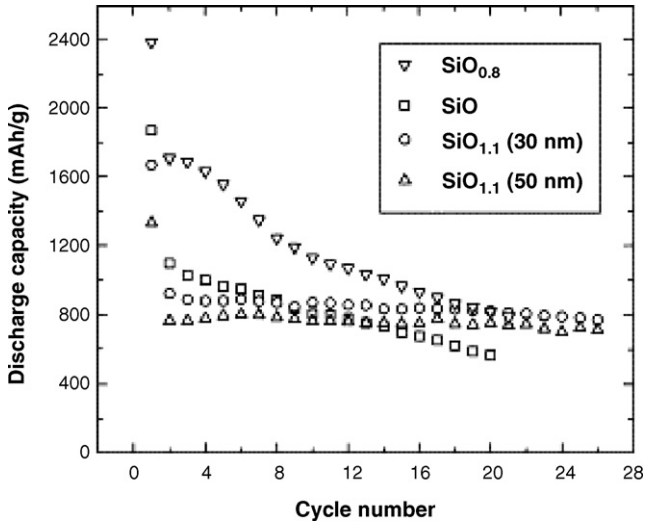

Fig. 7. §§Cycling behavior of SiO_x with different oxygen content and particle size [44].

between $Ni_{20}Si_{80}$ alloy and graphite particles, and surface modification. However, a decrease in reversible capacity close to 250 mAh g^{-1} was observed with carbon-coating. The reason for this reduction was unclear.

Unlike mechanically-milled Ni–Si and Fe–Si alloys, Cu–Si was formed by electroless deposition of Cu on Si powder [12]. To increase adhesion between Cu and Si, Cu was deposited on etched Si, followed by annealing at 400 °C. The Cu-coated Si powder showed higher electronic conductivity than the untreated material. However, its conductivity was reduced during annealing, which resulted in formation of resistive Cu_3Si alloys. When charged–discharged between 0.0 and 2.0 V, the Cu-coated Si electrode showed good capacity retention but unsatisfactory cycle life because of Cu detachment from the Si surface after few cycles, as was observed by SEM analysis. Increased Cu content with more effective annealing gave improved capacity retention and better cyclability. Its improved capacity retention resulted from its increased conductivity, which reduced contact and charge transfer resistances during alloying/de-alloying.

Apart from Ni–Si, Fe–Si, and Cu–Si alloys, highly oxidation-resistant alloys such as C–B–Si–N compositions were also investigated. They were prepared by co-pyrolysis of a light petroleum pitch fraction with polydimethylsilane followed by co-pyrolysis of the product with borane and pyridine, followed by heat treatment under nitrogen at 1200 °C [42]. When cycled at low current densities (0.01 mA cm^{-2}), a C–B–Si–N alloy anode showed a reversible capacity of 500 mAh g^{-1} and a columbic efficiency of 73%. Cycling performance of these anodes was not reported.

It had been reported earlier that Li insertion into tin oxides resulted in the formation of metallic Sn and an inert Li_2O matrix [43], which was believed to alleviate the volume change when Li alloys with Sn. Due to the superior cycling stability shown by tin oxide materials, silicon oxide powders with different oxygen contents (SiO, $SiO_{0.8}$, $SiO_{1.1}$) were also investigated as Li-ion anode materials [44]. Among anodes with different oxygen contents tested, those with lower oxygen content ($SiO_{0.8}$) showed higher reversible capacities (1600 mAh g^{-1}) but had poor capacity retention (Fig. 7). In contrast, anodes with higher silicon content ($SiO_{1.1}$) showed stable reversible capacities of 800 mAh g^{-1} over 25 cycles (Fig. 7). When the particle size of $SiO_{1.1}$ was reduced from 50 to 30 nm, capacity retention was further improved. Although high specific capacities and better cycle life were obtained with these anodes, they showed 50% irreversible capacities on the first cycle, which is undesirable for practical Li-ion cells. Their high irreversible capacity was due to formation of Li_2O, which was confirmed from neutron elastic scattering experiments [45].

To reduce the irreversible capacity of SiO_x anodes, Li was doped into them by the following procedure [46]: initially, an electrode was made from SiO powder on a nickel foam substrate, which was then immersed in a Li–organic complex solution obtained by dissolving naphthalene and metallic Li wrapped in porous polyethylene film into butyl methyl ether (BME) solvent. During immersion, naphthalene acted as a catalyst for doping Li into the SiO_x. When the electrode thus formed was immersed in electrolyte for 72 h, its equilibrium potential fell, finally stabilizing at 0.21 V versus Li/Li^+. Its discharge capacity was 670 mAh g^{-1}, which was higher than than that of pure SiO_x electrode, and its irreversible capacity was reduced. The extraction potential versus Li/Li^+ of such anodes is also raised. The resulting reduction in power density makes these materials unsuitable for commercial use.

Because of the advantageous electrochemical performance of lithium–transition metal oxynitrides as anode materials [47], lithium silicic oxynitride composites (LiSiPONS) prepared by HEMM of SiO_2 and Li_3N powders were investigated [48]. Although a reversible capacity of 600 mAh g^{-1} and a stable cycle life of 100 cycles were obtained, when the electrode was charged–discharged between 0.0 and 3.0 V, 75% of the capacity was obtained above 1.5 V, which cannot be considered to be practical.

Although the cycling stability of powder-based anodes prepared from Si covered by an inactive matrix was much better than that of pure Si anodes, it was not enough for commercial application. Recently, Sony has marketed its next generation Li-ion cells (Nexelion) which show a 30% capacity increase by using tin-based amorphous substrates. The large volume changes of tin anodes during Li insertion and extraction have been overcome by using alloys of the general formula $SnM^1_xM^2_yM^3_z$ [49], where M^1, M^2, M^3 are Co, Cr, and In. After testing anodes with $M = 0.2 < x < 1$ for all three compositions, a 92% capacity retention ability was observed. Since Co, Cr, and In do not react with Li, they can limit the change in particle shape and size and thus increase cycling stability. As a result, volume change was minimized, promising greatly improved Sn anode cycling stability.

The electrochemical performance of the anodes discussed in this Section shows that covering silicon with an inactive matrix reduces reversible capacity. When an active matrix such as graphite or pyrolyzed carbon is used to replace part of the inactive matrix, an increase in both reversible capacity and capacity retention are observed. To further improve Li-ion insertion ability, the outer inactive matrix should be completely replaced by an active matrix. In the next Section, the electrochemical performance of Si anodes covered by different active matrices is discussed.

4. Si-active material composites

4.1. Si-metal composites

Metallic silver and magnesium can reversibly react anodically with Li^+ at room temperature and form alloys (see Section 1). Mg_2Si alloy was therefore investigated as an anode material [50]. When charged–discharged between 0.0 and 1.5 V and 0.0 V at 10 mA g^{-1}, they showed a charge capacity of 1370 mAh g^{-1} and a discharge capacity of 1074 mAh g^{-1}. The charge capacity was equivalent to insertion of 3.9 Li atoms per Mg_2Si atom, which faded rapidly to only 100 mAh g^{-1} after 10 cycles. To understand this capacity fade, the Li-insertion reaction mechanism was studied by *ex-situ* XRD and atomic emission spectrography (AES). Differential capacity plots obtained for Si, SiO, and Mg were compared with those for Mg_2Si. It was determined that Si-containing materials followed similar Li insertion/extraction mechanisms because of the formation of Li–Si alloys, and the Li insertion mechanism in Mg and Mg_2Si anodes was the same near 0.0 V. Based on the XRD and AES analyses, the following reaction mechanism for Mg_2Si was proposed by Kim et al. [51]:

$$\text{First step}: \ Mg_2Si + xLi^+ + e^- \rightarrow Li_xMg_2Si$$

$$\text{Second step}: \ Li_xMg_2Si + Li^+ + e^- \rightarrow Li_{critical}Mg_2Si \rightarrow Li_{saturated}Mg_2S + Mg + \text{Li–Si alloy}$$

$$\text{Final step}: \ Mg + Li^+ + e^- \rightarrow \text{Li–Mg alloy}$$

It was therefore proposed that Li insertion into Mg_2Si was via three steps. First, Li inserts into octahedral Mg_2Si sites to form Li_xMg_2Si. When the Li concentration in Li_xMg_2Si reaches a critical value at 0.17 V, it decomposes into $Li_{saturated}Mg_2Si$, Mg, and Li–Si alloy phases as in Step 2. Finally, further insertion takes place into the Mg formed Step 2 with the formation of Li–Mg alloy. During extraction, the reverse reactions occur with formation of Mg_2Si. However, a small amount of Mg was still observed at the end of extraction. Comparison of XRD data for fresh and cycled anodes showed the presence of Li–Mg and Mg phases at the end of extraction. These incomplete reactions may be the reasons for capacity fade, since lithium is then trapped inside the anode. Li insertion into the remaining Mg phase results in volume change, which adds to that resulting from insertion into Mg_2Si, leading to cracking and disintegration of electrodes. A similar reaction mechanism was proposed by Moriga et al. [52] and Roberts et al. [53]. The latter [53] prepared Mg_2Si powders by ball milling and annealing of Mg and Si powders. In both cases, formation of Li_2MgSi was observed instead of $LiMg_2Si$. However, the formation of Li–Si phases was not reported. This may be due to the high current densities used, which reduced the kinetic possibilities for Li–Si reactions. While the Li insertion mechanism in Mg_2Si anodes observed in both these cases [52,53] is somewhat different from that previously reported [51], severe capacity fade was observed in all three cases, showing the inability of Mg_2Si anodes to suppress or accommodate volume changes on cycling.

SiAg anodes prepared by ball milling Si and Ag for 2, 15, and 50 h have also been examined [54]. XRD showed that Si was nano-scale and SEM analysis showed uniform dispersion of Si and Ag inside the anode. However, mechanical cracking due to the Li-insertion volume change resulted in poor cycling. Similarly, SiAg anodes prepared by electroless plating of Ag particles on Si powder were also tested [55]. X-ray energy dispersion analysis (EDAX) showed that the Si surface was covered by Ag particles. The improved performance of Ag-deposited Si was attributed to formation of an SEI film, which was not observed in pure Si anodes. The SEI film was believed to maintain contact between the pulverized Si particles. However, no galvanostatic cycling performance was reported for these anodes.

Sn is another metal allowing reversible Li insertion/extraction (see Section 1), so Si–Sn alloys with different compositions have been investigated as anodes. Among samples tested, a-$Si_{0.66}Sn_{0.34}$ film (a- = amorphous) showed high electronic conductivity. When charged–discharged between 0.0 and 1.3 V, a-$Si_{0.66}Sn_{0.34}$ anodes had an initial charge capacity of 2000 mAh g^{-1} and a discharge capacity ≈1900 mAh g^{-1} [56]. Charge–discharge curves were found to be smooth with no plateaus. Similarly, no sharp peaks were observed in differential capacity plots, which indicate the phase stability of the material during cycling. To determine their reaction mechanism, *in-situ* XRD experiments were conducted during cycling. Results showed that the film always remained amorphous. At the end of charge, a-$Li_{4.4}Si_{0.66}Sn_{0.34}$ was formed. While high reversible capacity was obtained with a-$Si_{0.66}Sn_{0.34}$, its cycle life is as yet unknown.

In the patent literature [57], efforts were made to improve electronic pathways between the current collector and Si active

material by forming multi-layer particles with Si inner, intermetallic middle, and synthetic graphite outer layers to give as-prepared active material containing between 30 and 70 wt% Si. Intermetallics such as Mg_2Si, $CoSi_2$, $NiSi_2$, were claimed. The middle layer was intended to suppress the cycling volume change, while the outer layer increased electronic conductivity. Previous attempts to mix conductive agents into the anode to improve its electronic conductivity resulted in too small an electronic contact area, which resulted in major cycling fade for anodes showing large volume changes. This effect was prevented by surface coating of the intermetallic compound by fusion, then subjecting the resulting powder to mechano-fusion to coat synthetic graphite onto the surface. This gave an anode with greater than 80% capacity retention over 300 cycles.

A similar approach in published US patent applications [58–60] has involved dispersing Si into a metal (Sn, Zn, Al) acting as an active matrix, but including a lesser proportion of another inactive metal (Cu, Co, Ni, Ti, B, Sb). Impregnation was done via melting the elements with Si to form an alloy, followed by water atomization and HEMM. The resulting powder contained uniformly-dispersed Si in an active metal matrix and an intermetallic compound, e.g., Cu_6Sn_5, Cu_5Zn_8, Ni_3Sn_2, etc.) formed from an Li-active and Li-inactive metal. When charged–discharged between 1.2 and 0.0 V for 30 cycles, such anodes showed reversible capacities in the 1100–1700 mAh g^{-1} range [58–60]. In particular, Si–Sn–Ni alloy anode showed superior capacity retention ability [58]. A charge–discharge test in a complete cell using a $LiCoO_2$ cathode and one of the above anode anodes gave a capacity retention of 75% at the 100th cycle [58]. The improved cycling stability of this anode may be due to the minimization of volume change by dispersing Si in the complex matrix.

4.2. Si/C composites

Although the cycling performance of Si-metal inactive/active matrix composite anodes discussed in the last Section is much better than that of pure Si anodes, capacity fade has still been unavoidable. Even relatively strong metals may not be able to sustain the 400% volume expansion of Si, and their pulverization will result in loss of interparticle electronic contact. Carbon has been used as an active matrix because of its softness and compliance, relatively low mass, good electronic conductivity, reasonable Li-insertion ability, and small volume expansion. Silicon dispersed in carbon matrices (Si/C composites) were therefore tested as anodes.

Various methods have been employed for preparing Si/C composite anodes. Based on their preparation procedure, we classify Si/C composite anodes into five types:

1. Pyrolysis or chemical/thermal vapor deposition (CVD/TVD).
2. Ball milling or mechanical milling.
3. Combination of pyrolysis/CVD/TVD and mechanical milling.
4. Chemical reaction of gels.
5. Other methods.

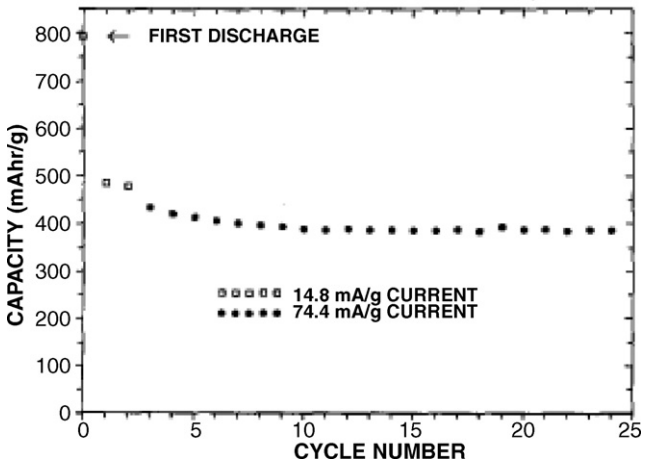

Fig. 8. §§Capacity vs. cycle number for anode made from polymethylphenylsiloxane (PMPS) pyrolyzed at 1100 °C [61].

4.2.1. Si/C composite anodes prepared by pyrolysis reactions or TVD.

Work on Si/C composite anodes started in the early 1990s. Dahn et al. appear to have been the first to prepare Si/C composites from various polymers containing silicon and carbon. The first anode was prepared from thermal pyrolysis of polymethylphenylsiloxane (PMPS) and polyphenylsesquisiloxane (PPSSO) polymers in the 900–1300 °C temperature range [61]. These start to decompose above 500 °C, rapidly evolving large amounts of benzene and small amounts of methane and hydrogen at higher temperatures. Thermogravimetric analysis (TGA) showed final estimated compositions at 1000 °C as $C_{2.9}SiOH_y$ and $C_{3.9}SiO_{1.5}H_y$, respectively, with y ranging from 0 to 1. Both were amorphous and had reversible capacities of 550 mAh g^{-1} and an irreversible capacity close to 300 mAh g^{-1} (Fig. 8). When pyrolysis was performed at 1300 °C and above, anodes showed low reversible capacities (close to 200 mAh g^{-1}) and large irreversible capacities because complete oxygen removal occurred with formation of silicon carbide. Siloxane polymers were also synthesized and investigated as anode materials [62,63]. They were derived from mixtures with generic structures $(R^1R^2R^3SiO_{0.5})_w$ $(R^4R^5SiO)_x$ $(R^6SiO_{1.5})_y$ $(SiO_{4/2})_z$, where R^1–R^6 are hydrogen or alkyl groups and w, x, y, and z are molar ratios [63]. Their electrochemical performance was explained by constructing a Gibbs triangle for Si, C, and O. Most of the samples lay near the line connecting carbon to $SiO_{1.3}$. Along the line, reversible capacities increased from 340 mAh g^{-1} for pure carbon, to a maximum capacity of 890 mAh g^{-1} for the composition of 25 wt% Si, 45% C, and 30% O. When the amount of carbon was further decreased, it led to a decrease in reversible capacity with 0 mAh g^{-1} capacity at 0% carbon. These results indicate the role of carbon in improving their reversible capacity. Although amorphous Si–C–O glass can reversibly react with Li, conduction pathways for electrons and Li^+ ions are necessary, which are provided by carbon. XRD of the composition 25% Si, 45% C, and 30% O showed that it consisted of amorphous Si–C–O glass dispersed in disordered carbon. From comparison of stoichiometries, it was concluded

that increase in oxygen content increased irreversible capacity and discharge potential. Although higher specific capacities were obtained with pyrolyzed polysiloxane materials, samples with desired Si/C compositions could not be prepared, since the Si/C compositions of the polymer precursor was fixed.

To prepare anodes with desired Si/C compositions, an epoxy-silane composite was prepared from the non-silicon-containing polymer poly[(phenylglycidylether)-*co*-formaldehyde)], an epoxy resin, and the epoxy-functional silane 3-glycidoxypropyltrimethoxysilane [64]. The epoxy-silane composite obtained was pyrolyzed at 1000 °C and the resulting powder made into an anode. When epoxy resin was pyrolyzed, it gave disordered carbon in the form of single graphene layers. Pyrolysis of silane gave an amorphous glassy compound with the composition $C_{0.5}Si_{0.19}O_{1.31}$. Pyrolysis of the epoxy-silane composite gave a compound of composition $C_{1-y-z}Si_zO_y$. The amount of carbon was found to depend on the silane concentration in the precursor, first increasing, then decreasing as silane increased. An optimum composition was obtained using 50% silane and 50% resin, which gave a mixture of carbon single layer phase and amorphous glassy phase. As the amount of silicon and oxygen in the anode was increased, the reversible capacity also increased. Increase in silicon and oxygen concentration also resulted in increase in charge potential, which led to significant capacity above 1.0 V. When the anode was made from 50% silane and 50% resin, it showed a reversible capacity of 770 mAh g^{-1}, but with a large irreversible capacity. Although Si/C composite anodes with desired compositions can be prepared by the epoxy-silane approach, the large irreversible capacities observed for these materials were disadvantageous.

Apart from polysiloxanes and epoxy-silanes, pitch-polysilane composites in various ratios were also pyrolyzed at 1000 °C to form Si/C composites [65]. Stoichiometries of these samples corresponded to the entire region of the C, SiC, and SiO_2 Gibbs triangle. As with the epoxy-silane composite precursors, anode materials prepared from material with higher silane content exhibited an amorphous glassy structure dispersed in disordered carbon. Increasing silane in the pitch blend increased both reversible and irreversible capacity. A study of electrochemical performance as a function of composition led to the conclusion that materials in the SiO_2 and SiC corners should not be used for the preparation of Si/C composite anodes. Using these results, a silane polymer with composition $(Me_2Si)_x(PhMeSi)_y$ was selected for further investigation [66]. As with the anodes made from siloxane polymers [63], the presence of oxygen was found to be the main reason for high irreversible capacity. This was confirmed from X-ray absorption spectroscopy (XAS) and charge–discharge curves, where the presence of oxygen gave an additional plateau between 0.6 and 0.8 V.

The effect of oxygen and sulfur content on Si/C irreversible capacity was examined by electrochemical tests on anodes containing pyrolyzed mixtures of pitch and polysilanes [67,68]. Polyphenylmethylsilane (PPMS), polydimethylsilane (PDMS), polydimethylphenylmethylsilane (PDMPMS), polydiphenylsilane (PDPS), and PDMS/PPMS and PDMS/PDPS mixtures were used along with Ashland Chemical pitches with different sulfur contents, naphthalene pitches, and PVC pitch with very low sulfur and oxygen content. Anodes made from pitches other than PVC pitch showed irreversible capacities between 150 and 170 mAh g^{-1}. When PVC pitch was used, a considerable decrease in irreversible capacity was observed. However, it also resulted in reduction in reversible capacity due to loss of active Si and inactive Si–C phase formation. When significant amounts of Si and S were present, a large amount of Li was inserted, but it also resulted in increased irreversible capacity since some Li was trapped by S. Similarly, reversible capacity between 320 and 450 mAh g^{-1} and irreversible capacities of 300 mAh g^{-1} were reported for Si/C composite anodes prepared by pyrolysis of coal tar pitch and silane polymers, such as PDMS, PPMS, PDMPMS, and PDPMPS [69]. From these results, it was concluded that pitch-polysilane blends were not suitable for preparing anodes with high reversible and low irreversible capacities.

Similarly, Hayes et al. [70] reported formation of Si/C composites from polymethacrylonitrile/divinylbenzene (PMAN/DVB) copolymer as a carbon precursor and tetramethylsilane (TMS) or tetravinylsilane (TVS) as Si precursor. These were mixed to form an emulsion which was polymerized at 65 °C, thermally stabilized in air at 240 °C, and finally pyrolyzed at 700 °C. The resulting material was found to have large oxygen content (22.5 wt%), negligible nitrogen content (2.99 wt%), and 10 wt% Si. Structural studies showed that the material consisted of mostly Si–O–Si bonds with a few Si–O–C bonds, but no Si–C bonds, possibly showing that these were converted to Si–O–C bonds during oxidative stabilization, with further conversion to Si–O–Si bonds during pyrolysis. These Si–O–Si and Si–O–C glasses were found to be dispersed in disordered carbon. When cycled between 0.10 and 1.0 V, anodes made from PMAN/DVB–TMS emulsion showed a reversible capacity of 394 mAh g^{-1} with a large irreversible capacity of 576 mAh g^{-1}. The anode made from PMAN/DVB–TVS showed a reversible capacity of 363 mAh g^{-1} and an irreversible capacity of 601 mAh g^{-1}. Their first cycle columbic efficiency was 26%, which was very low compared with the columbic efficiency of Si/C composite anodes obtained from pitch-polysiloxane materials [63]. Although the structures of the both materials were the same, the reversible capacity was very low for anodes made from PMAN/DVB–TVS/TMS. The difference in electrochemical performance was attributed to the different polymer precursors used. Li intercalation into the last anode resulted in formation of silicates, accounting for their irreversible losses. Their large irreversible capacities and low reversible capacities make the above materials unsuitable as anodes.

The electrochemical performance of Si/C composite anodes prepared by pyrolysis of various polymer precursors makes it clear that the presence of oxygen in the anode leads to irreversible capacity. To overcome this, oxygen free materials have been used as carbon and silicon precursors. Wilson et al. [71,72] used benzene as a carbon precursor, with $SiCl_4$ and $(CH_3)_2Cl_2Si$ as Si precursors. Precursor materials were deposited by thermal vapor deposition (TVD) at 850, 950, or 1050 °C. The materials obtained showed the absence of a-Si, SiC, and SiO_2. It was thought that Si was located in unorganized graphitic regions.

Anodes made from this material showed reversible and irreversible capacities of 640 and 120 mAh g^{-1}, respectively.

Similarly, Xie et al. [73] deposited Si particles on Meso carbon microbeads (MCMB) by TVD of silane (SiH_4) at 450 and 500 °C. Raman spectra indicated that crystalline Si was coated on the MCMB, but only in small amounts (0.036 and 0.05 at.% at 450 and 500 °C, respectively). Although the 450 °C preparation showed higher reversible capacity (462 mAh g^{-1}) than that of an uncoated MCMB anode (290 mAh g^{-1}), its coulombic efficiency was only 45% compared with 77.5% for MCMB. The low coulombic efficiency was attributed to SEI film formation, irreversible Li^+ trapping, and loss of active material. Similarly, nano-Si deposited on Timcal KS-6 graphite by TVD of silane was tested as an anode [74,75]. From SEM analysis of the Si/C composite obtained, 10–20 nm of spherical Si particles were found to adhere to the graphite surface [75]. From microanalysis, the Si content was found to be 7.1 wt% [74]. During the initial charge–discharge of this anode, Li-insertion simultaneously took place in nano-Si and graphite. During continuous cycling between 0.005 and 1.0 V, a capacity loss of 0.15% per cycle was observed. When the Si content was increased to 20 wt%, this anode showed initial charge and discharge capacities of 1350 and 1000 mAh g^{-1} with a non-restricted cycling procedure, with 26% irreversible capacity attributable to the high surface area of KS-6 graphite [75]. However, the 20 wt% nano-Si deposited on the graphite surface was exposed to electrolyte and had a high surface area available for SEI film formation, which will better account for the high irreversible capacity. As shown in Fig. 9, after 100 cycles this anode showed reversible capacity higher than 900 mAh g^{-1}, i.e., a capacity fade rate less than 1%. Its superior cycling performance was attributed to the smaller silicon particle size (50 nm) and its strong adhesion to the graphite matrix. The amorphous oxide layer on the Si surface was believed to play an important role in improving cycling performance. During intercalation, Li would react with this oxide to form Li_2O, which would act as an Si particle binder during cycling. The cycling performance of this anode is the best so far observed for Si, excluding thin film anodes whose cycling performance is known to depend on microstructure. These results made further investigation of Si/C composite anodes a priority. However, their observed high irreversible capacity should be reduced.

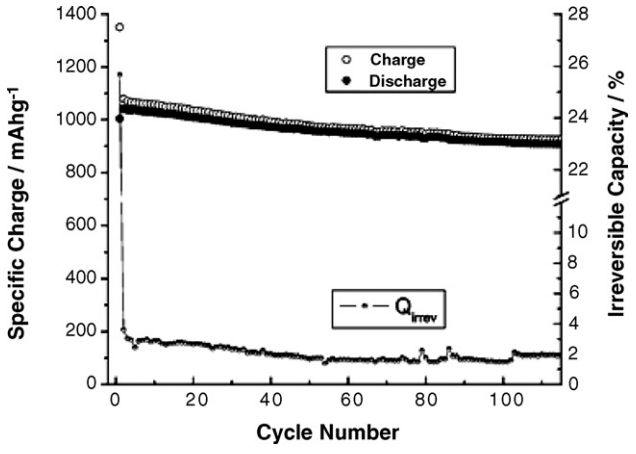

Fig. 9. Specific capacity and percent irreversible capacity as a function of cycle number for Si/graphite composite anode obtained by depositing Si on graphite [75].

Since carbon has less surface area than Si, carbon has been deposited on pure Si powder to attempt to reduce SEI film formation and irreversible capacity. Since performance depends on the precursor used and on deposition parameters, different precursors such as polyvinylchloride, polyvinylalcohol (PVA), and pitch have been used. Using this approach, Dimov and coworkers [76–79] and Liu et al. [81] prepared Si/C composites and tested their electrochemical performance as anodes. They deposited carbon on ground Si particles by TVD of benzene in a nitrogen stream using at 1000 °C. The high columbic efficiency and low irreversible capacity resulted from suppression of electrolyte decomposition by carbon coating, which was demonstrated by cyclic voltammetry. Charge–discharge capacities of this anode for the first 50 cycles were found to be very close, demonstrating high coulombic efficiency. In addition, limiting Li insertion capacity to below $Li_{1.71}Si$ also improved capacity retention. Irrespective of the charge–discharge mode, the Si lattice is gradually destroyed by Li insertion/extraction, and the carbon coating was not itself sufficient to suppress the large volume change [78]. Though capacity fade was observed after a certain number of cycles, carbon-coated Si anodes also showed low irreversible capacities in propylene carbonate (PC) based electrolytes, with better thermal stability than conventional graphite anodes.

Addition of graphite was examined to improve the cycle life of these anodes. Si and graphite in 1:1 weight ratio were homogenously mixed and carbon was deposited on the mixture [79]. The deposition procedure and charging–discharging modes were the same as in the previous paragraph. The anodes contained two types of carbon, viz., graphite and disordered carbon obtained from thermal vapor decomposition of benzene. A single plateau was seen in the charge–discharge curve, which did not correspond to any of the four Li–Si phases. From the differential capacity curves [79] and *in-situ* XRD studies [80] during Li insertion/extraction, it was concluded that during the first insertion process, Li^+ saturates the carbons first and then starts to alloy with Si, so Li-saturated carbon and amorphous Li–Si alloy coexist. During the second cycle, Li alloys with C and amorphous Si simultaneously. On further cycling, a decrease in Si peak intensity was observed, indicating a decrease in the Si contribution to overall capacity. *Ex-situ* XRD studies [79] showed that the anode consisted of only Si and C phases. Even after Li insertion in the first cycle, the anode was found to contain a dominant percentage of Si particles, showing the non-uniform distribution of Li inside the anode. However, the distribution was found to be more uniform than that of a pure Si anode due to the presence of deposited carbon and graphite, which provided a uniform and distributed Li buffer [80]. These anodes also showed better cycling performance than those made from pure Si, however, capacity fade occurred after extended cycling. To determine the reason for the capacity fade, anodes with different water contents and cells with fluorine-free electrolytes were made. Water content was found to have detrimental effect on anode cycle life,

but the presence of fluorine did not. Anodes with low water content (<20 ppm) showed reversible capacities of 800 mAh g^{-1} for 30 cycles, after which rapid capacity fade occurred. At 250 ppm water, cycling could only be performed over 10 cycles. During 30 charge–discharge cycles, anodes containing less water showed a total irreversible capacity of 1000 mAh g^{-1}, i.e., some lithium was trapped inside the anode during each insertion. As shown earlier, the non-uniform distribution of lithium in the anode gave dead areas unavailable for further insertion, which in turn resulted in increased irreversible capacity and capacity fade.

Capacity fade for Si and Si/C composites was explained in terms of electrode microstructure by Liu et al. [81]. Si and Si/C composite anodes containing conductive additives (KS-6 graphite and Super P carbon black) added to Si and carbon-coated Si were prepared. These were mixed with styrene butadiene rubber-sodium carboxymethylcellulose (SBR–SCMC) to give a slurry which was coated on Cu foil to prepare electrodes. Both pure Si and carbon-coated Si anodes were charged at constant capacity and discharged until a cut-off potential of 1.2 V was reached. After 70 cycles, the capacity versus cycle number for pure Si electrodes was found to contain two regions with different capacity fade rates, shown in Fig. 10. When the designated charge capacity was limited to 800 mAh g^{-1}, the first region was found between cycle 25 and cycle 52, during which the designated charge capacity was reached easily but the coulombic efficiency started to decrease. The results show that Si particles were in good contact during charge, but during discharge certain particles started to lose electronic contact, which was also observed for thin film Si anodes. After the 52nd cycle, a second region was observed, where the charge capacity was less than the designated value. This was due to poor electronic contact between Si particles even during charge, with the conclusion that the entire anode structure had then disintegrated. Results showed that capacity fade in the first region were locally associated with individual particles, while that in the second region was global and associated with failure of the entire electrode structure. When the latter occurred, a negligible capacity was seen within a few cycles. When the designated charge capacity

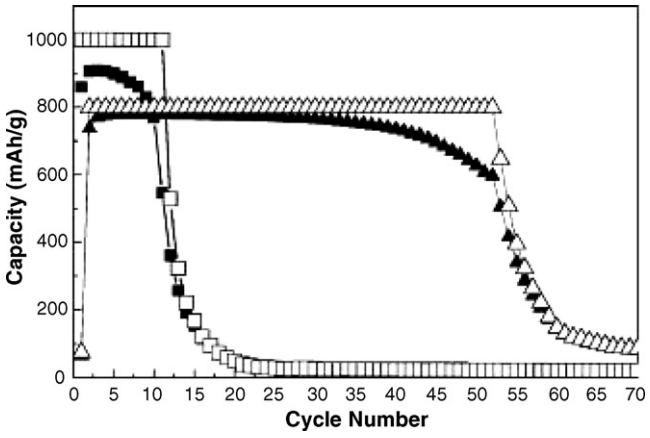

Fig. 10. Capacity vs. cycle number for pure Si electrode at designated discharge capacities of 800 and 1200 mAh g^{-1}. Open symbols: charge; solid symbols: discharge [81].

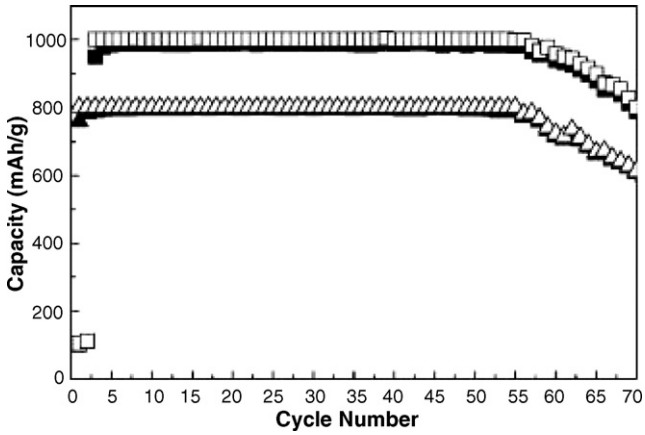

Fig. 11. Capacity vs. cycle number for carbon-coated Si anode at designated discharge capacities of 800 and 1200 mAh g^{-1}. Open symbols: charge; solid symbols: discharge [81].

was increased to 1000 mAh g^{-1} for pure Si, the occurrence of the first and second regions was observed much earlier than at 800 mAh g^{-1}, the transition occurring between the 9th and 10th cycles, as shown in Fig. 10. For Si/C composite anodes, only the global fading mode was observed, as shown in Fig. 11, when the capacity fade rate was lower than that of Si anodes. The overall improvement observed for Si/C composite anodes was attributed to the stability of the electrode structure obtained by carbon deposition. The absence of the local degradation mode was due to the conductive network formed by deposited carbon and graphite, which preserved electronic connection between fractured Si particles during cycling. A lower measured resistance (26 μΩ) across a Si/C composite anode compared to a Si anode (55 μΩ) also justifies the above reasoning. Though significant improvement was observed in cycling by using carbon deposition, severe capacity fade was still observed after 55 cycles. Limiting Li insertion to a certain capacity limit will reduce volume expansion and give improvement in cycle life.

Similarly, Si/C composites were prepared by pyrolyzing nano-Si (100–150 nm), pitch and graphite in 1:3:1 weight ratio at 900 °C for 1 h [82]. Anodes prepared from the pyrolyzed mixture were found to be very porous. Since many Si nano-particles are attached to carbon, voids might have formed between the particles, which improved capacity retention of nano-Si/C compared with that of pure Si. Generally, electrolyte contact with Si results in the separation of conductive pathways between Si and other particles present, leading to loss of active material. Here, the composite structure obtained by carbon coating apparently reduced the possibility for contact between Si and the electrolyte. The porous nano-Si/C anode structure also helped to maintain its mechanical stability by relieving stresses resulting from Si volume change. Further improvement in cycling performance was obtained by adding $CaCO_3$ to the Si/C composite [83]. Improved electrochemical performance was due to the formation of $CaSi_2$ and Ca_2Si alloys, which were evident from XRD analysis. The alloy layer formation increased the interfacial stability between Si and C, and also suppressed the volume change in Si.

Apart from pitch, PVC was also used as carbon precursor by Yang et al. [84]. Nano-Si and graphite were mixed with a PVC

solution, dried, then pyrolyzed at 900 °C for 2 h. Although its cycling stability was same as that of an anode without graphite, its initial reversible capacity and coulombic efficiency were higher due to the graphite additive, which enhanced Si distribution uniformity in the pyrolyzed carbon. When some pyrolyzed carbon was replaced by graphite, the resulting lower surface area reduced the potential hysteresis between charge and discharge. High cycling stability of such anodes with and without graphite resulted from the pyrolyzed carbon coating. The latter not only acts as a carrier and matrix, but also as a binder for Si and graphite. As a result, Li alloying and de-alloying kinetics were improved, giving improved cycling stability. Compared to Si/C composites made from pitch [82], Si/C composite anodes made from PVC showed higher cycling stability. This was attributed to their less porous structure.

As stated in Section 3, Si–TiN composite covered by carbon has shown high reversible capacity and high capacity retention. Accordingly, the effect of introducing an inert element such as Cu into Si/C composites was investigated [85]. Initially Cu was deposited on Si particles by simple chemical reduction followed by drying. The Si/Cu composite was mixed with PVA solution, which was dried and pyrolyzed at 900 °C for 2 h. XRD patterns of the initial powder contained peaks related to Cu, Cu_2O, and Si, whereas patterns obtained after pyrolysis showed Si and Cu_3Si. Oxidation of Cu had therefore occurred during the initial processes, while during pyrolyzation, both Cu_2O and Cu reacted with Si to form Cu_3Si alloy. Electron-probe X-ray microanalysis (EPMA) showed that the composite particles obtained by pyrolysis contained both randomly distributed Cu particles, and Si particles to which Cu_3Si particles adhered. When cycled between 0.0 and 2.0 V, electrodes prepared from Si–Cu–Cu_3Si/C composites showed a first discharge capacity of 680 mAh g^{-1} and a coulombic efficiency of 82%. After 30 cycles, they showed 87% capacity retention ability. Improved cycling stability of Si–Cu/C anodes was due to the high electronic conductivity of the Cu_3Si alloy and the carbon coating. From EPMA analysis, the high electronic conductivity of the Cu_3Si alloy was found to increase the adherence strength of Si particles with the current collector, which resulted in good interparticle electronic connection. Increasing adherence resulted in suppression of the Si volume changes.

So far, the electrochemical performance of Si/C composite anodes prepared by various procedures has been discussed. In most cases, the carbon was prepared by pyrolysis of different organic precursors giving disordered carbon. In contrast, carbon nanotubes (CNTs) were used in Si/C composite anodes by Shu et al. [86]. They deposited these on Si powder by decomposition of acetylene at 800 °C in the presence of Ni–P catalyst. The nanotubes were found to be in the form of 400 nm long, 30 nm diameter coils which SEM analysis showed to be cage-like, enveloping each Si particle. When cycled between 0.0 and 2.0 V, their Si/CNT composite anode showed an initial reversible capacity of 1120 mAh g^{-1} and a coulombic efficiency of 80%. After 20 cycles, its reversible capacity was 940 mAh g^{-1}. Anodes made from a simple mixture of Si and CNTs showed severe capacity fade, indicating the importance of good electronic contact. When the length of carbon nanotubes was increased to 15 μm by increasing deposition time, the cycling performance of the composite anode was greatly improved, which was attributed to their better electronic conduction network. A further effort was made to improve Si/CNT anode cycle life by increasing its electronic conductivity by doping Cr into Si by ball-milling prior to deposition [87]. However, this did not result in a cyclability enhancement over the results of Shu et al. Since CNTs act as a conductive and mechanical network, they may be sufficient to maintain mechanical integrity. Although carbon coating on Si and Si coating on carbon have been found to be effective in reducing capacity degradation during cycling, high cycling performance was not in fact achieved by either method.

4.2.2. Si/C composite anodes prepared by ball milling

Structure, particle size, and composition in Si/C composite anodes cannot be controlled by using TVD or pyrolysis reactions. Maintaining homogeneity throughout the sample is also difficult. However, ball milling or mechanical milling can result in alloy systems with desired compositions, structures, and particle sizes. Recognizing these advantages, Wang et al. [88] used this method to prepare Si/C composite anodes by ball-milling graphite and crystalline Si in different atomic ratios ($C_{1-x}Si_x$, $x = 0$, 0.1, 0.2, and 0.25) for 150 h, then mixing the powder with colloidal polytetrafluoroethylene (PTFE) in anhydrous alcohol to prepare anodes. During milling, collision of C and Si resulted in particle size reduction. After 150 h of milling, graphite was found to form a metastable phase identical to that of disordered pyrolytic carbons. XRD showed no peaks other than metastable C and Si, and the Si/C composite was found to contain nano-Si particles encapsulated in amorphous carbon. At low Si content ($x = 0.1$), an agglomeration of 50 nm graphite particles occurred, forming 0.5 μm mean diameter lamellar particles. Increased Si content avoided such agglomerations. When charged–discharged between 0.005 and 1.5 V, a flat plateau at 0.4 V was seen for all compositions, whose reversible capacity corresponded to insertion of 1.5 Li atoms per Si, i.e., lower than the usual maximum. All anodes prepared by milling showed higher reversible capacities and lower irreversible capacities than a nominal $C_{0.6}Si_{0.4}$ anode made by simply mixing C and Si, due to the presence of nano-Si which reduced disintegration. Among compositions tested, an anode with 20 wt% Si had a reversible capacity of 1039 mAh g^{-1}, an irreversible capacity of 1500 mAh g^{-1}, and the best cycle life, which decreased with increasing Si content due to disintegration. As already stated, the cycle life of Si/C composite anodes prepared by milling can also be improved by changing the degree of charge, e.g., reducing the Li insertion capacity from 900 to 500 mAh g^{-1} increased life from 25 to 90 cycles [89]. In spite of their relatively good capacity retention, these anodes have shown unacceptable irreversible capacities of greater than 100% due to disintegration of Si and irreversible lithium insertion. To attempt to further improve cycling stability, Si–graphite composites were milled with multi-walled carbon nanotubes (MWNTs) and their electrochemical performance was tested [90]. However, neither capacity decay nor irreversible capacity was reduced.

To reduce irreversible capacity and increase the coulombic efficiency of Si–graphite anodes, Liu et al. [91] included the compound $Li_{2.6}Co_{0.4}N$ into Si/C composite by milling. Initially Si and graphite were milled for 10–15 h. The appropriate amounts of Li_3N and Co were homogenously mixed and sintered at 700 °C for 12 h under nitrogen to form $Li_{2.6}Co_{0.4}N$, which was milled with Si/G composite for 2 h. Anodes were made from milled Si–G and Si–G–$Li_{2.6}Co_{0.4}N$. Addition of $Li_{2.6}Co_{0.4}N$ to Si/C composite anodes resulted in an initial coulombic efficiency increase from 44% to 90%. During discharge, a new plateau for Li extraction from $Li_{2.6}Co_{0.4}N$ appeared at 1.0 V. It was supposed that this extraction capacity above 0.8 V resulted in suppression of charge–discharge potential hysteresis, but such capacity should not count towards that of a practical anode. Addition of this compound to milled Si–G powder decreased open circuit voltage to 0.8 V, giving lower anode power density. Although irreversible capacity was decreased by addition of $Li_{2.6}Co_{0.4}N$, for the reasons given this approach is not suitable for a practical anode.

Like graphite, 10 μm Meso carbon microbeads have been used as a dispersion medium for 80 nm nano-crystalline Si by ball-milling for 5, 10, and 20 h [92]. SEM showed that MCMB remained spherical even after milling for 10 h. However, after 20 h, it became a fine powder. XRD showed that the Si/C composite contained nanocrystalline Si and MCMB with reduced particle size. Cyclic voltammetry showed insertion peaks at 0.2 V and close to 0.0 V and oxidation peaks at 0.3–0.4 and 0.51 V. The 0.2 and 0.51 V peaks were attributed to Li insertion and extraction in Si, while the remaining peaks corresponded to Li insertion and extraction in MCMB. When cycled between 0.01 and 3.0 V, a 10 h milled anode showed an initial reversible capacity of 1066 mAh g^{-1} and a reversible capacity of 700 mAh g^{-1} on the 25th cycle, while a 5 h milled sample showed lower capacity retention, indicating better dispersion of nanocrystalline Si in the MCMB matrix with longer milling. However, an anode prepared after 20 h of ball-milling showed lower capacity retention ability and higher irreversible capacity due to the destruction of the MCMB structure, and to its higher surface area, giving more extensive SEI film formation. Superior cycling shown by the anode milled for 10 h was not only due to better dispersion, but also from limiting the insertion potential. These anodes showed lower irreversible capacities than those made from milled Si and G when the Li insertion potential was limited to 1.0 V. In general, SEI film formation and irreversible capacity occurred starting at 0.8 V.

Cu_5Si–Si/C composites prepared by ball milling were also electrochemically evaluated [93]. Initially Cu and Si powders were milled together to form a Cu_5Si–Si composite, which was then milled with graphite to form the Cu_5Si–Si/C product. XRD showed the presence of Cu_5Si and low crystallinity Si. The initial reversible capacity of these anodes was much less than that of Cu–Si anodes prepared by electroless deposition (see Section 1), and their first cycle involved 60% irreversible capacity.

These results show that Si/C composite anodes prepared by either milling or pyrolysis have better cycle life than pure Si anodes, but they still show capacity fade after a certain number of charge–discharge cycles because of microstructural changes on cycling which give macrostructural deformation [94]. To replace graphite or carbon with Si as an anode material, it is essential to develop electrodes able to maintain electrochemical reversibility in spite of microstructural deformation [94].

4.2.3. Si/C composite anodes made by ball-milling and pyrolysis

It is evident from the above that addition of carbon to Si by milling or pyrolysis can enhance interparticle electronic connection during charge–discharge, giving improved capacity retention. However, composite anodes prepared by pyrolysis but not initially including graphite gave unsatisfactory cycling performance and coulombic efficiency due to non-uniform distribution of Si and to the high porosity of pyrolyzed carbon. Si/C composite anodes prepared by mechanical milling had a large initial irreversible capacity. These suggested that pyrolysis and HEMM should be used in the preparation of Si/C composites. Zhang et al. [95] milled Si with PVC for 24 h, then heat-treated the mixture at 650, 800, 900, and 1050 °C. The electrochemical performance of anodes thus formed was found to be dependant on heat treatment temperature. Thirty-three weight percent of Si–PVC-based disordered-C anodes prepared at 800 and 900 °C showed high reversible capacity (548.8 and 468.3 mAh g^{-1}, respectively) due to their low interfacial impedance which resulted from incomplete C coating on Si. At reduced Si content, a more uniform dispersion of Si in carbon was achieved, resulting in improved Li insertion and extraction.

To further improve the capacity retention of Si–PVC-based disordered carbon anodes, two pyrolysis reactions were performed during preparation with one intermediate high energy mechanical milling reaction [96,97]. Electrodes were prepared using the following procedure: PVC and Si in 3:7 weight ratio were homogenously mixed and pyrolyzed at 900 °C for 1 h. The pyrolyzed powder was milled for 2 h, again mixed with PVC in same ratio, then pyrolyzed at the same temperature. An anode prepared from final powder showed a first cycle coulombic efficiency of 80%. Anodes prepared using one pyrolysis reaction showed severe capacity fade due to poor distribution of Si in the carbon matrix and poor interfacial contact between Si and C. When two pyrolysis reactions were performed, the anodes showed increased cycling stability. However, capacity fade was observed after 15 cycles. When one pyrolysis and one HEMM were used, the anode showed a capacity decrease during initial cycling, then capacity retention increased during further cycling. This improvement was attributed to HEMM, which crushes the least stable parts of the Si/C composite, forms Si–C cores, improves the uniformity of Si distribution in C, and reduces the porosity of pyrolyzed C. Pyrolyzed PVC from the first pyrolysis also works as a separator and prevents the agglomeration of Si particles during the HEMM process. As a result, the filling density and mechanical strength of the anode increases. However, milled samples showed highest irreversible capacity due to the reduced particle size and increased surface area. To overcome this, the second pyrolysis carried out after the HEMM process reduced this surface area and gave Si completely embedded in a carbonaceous matrix. During the initial

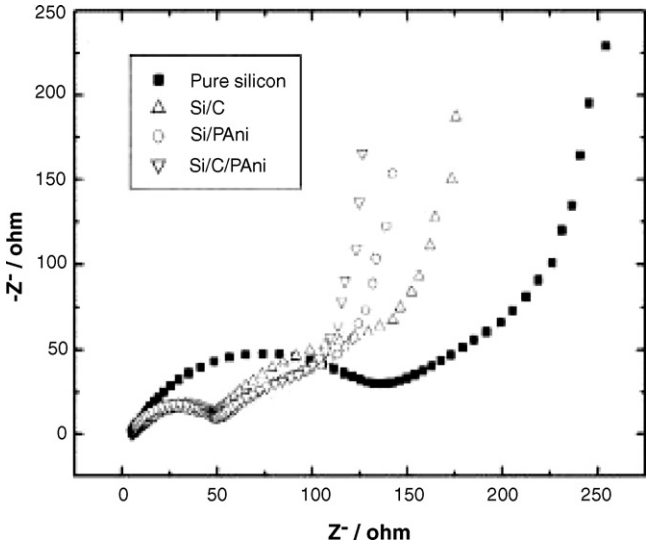

Fig. 12. Impedance measurements for pure Si, Si/PAni, Si/C, and Si/C/PAni composite anodes (PAni = emeraldine-base polyaniline/$LiClO_4$) [98].

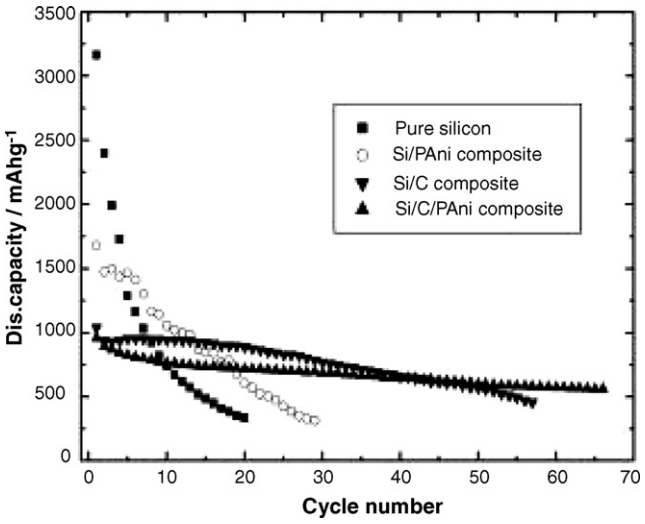

Fig. 13. §§Cycling of pure Si, Si/PAni, Si/C, and Si/C/PAni composite anodes [98].

cycle, an anode prepared from 2 pyrolysis reactions and one HEMM showed a reversible capacity of 1100 mAh g^{-1}. After 40 cycles, it showed a capacity retention ability of 69%. Compared to a pure Si anode, one prepared by two pyrolysis reactions and one intermediate HEMM showed very high coulombic efficiency, capacity retention ability and cycling stability because of the multiphase structure of the Si/C composite, which reduced mechanical stresses resulting from the Si volume change. To improve their capacity retention ability, pores in the composite were filled by conducting emeraldine-base polyaniline solution containing $LiClO_4$ (PAni/$LiClO_4$) [98]. This resulted in higher mechanical integrity, as shown by the decrease in charge transfer resistance in Fig. 12. When charged–discharged between 0.02 and 1.5 V, an Si/C/PAni anode showed a capacity retention of 63% with a reversible capacity of 560 mAh g^{-1} on the 67th cycle (Fig. 13), which was explained by its low porosity determined by SEM after 200 cycles, giving an improved capacity retention over that of Si/C, Si/PAni, and pure Si. As Fig. 14(a) shows, an Si/C composite after 200 cycles had many 3–5 μm diameter pores with surface cracks, perhaps due to the inability of pyrolyzed PVC to accommodate volume changes. As seen in Fig. 14(b), no such porosity or cracks were seen in Si/C/PAni anodes covered by the conducting PAni/$LiClO_4$ film. These results show the importance of microstructure in suppressing the large Si volume change on cycling. Although cycle life was significantly improved by coating of the polyaniline derivative on Si/C composites, pulverization of Si during extended cycling was still unpreventable. A further procedure of Zhang et al. [95] prepared Si/C composite anodes in which PVC was replaced by polyparaphenylene (PPP). As prepared these Si–PPP-based disordered carbon materials showed lower reversible capacity and capacity retention than those derived from Si–PVC.

Using polystyrene (PS) resin as a carbon precursor, Si/C composites were prepared by milling and pyrolysis [99]. In the first step, PS resin was milled with Si for 12 h and the powder obtained was again milled with PS resin for 12 or 24 h. The weight ratio of Si to C in the final powder was 1:2. The powder from the second milling was heated at 600, 800, or

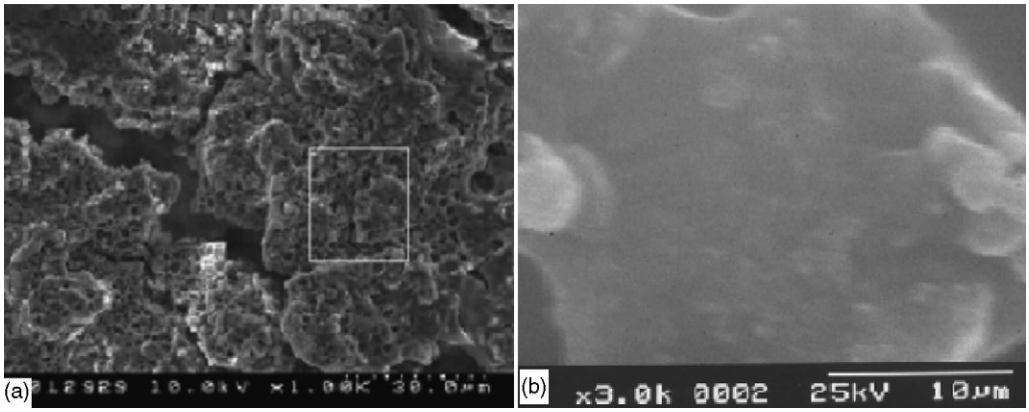

Fig. 14. Cross-sectional SEM image of (a) Si–PVC-based disordered C composite anode after 200 cycles; (b) PAni/$LiClO_4$ coated Si–PVC-based disordered C composite anode after 200 cycles [98].

1000 °C for 5 h. The capacity retention ability in the cycling voltage range 0.02–1.2 V of an anode with a 12 h second milling was found to increase with increase in heat-treatment temperature due to the formation of a high-density, hard carbon which relieved anode mechanical stress. Encapsulation of Si in this hard carbon resulted in only a small amount of inactive Si, which gave a slight decrease in reversible capacity with increasing heat-treatment temperature. TEM images showed that Si was uniformly distributed inside the carbon matrix. When the second milling time was increased to 24 h, reversible capacity decreased to 540 mAh g^{-1}, but capacity loss was only 0.67% per cycle. However, the reversible capacities of these anodes after 30 cycles were still too low to meet requirements.

Kim et al. [100] reported the electrochemical performance of two types of Si/C composite anodes designated as H-C and I-C. To prepare H-C, Si was milled for 3 h to produce nano-particles, which were milled with pitch, then mixed with graphite. The resulting powder was pyrolyzed at 900 °C for 1 h. For I-C samples, Si powder was milled with Cu powder before following the H-C procedure. The H-C anode contained 100–150 nm Si particles uniformly dispersed in a carbon matrix, while the I-C anode had 15 nm Si–Cu composite particles heterogeneously distributed in the matrix. XRD analysis showed that H-C sample contained nanocrystalline Si, whereas the I-C sample contained Cu_3Si phases. SEM, TEM, and energy loss electron spectrometry (EELS) showed that the H-C sample contained nano-Si tightly encapsulated in the carbon matrix, while in the I-C sample, micro-spaces were present between Si–Cu composite particles encapsulated in carbon matrix. When cycled between 0.0 and 1.5 V, both H-C and I-C samples showed an initial reversible capacity of 700 mAh g^{-1}. While both showed similar reversible capacities, capacity retention of an H-C anode was much lower than that of an I-C anode. After 15 cycles, the former had 50% capacity retention while the latter showed 90%. The better cycling stability of I-C anodes was attributed to the presence of micro-spaces which could accommodate the Si volume changes on cycling. The formation of Cu_3Si alloy also relieved some mechanical stress. The I-C anode still must be extensively cycle-tested to determine whether it can replace graphite.

Similarly, a Si/disordered carbon composite anode was prepared by mechanical milling followed by pyrolysing a mixture of nano-Si and PVA or sucrose carbon precursor [101]. XRD and Laser Raman Spectroscopy (LRS) showed that carbon present in the Si/C composite had an amorphous and disordered structure. When cycled between 1.2 and 0.02 V, Si-PVA and Si-sucrose anodes showed coulombic efficiencies of 80.3% and 67.1%, respectively. The low coulombic efficiency of the Si-sucrose anode was attributed to irreversible decomposition of electrolyte, which was evident from cyclic voltammetry. The Si-PVA anode showed better capacity retention (80%) with a reversible capacity of 754 mAh g^{-1} after 20 cycles. Its better capacity retention and high coulombic efficiency resulted from the uniform carbon dispersion from the PVA precursor, as seen by SEM analysis.

Following carbon deposition on Si, it was also used on materials prepared by reducing SiO [102]. SiO, Al, and Li_2O powders in 1:1:2 molar ratios were mechanically milled using HEMM. XRD analysis of milled powder showed evidence of nano-Si (15 nm) and Al_2O_3 peaks. Since aluminum oxide was present, the powder after milling was referred to as "Si-dispersed oxide." This was mixed with graphite in a 1:1 weight ratio, then milled with coal tar pitch and pyrolyzed at 900 °C for 1 h. When cycled between 0.0 and 1.2 V, an Si-dispersed oxide-graphite anode showed good capacity retention, with a stable reversible capacity of 600 mAh g^{-1} over 40 cycles. However, its irreversible capacity was close to 33%. Increased milling time increased its irreversible capacity. A carbon coating gave an increase in cyclability and a decrease in irreversible and reversible capacity. The irreversible capacity reduction was due to reduction in the specific surface area. As Fig. 15, shows, carbon-coated nano-Si-dispersed oxide/graphite had a stable reversible capacity of 525 mAh g^{-1} over 40 cycles. Capacity retention improvement was attributed to carbon coating on dispersed nano-Si-graphite particles, which improved electronic connection throughout.

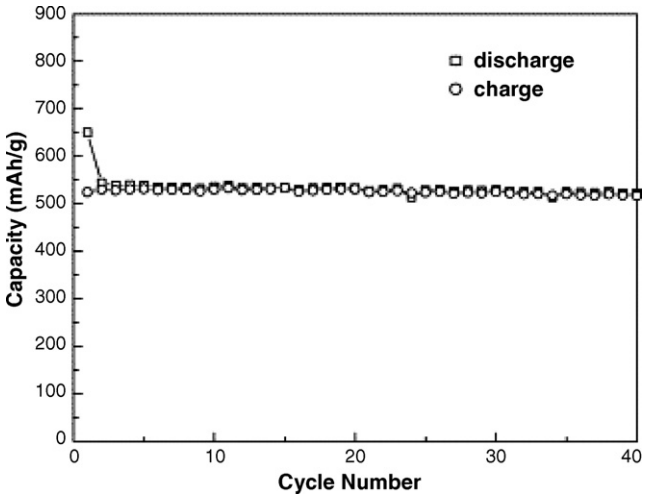

Fig. 15. §§Cycling performance of carbon-coated nano-Si-dispersed oxide/graphite composite anodes [102].

As with nano-Si dispersed oxide anodes, nano-silicon clustered –SiO_x–C composite anodes were prepared by the following procedure [103]. SiO and graphite powders were ball-milled for 18 h and the resulting powder was mixed with furfuryl alcohol, ethanol, and water. The resulting slurry was mixed with hydrochloric acid for polymerization, which was followed by heat treatment at different temperatures (850, 1000, and 1100 °C) for carbonization. During the heat treatment, SiO was believed to decompose into Si and SiO_2 phases. XRD, SEM, and TEM analysis showed that all final composites contained 5–10 nm Si particles uniformly dispersed in SiO_x particles, which were in turn dispersed in carbon matrix. However, the 1100 °C preparation showed evidence of SiC formation. Although excellent cycling stability was observed for all the three electrodes, a higher initial reversible capacity and capacity retention were seen in the anode prepared at 1000 °C (Fig. 16). When galvanostatically charged–discharged between 0.01 and 1.5 V, the 1000 °C anode showed an initial reversible capacity of 700 mAh g^{-1} and a reversible capacity close to 620 mAh g^{-1} in the 200th cycle (Fig. 16). This is the longest cycling stability

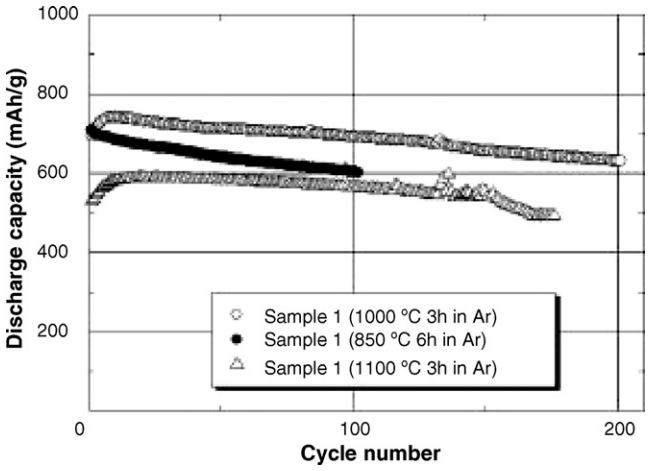

Fig. 16. Cycling performance of nano Si cluster–SiO_x–C composite anodes prepared at different temperatures [103].

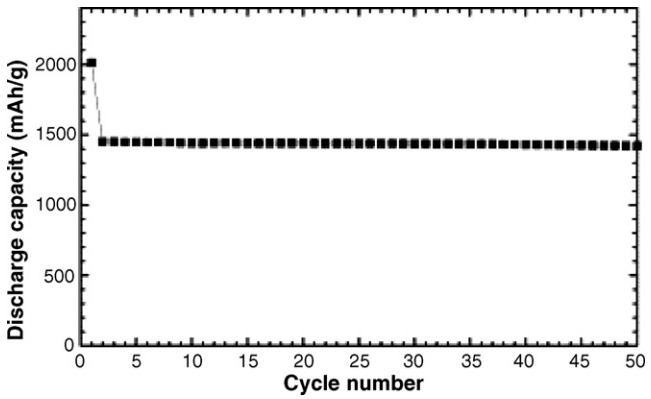

Fig. 17. §§Cycle life for Si/C composite anode prepared from carbon aerogel [104].

over time so far reported for powder-based Si anodes. The good cycle performance was attributed to the structural stability of the electrode, resulting from retention of nano-Si in SiO_x by stable Si–O bonds, along with carbon deposition. However, a large irreversible capacity was seen in the first cycle, which must be eliminated for use in practical Li-ion cells. This high irreversible capacity was due to the alloying of Li with the SiO_x phase, giving lithium silicate phases such as Li_2SiO_3 and Li_4SiO_4. Despite its high irreversible capacity, the improved cycling stability of this material seems to be promising for future applications if its irreversible capacity can be controlled.

The electrochemical performance the Si/C composite anodes discussed in this Subsection shows that both milling and pyrolysis during preparation improve capacity retention and cycle life. However, the cycle life reported for these anodes is still insufficient.

4.2.4. Si/C composite anodes prepared from chemical reaction of gels

Apart from by ball milling and pyrolysis, carbon has been deposited on Si particles using carbon gels. One was a carbon aerogel prepared from resorcinol and formaldehyde [104,105]. Its preparation was by mixing measured amounts of resorcinol and formaldehyde and heating to 85 °C [104]. When the resulting mixture became viscous, nanocrystalline Si was added. This was heated at 85 °C for 10 h to form a carbon aerogel, which was sintered at 650 °C to form Si/C composites. During initial heating at 85 °C, resorcinol reacted with formaldehyde to form hydroxymethyl resorcinol derivatives, which further reacted with formaldehyde to form a cross-linked three-dimensional network called RF gel. After heat treatment at 650 °C, this formed an amorphous carbon. XRD results on Si/C composites prepared by this process showed peaks related to Si and amorphous carbon, and TEM images showed that Si was uniformly dispersed in the latter. When cycled between 0.02 and 2.0 V, these anodes showed a reversible capacity of 1450 mAh g^{-1} and an irreversible capacity of 550 mAh g^{-1}, shown in Fig. 17. During further cycling, they showed high cycling stability with a reversible capacity of 1400 mAh g^{-1} after 50 cycles. Their excellent cycling performance was due to the nano-sized Si and its dispersion in a three-dimensional carbon network.

Si/C composite anodes were similarly prepared by adding Si to an aqueous phase during the inverse emulsion polymerization reaction of resorcinol and formaldehyde, followed by drying and carbonization under an inert atmosphere [105]. The nature of the final composite depended on the method of drying. With freeze-drying, carbon cryogel microspheres (CCM-Si) resulted, while hot air gave carbon xerogel microspheres (CXM-Si). SEM images of CCM-Si and CXM-Si anodes showed encapsulation of Si in carbon gel spheres. When the Si/resorcinol ratio was 1, CCM-Si and CXM-Si anodes showed reversible and irreversible capacities of 787 and 402 and 763 and 442 mAh g^{-1}, respectively. Their large irreversible capacities were due to the presence of large amounts of oxygen. While their initial properties were similar, a large capacity decrease occurred for CXM-Si during initial cycling, while CCM-Si showed a slower decrease, giving a reversible capacity of 600 mAh g^{-1} after six cycles. The better cycling performance of the latter was attributed to the larger mesopore volumes of the carbon cryogels, which acted as a buffering matrix, so that the shrinkage volume of CCM was smaller than that of CXM. When the carbonization temperature was increased to 1523 K, the irreversible capacity was reduced to small values, however a decrease in reversible capacity was simultaneously observed due to SiC formation, confirmed by XRD. When a higher Si/resorcinol ratio was used, reversible capacities increased to 1000 mAh g^{-1}. However, increase in Si content resulted in more capacity degradation. The difference in cycling performance of Si/C composite anodes prepared from carbon aerogels by these methods [104,105] shows the influence of preparation procedure and conditions on electrochemical performance.

Si/C composite anodes have also been prepared by dispersing Si in a sol–gel graphite (SGG) matrix [106]. The SGG was prepared from KS-6 graphite and methyltrimethoxysilane (MTMOS) by gelling at room temperature [107]. The SGG powder obtained from the sol–gel had an open three-dimensional ceramic network with percolating graphite particles. The SGG

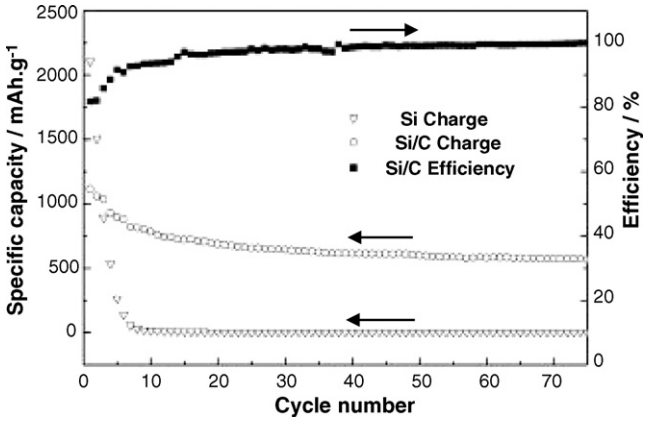

Fig. 18. §§Cycling performance of pure Si anodes and Si/C composite anodes prepared at room temperature [108].

matrix powder obtained was milled with differing amounts of Si (4.6–38.6 wt%) to form Si/C composite anodes. SEM images of the various composites showed a uniform distribution of Si in the SGG matrix.

4.2.5. Si/C composites prepared by other methods

Other than those prepared by ball milling, all of the above Si/C composite anodes were prepared between 600 and 900 °C. To protect Si from oxidizing at such temperatures, the process must be carried out in vacuum or in the presence of inert gases, which may increase cost. To reduce cost, Si/C composite anodes were prepared at room temperature by Yang et al. [108] by dehydration of a carbon precursor. Initially Si and sucrose were ultrasonically agitated under infrared light to form a syrup, which was dehydrated at room temperature by H_2SO_4 for 2 h, giving a Si/C composite consisting of amorphous carbon and nano-crystalline Si (<30 nm). Anodes prepared from this showed an initial discharge capacity of 1115 mAh g^{-1} and a coulombic efficiency of 82% when galvanostatically cycled between 0.02 and 1.5 V. After 75 cycles, they showed a reversible capacity of 560 mAh g^{-1} (Fig. 18). Their improved cycling compared to that of pure Si was attributed to the presence of amorphous carbon, which not only prevented the agglomeration of Si particles, but also reduced the cycling volume changes. Addition of graphite into the Si/C composite further increased cycling stability, and also resulted in a better rate capability [109]. However, the number of charge–discharge cycles tested for this anode was limited to 50.

5. Si anodes prepared by using different binders

For powder-based Si anodes, the type of binder and its overall content also have a major impact on cycle life. Generally, the binder must keep the particles together in powder-based anodes and make them adhere to the current collector. Most of the Si anodes discussed in this review were prepared by using polyvinylidenefluoride binder. PVDF is thermoplastic and does not exhibit much elongation, so it may not be able to sustain the large Si volume expansion on Li insertion. To attempt to overcome this, different anode binders have been examined. In this Section, the electrochemical performance of Si anodes prepared with different binders are discussed and are compared with the performance of those using PVDF.

Wang et al. [110,111] prepared Si/C composite anodes using polyethylene oxide with lithium perchlorate (PEO–$LiClO_4$) and cross-linked polyethylene glycol with lithium perchlorate (PEG–$LiClO_4$) as binders. Si/C composite anodes were prepared by mixing nano-Si with Timcal KS-15 graphite, $(Li_2S)_4(P_2S_5)$ powder (a fast Li^+-ion conductor), and one of the above binders in solution. The PEO–$LiClO_4$ binder solution was prepared by dissolving polyethylene oxide and $LiClO_4$ in 8.5:1.5 wt% ratio in acetonitrile. A cross-linked PEG–$LiClO_4$ solution was prepared by measuring 6 ml of polyethylene glycol (PEG, MW 600) containing 15 wt% $LiClO_4$ in a burette which was added to 4 ml of 1,3-bis(isocyanatomethyl)cyclohexane cross-linking agent. The solution was kept at 60 °C for 1.0 h for pre-polymerization. Ten milliliters of dimethylformamide (DMF) solvent was added, which was followed by heating to 60 °C for 2.0 h. After this, 0.5 ml of ethylene glycol, 10 drops of tin(II) 2-ethylhexanoate catalyst and 10 ml of DMF were added. The resulting solution was heated for 1.0 h for polymerization reaction to take place. The reason for adding $LiClO_4$ to both binders was to improve their ionic conductivity. Compared to films made from PEO–$LiClO_4$, the film made from cross-linked PEG–$LiClO_4$ showed high elasticity and mechanical strength. Both acetonitrile slurries were coated onto a Cu foil and dried to form anodes.

When charged–discharged between 0.0 and 1.5 V, anodes containing cross-linked PEG and PVDF binders had better performance than anodes containing PEO–$LiClO_4$. The higher capacity and capacity retention of the latter shows the effect of cross-linking in improving mechanical strength. Although the anode with cross-linked PEG–$LiClO_4$ binder showed a higher initial reversible capacity than that with PVDF, its capacity faded in subsequent cycling and by the 11th cycle both had the same capacity. Hence, anodes with PVDF binder appear to have better cycling performance than those with cross-linked PEG–$LiClO_4$.

Oppanol B200 (BASF), a rubber-like polyisobutene with high elasticity, was investigated as a binder for Si/C composite anodes by Holzapfel et al. [74]. Chemically vapor-deposited Si on particulate graphite (90 wt%) was mixed with 10 wt% Oppanol in a 5 wt% petroleum ether solution to give a slurry which was pasted onto Cu foil. The reversible capacity and capacity fade of this anode were similar to that made with PVDF binder, but its irreversible capacity was slightly higher. Similarly ethylene propylene diene monomer (EPDM) was used as binder for Cr-doped Si/CNT composite anodes by Ishihara et al. [87]. Although the initial reversible capacities of this anode were the same as that of anode made with PVDF binder, its cycling showed more fade. After 10 cycles, the PVDF and EPDM anodes had reversible capacities of 1250 mAh g^{-1} and less than 500 mAh g^{-1}, respectively. Efforts were then made to improve the mechanical strength of the PVDF binder by cross-linking [112]. This was performed by adding triethylenetetramine (TETA) to a mixture containing poly(vinylidene

fluoride–tetrafluoroethylene–propylene) P(VDF–TFE–P) and Super-S carbon black. As a surface coupling agent or adhesion promoter, 3-aminopropyltriethoxysilane was added to the resulting solution. To determine the effect of cross-linking PVDF on cycling performance, a-$Si_{0.64}Sn_{0.36}$ anodes were prepared using cross-linked PVDF and PVDF as binders and were galvanostatically cycled between 1.0 and 0.22 V [113,114]. With non-cross-linked PVDF binder, an a-$Si_{0.64}Sn_{0.36}$ anode showed 60% of initial reversible capacity (810 mAh g^{-1}) after 30 cycles. When P(VDF–TFE–P) was used, a stable reversible capacity of 800 mAh g^{-1} was obtained over 40 cycles. This was attributed to the improvement in mechanical properties of the binder for the following reasons: (1) the amine groups in the adhesion promoter would react with acidic functional groups on the surface of the solids, while its end groups would react with unsaturated carbon–carbon double bonds in the P(VDF-TFE-P) backbone at room temperature, binding this polymer to the solids; (2) the TETA used in anode preparation would suppress visco-elastic flow of the polymer chains; (3) addition of carbon black to the binder would provide electronic contact between active material particles and the current collector.

With these additives, the P(VDF–TFE–P) binder was found to have an elongation of 150%. Because of its high elasticity, it was able to contain the large volume change in the a-$Si_{0.64}Sn_{0.36}$ active material under the cycling conditions used. However, when cycled between 1.0 and a cut-off of 0.06 V rather than 0.22 V, these anodes showed an 80% capacity decrease within 20 cycles. These results show the inability of cross-linked PVDF binder to completely suppress larger volume changes in a-$Si_{0.64}Sn_{0.36}$ anodes.

An electronically-conducting polypyrrole (PPY) has also been used to enhance the conductivity of Si anodes [21]. Initially, a polypyrrole film obtained by deposition followed by drying was milled with nano-Si powder. The resulting powder was mixed with PVDF to produce anodes. SEM showed dense agglomerates (0.3–3.0 μm) of Si particles connected by polypyrrole. The capacity retention of this anode was better than one with PVDF, but was insufficient for continued cycling. While increasing ball-milling time from 4 to 8 h gave no improvement, increasing PPY content resulted in better cycling. An Si/PPY anode with a 1:1 weight ratio of Si to PPY showed a stable reversible capacity close to 1000 mAh g^{-1} for 10 cycles. The improved performance of such anodes was attributed to the buffering action of the conductive PPY matrix, together with its binding ability, which allowed better interparticle contact during cycling. This was confirmed by AC impedance measurements on Si and Si/PPY anodes before and after cycling. The cycle life of Si/PPY anodes requires further testing to see if they might meet commercial requirements. Similar results were reported for anodes derived from PPY-coated Si particles prepared by *in-situ* polymerization [115].

In addition to the above polymers, high-elasticity materials such as styrene butadiene rubber (SBR) have been examined as Si anode binders. Since solid SBR is insoluble in common solvents, a mixture of its aqueous emulsion and sodium carboxymethylcellulose (SCMC) was examined [116]. When

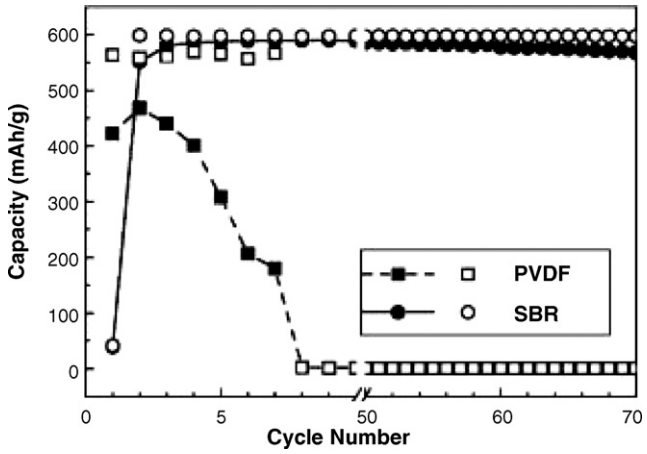

Fig. 19. Charge–discharge capacities of Si anodes with PVDF and SBR binders as a function of cycle number (open symbols: charge; solid symbols: discharge) [116].

cycled with a capacity limitation of 600 mAh g^{-1}, an Si anode containing SBR–SCMC binder showed a high capacity retention over 70 cycles. Its cycling performance was much better than that of a PVDF anode (Fig. 19). When Li insertion was limited to 600 mAh g^{-1}, an Si-SBR anode took several cycles to reach the designated capacity, after which it maintained 95% of the original value over 70 cycles. With PVDF binder, the capacity never reached the designated value and severe capacity fade was observed over the first 10 cycles. Improvement in electrochemical performance was attributed to the better mechanical and electrical properties of elastomeric SBR binder compared to those of PVDF. SBR has a higher elongation-to-breakage and a smaller modulus than PVDF, allowing anodes to freely expand and contract, relieving the forces exerted between particles. It also has a higher adhesive strength, so its sticks well to the active particles and current collector. It also has a swelling ratio of 1%, which is very low compared to the PVDF value of 60%. If the swelling ratio is high, electrolyte can easily penetrate between the particles, resulting in lack of electronic contact. Although Si-SBR anodes showed better capacity retention than Si-PVDF, a decrease in capacity was still observed after 20 cycles when the Li insertion capacity was increased to 800 mAh g^{-1}.

6. Si thin films

Because of the improved initial reversible capacity and better capacity retention of nano-Si compared to the bulk material, thin film silicon anodes with nano-Si particles may have longer cycle life. Normal anodes contain up to 10–20 wt% of inactive binders and conductive additives, while silicon thin film anodes contain no inactive materials, giving increased specific capacity. Generally, thin film Si anodes can be classified into nano-crystalline thin film anodes and amorphous (a-) thin film anodes. Amorphous materials in general do not exhibit any of the long-range atomic order which is characteristic of crystalline material. This Section discusses the electrochemical performance of pure Si, and binary and ternary Si alloy thin film anodes and their applications in thin film secondary cells.

6.1. Pure Si thin film anodes

6.1.1. Mechanism of Li insertion and extraction in Si thin films

Improving the cycling stability of Si thin-film anodes requires a fundamental understanding of their Li insertion/extraction mechanism. Structural and morphological changes in silicon anodes during charge–discharge cycling have been determined and analyzed by XRD, SEM, high-resolution transmission electron microscopy (HRTEM), and Raman spectroscopy [117–121]. During Li insertion, it was shown that the crystal structure of nano-Si was destroyed and at its end at 0.0 V the anode was converted into an amorphous metastable structure without formation of any intermediate phase [117]. During extraction of Li^+, recrystallization took place. However, at the end of extraction, anodes were found to have both amorphous and crystalline regions, with internal trapping of Li^+ ion. In both charged and discharged states, agglomerates of nano-Si particles were found. Because of the large volume expansion during charge, neighboring Si particles contact each other, resulting in the formation of agglomerates. The size of these agglomerates was very large compared with the particle size of the parent Si. This size increase resulted in poor Li insertion/extraction kinetics, resulting in further capacity fade and short cycle life. To obtain improved cycle life, it is therefore essential to prevent the formation of such agglomerates.

How amorphous alloys may be formed by diffusive reactions in multilayer films may be explained by solid state amorphization theory, which has been used to explain the formation of metastable amorphous Li–Si during insertion [118,119]. XRD studies were performed on Si thin film anodes before and after galvanostatic cycling at various Li insertion levels. A Si anode was electrochemically lithiated so that it contained 74 mol% Li. According to the binary phase diagram, three crystalline Li–Si phases should form during insertion to this composition. However, the XRD pattern showed no peaks corresponding to crystalline phases other than Si itself: only a few broad peaks not matching any of the three crystalline phases were present. High resolution TEM showed that crystalline Si co-existed with one unknown amorphous phase. From this, it was concluded that electrochemical Li insertion results in the formation of an amorphous Li–Si phase without first forming any of the three crystalline phases in the phase diagram. This was explained by constructing a Gibbs phase diagram for pure Li and Si species, four Li–Si phases, and the amorphous Li–Si phase apparently formed. The Gibbs free energy of the amorphous Li–Si alloy was calculated from the Nernst equation. The four Li–Si crystalline phases have a lower Gibbs free energy than Li and Si. Since crystallization cannot take place at room temperature, reduction of the Gibbs free energy to achieve thermodynamic equilibrium must be via some other process. This suggests that a metastable amorphous Li–Si phase with a lower Gibbs energy than that of pure Li, Si, and the other stable crystalline alloy phases is formed by diffusion.

The structural change from crystalline Si to amorphous Si during insertion was also confirmed by Obrovac and Christensen [120] and Hatchard and Dahn [121] by conducting *ex-situ* XRD studies on electrodes in various insertion/extraction states. During initial Li insertion, crystalline Si was converted into an amorphous lithiated Si phase leading to the formation of a two-phase region, which was present until the potential reached 0.050 V. At lower potentials, a new crystalline compound was formed with the structure $Li_{15}Si_4$. However, the formation of $Li_{22}Si_5$ expected from the binary phase diagram was not observed. As a result, the Si anode showed a charge capacity of 3400 mAh g^{-1}, close to the theoretical capacity of $Li_{15}Si_4$ (3579 mAh g^{-1}). During extraction, crystalline $Li_{15}Si_4$ was converted to amorphous lithiated Si, leading to the formation of a two-phase region. During the second Li insertion cycle, amorphous Si was converted to amorphous lithiated Si, and below 0.050 V it was converted to the crystalline $Li_{15}Si_4$ phase, resulting in two-phase formation. Similar results were reported for amorphous Si anodes. From galvanostatic cycling of both crystalline and amorphous Si anodes, it was concluded that limiting the Li insertion voltage to above 0.030–0.050 V improved cycling performance, since it avoided the formation of two-phase regions. Such two-phase regions are usually associated with high internal stresses, which lead to pulverization of active material, loss of electronic contact and severe capacity fade. In the published US patent application literature, Konishiike et al. [122] have reported that cycling stability of Si thin film anodes can be improved by depositing a Li layer on Si films by vacuum deposition. When the amount of Li deposited on the Si film was limited to 0.5–40% of the theoretical Li insertion amount, a capacity retention between 88% and 97% (after 50 cycles) was obtained. When the Si film alone was used as the anode, 71% capacity retention was achieved, which may show the cycle life influence of alloying Li prior to charging. This is mainly due to the formation of amorphous Li–Si compounds, which may eliminate the formation of two-phase regions. When small amounts of residual Li were present in the anode after discharge, an improvement in cycling stability was observed, which may explain the effect of two-phase regions on the cycle life of Si anodes.

The stress changes inside an a-Si thin film anode during Li insertion and extraction were measured by Lee et al., using an optical cantilever method [123]. Fig. 20 shows the voltage profile of an a-Si anode during the first cycle. The right voltage scale indicates stress, for which negative values are compressive. From Fig. 20, stress was found to vary with Li insertion voltage as follows: During the decreasing potential range 1.5–0.3 V, compressive stress was found to increase rapidly with a steep slope, which was attributed to the formation of Li_2Si phase near the surface. When the potential decreased from 0.3 to 0.1 V, compressive stress was found to increase with reduced slope. This was attributed to the formation of Li_2Si phase over the entire electrode. When the potential further decreased to 0.0 V, reduction in compressive stress was observed. This was attributed to micro-cracks resulting from formation of $Li_{4.4}Si$ alloy, which has a volume four times larger than that of the parent Si. Because of these micro-cracks, stresses were relieved, which resulted in reduction of compressive stress. During the discharge process, the compressive stress was observed to further decrease. These results again confirm that stress resulting from large volume

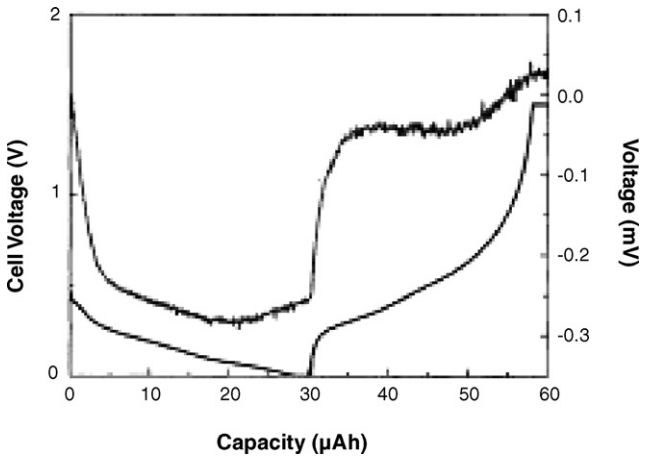

Fig. 20. (Top curve) Stress variation (compressives stress negative, right axis) in amorphous (a-Si) 35 nm thick film prepared by rf magnetron sputtering in the potential range 0.0–1.5 V (*V*–capacity curve below and left axis) [123].

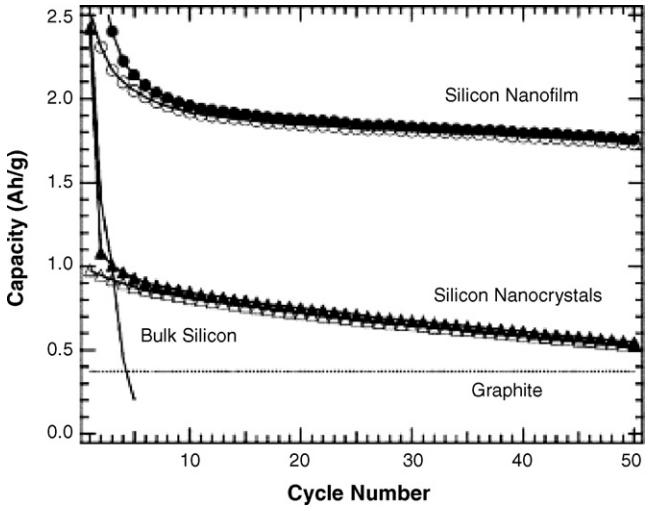

Fig. 21. Specific capacity vs. cycle number for nano-crystalline Si and nano-amorphous Si thin film anodes prepared by thermal vapor deposition. Specific capacity of graphite and bulk-silicon anodes also shown [126].

changes are the reason for the low cycle life of Si anodes. These stresses must be accommodated to obtain improved cycle life.

6.1.2. Methods for improving the cycling stability of Si thin-film anodes

6.1.2.1. Decreasing thickness using nano-crystalline or amorphous Si film. Cyclic voltammetry and galvanostatic cycling [121] have shown that film thickness also has an influence on the formation of the crystalline $Li_{15}Si_4$ phase. Films with a thickness lower than 2.5 μm did not crystallize upon lithiation, and films with a greater thickness always show crystalline phase formation. In addition, thickness also influences anode rate capability. Increasing film thickness gives an increase in charge transfer resistance, leading to lower rate capability [124]. These results stress the importance of film thickness on cycle life of a-Si anodes. Ohara et al. [125] investigated the influence of deposition rate on cycling performance of amorphous Si anodes (77 nm). a-Si thin film anodes were prepared on Ni foil by vacuum deposition. When the deposition rate was very fast, the film formed was not homogeneous, which resulted in poor cycle life. When the deposition rate was very slow, Li insertion did not occur at high currents. A film with an appropriate deposition rate was found to have a reversible capacity of 1500 mAh g^{-1} which was stable for 700 cycles in both ethylene carbonate (EC) and propylene carbonate solvents.

Graetz et al. [126] investigated nano-crystalline Si thin film anodes prepared by physical vapor deposition. The films were found to contain 12 nm diameter Si particles. When cycled between 0.0 and 1.5 V at the *C*/4 rate, they showed an initial charge capacity of 2400 mAh g^{-1} and a discharge capacity of 1000 mAh g^{-1}. During further cycling, a capacity fade of 20 mAh g^{-1} per cycle was observed, which resulted in a reversible capacity of 525 mAh g^{-1} after 50 cycles. This performance is much better than that of as bulk Si anode, as shown in Fig. 21. This was attributed to lack of dislocations in nanocrystals [126]. It was believed that for brittle materials such as Si, particle break-up takes place through the formation and propagation of cracks by dislocation emission from the crack tip. Due to the lack of dislocations, the material was strained uniformly, which alleviated the stresses inside the anode film. If this is the only reason for improved performance, similar results should be obtained for nano-crystalline Si powder anodes. However, the cycle life of such anodes is much lower than that of thin film anodes [22], which suggests that there might be some other reason for their improved performance. Deposition processes normally give good adhesion between deposited particles and the substrate current collector, which maintains contact during volume changes, thereby increasing capacity retention ability and cycle life. Though better cycling performance was obtained with nano-crystalline thin film anodes, their capacity retention after 50 cycles was 52%, which is insufficient to meet practical requirements.

As with nano-crystalline Si thin films, a-Si thin films have been deposited on nickel foil by physical vapor evaporation [126] and vacuum evaporation [125]. As shown in Fig. 21, a 100 nm thick a-Si anode deposited on Ni had an initial reversible capacity of 2500 mAh g^{-1} and a stable reversible capacity of 2000 mAh g^{-1} after 50 cycles. The amorphous thin film exhibited a mean capacity loss of only 8 mAh g^{-1} per cycle, much less than that of a nanocrystalline Si anode (Fig. 21).

6.1.2.2. Limitation of state of charge (SOC) and discharge (SOD) of thin-film Si anodes using capacity or voltage control. One way to decrease stress, pulverization, and disintegration of thin-film Si anodes is by limiting Li insertion by controlling SOC and SOD. Jung et al. [127] measured the cycle life of 50 nm a-Si thin film anodes at 0.25 mAh cm^{-2} with Li insertion for 10 min. With this limitation, a stable reversible capacity of 3000 mAh g^{-1} was obtained to 80 cycles. Fig. 22 shows the effect of capacity limitation on the cycle life of 50 nm a-Si thin film anodes prepared by low pressure chemical vapor deposition (LPCVD) [128]. At a designated charge capacity of 4200 mAh g^{-1}, a cycle life of 40 cycles was attained, whereas 430 mAh g^{-1} gave 1500 cycles (Fig. 22). This again suggests the strong influence of cycling voltage or capacity on cycle life,

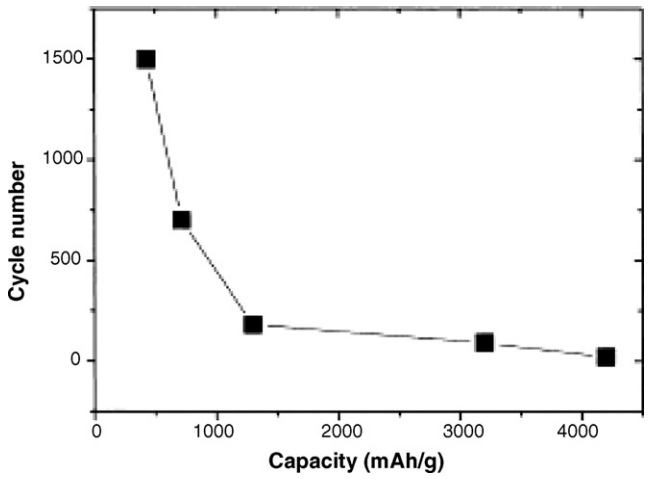

Fig. 22. Cycle life of 0.5 μm a-Si thin film anode as a function of designated charge capacity under capacity limitation conditions [128].

since limited insertion of Li into Si greatly reduces anode volume change. However, limiting the Si anode potential in practical Li-ion cells is not feasible.

In addition to Ni substrates, the performance of Cu with 250 nm a-Si thin films deposited by radio-frequency magnetron sputtering was also investigated [129,130]. Cycled between 0.02 and 1.2 V at the *C*/2.5 rate, these anodes showed an initial charge capacity of 4100 mAh g^{-1}, very close to the theoretical capacity of Si. During the next discharge, 3800 mAh g^{-1} was obtained, which was stable for 29 cycles [129]. However, after the 29th cycle severe capacity fade occurred, giving a reversible capacity of 1800 mAh g^{-1} in the 40th cycle [130]. SEM images of 250 nm Si films after the first cycle (Fig. 23(a)) showed that the entire anode surface was cracked and separated into islands. During 30 charge–discharge cycles, the gaps between these islands widened, as may be seen in Fig. 23(b). The greater capacity retention shown by 250 nm Si films up to the 29th cycle was attributed to its structural stability. It was believed that during cycling, the underlying part of the active material was strongly bonded to the current collector, while the outer surface participated in the alloying/de-alloying process [129]. SEM, TEM, *in-situ* atomic force microscope (AFM) analysis, and differential capacity plots showed that rapid capacity fade of 250 nm Si films after 30 cycles resulted from incremental plastic strain (strain ratcheting) in the Cu substrate during charge–discharge. This plastic strain and interfacial impurity formation resulted in reduction of adhesive strength [130].

6.1.2.3. Increasing Si thin film electronic conductivity by using n-type, p-type, and pure intrinsic amorphous Si. The influence of electronic conductivity on cycling performance of amorphous Si anodes has been studied [131,132] by cycling n-type, p-type, and pure intrinsic amorphous Si anodes with different film thicknesses. N-type materials had high columbic efficiency, high specific capacities, and longer cycle life. Among those tested, a 150 nm thick n-type a-Si anode showed a stable reversible capacity of 2200 mAh g^{-1} for 200 cycles at the 1*C* rate, indicating an excellent cycle life, which was attributed to its high electronic conductivity and thinness. When thickness was reduced to 50 nm, n-type Si anodes showed a stable reversible capacity of 3600 mAh g^{-1} for 200 cycles, which is shown in Fig. 24(a). At the 12*C* rate, this anode had a reversible capacity of over 3000 mAh g^{-1}, which was stable for 1000 cycles (Fig. 24(b)) [133]. Cycled at 30 C, a reversible capacity over 2000 mAh g^{-1} was obtained, which was stable for 3000 cycles (Fig. 24(c)). These results show the superior rate capability of these anodes. The impact of film thickness and electronic conductivity on their specific capacity, rate capability, and cycle life is also evident.

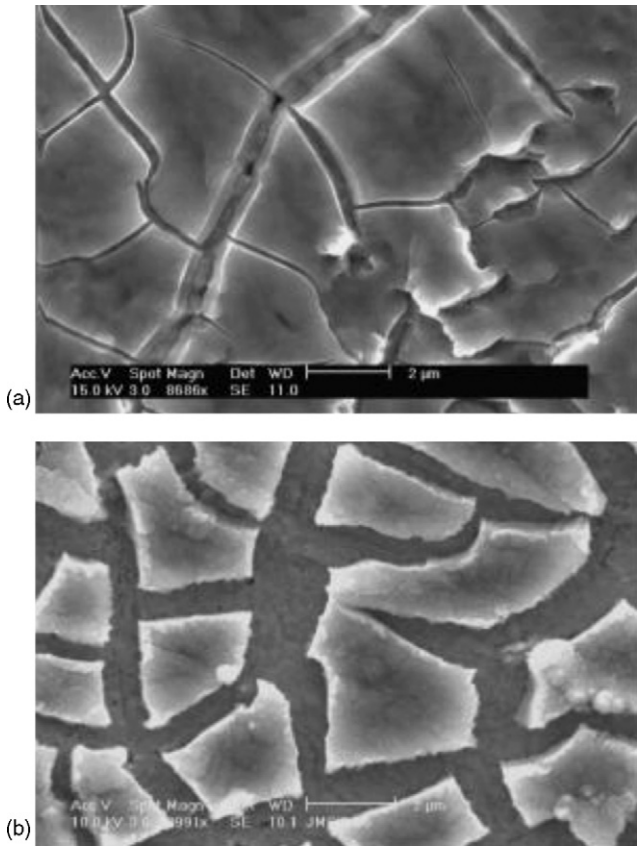

Fig. 23. SEM morphology of 250 nm a-Si film on Cu cycled at *C*/2.5 for (a) 1 cycle, and (b) 30 cycles [130].

6.1.2.4. Improving adhesion between the current-collector substrate and the thin active film. Although 50 nm a-Si thin film anodes [132,133] have shown excellent electrochemical performance, their very low active material content reduces the volumetric capacities of cells using them. Improving their volumetric capacities requires an increase in anode thickness. However, from the results discussed above, it is evident that increase in thickness results in severe capacity fade. To attempt to overcome this, the current-collecting surface of the substrate on which Si was deposited was roughened [134,135] by different methods such as sanding [134,135], etching in aqueous $FeCl_3$ solution [135], and by electrolytic deposition of Cu [135]. The last two were found to be more effective than the first. An a-Si 1.0 μm thick film deposited on a Ni substrate roughened by etching had a reversible capacity of over 1500 mAh g^{-1}, which was stable for 200 cycles. An electrolytically-deposited 3.6 μm

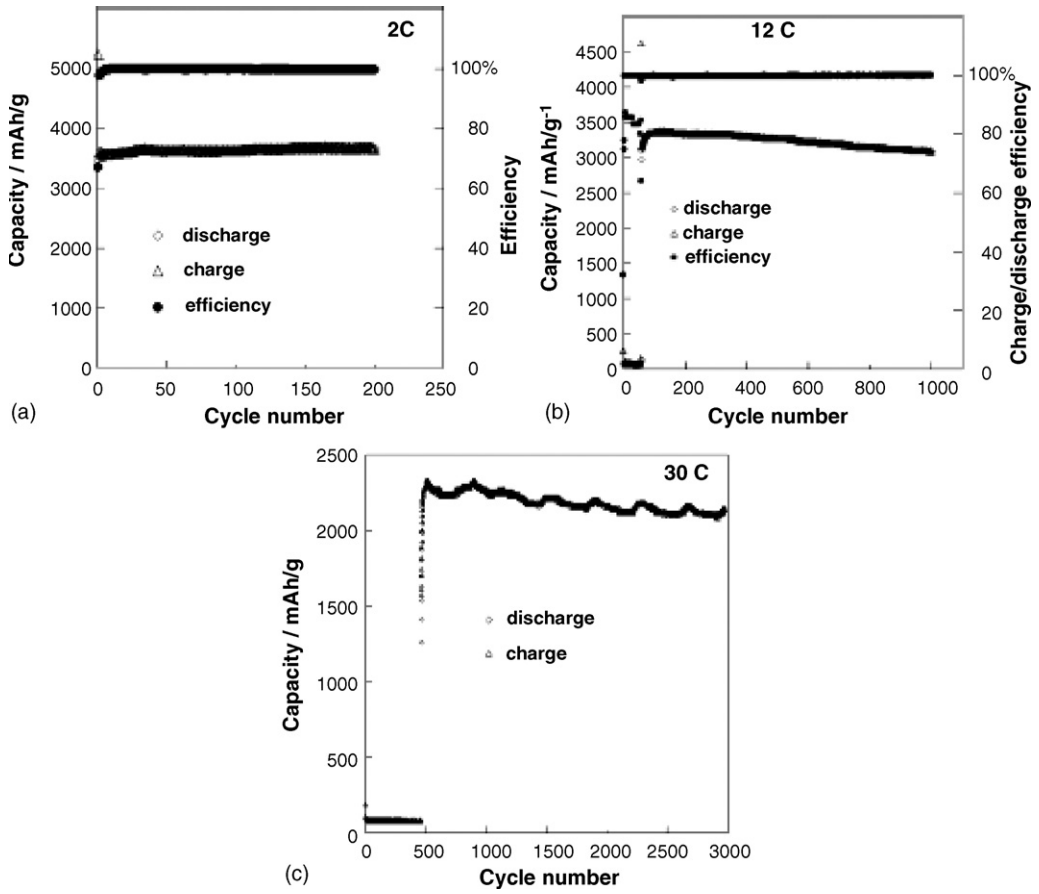

Fig. 24. Capacity retention and efficiency of 50 nm a-Si thin film anode during galvanostatic charge/discharge at: (a) 2*C*; (b) 12*C*; (c) 30*C* rates (for 30*C*, efficiency not shown) [133].

a-Si thin film deposited on a modified Cu substrate showed a stable reversible capacity of 2000 mAh g^{-1} for 50 cycles. The improved performance of such thicker a-Si film anodes resulted from the roughened Ni and Cu substrate surfaces, which gave better adhesion [135]. These results show that the surface properties of the current collector may have a strong influence on cycle life. The electrochemical performance of the various a-Si thin film anodes discussed show that by maintaining appropriate microstructure, deposition rate, thickness and substrate surfaces, reasonably high specific capacities, and cycle life can be obtained. It was previously thought that voids in the substrate may be helpful in accommodating the Si volume change, so a-Si thin films deposited on porous nickel substrates by chemical vapor deposition were tested [136]. This amorphous Si deposited on porous nickel showed a lower initial reversible capacity (1000 mAh g^{-1}) and poor cycle life.

6.1.2.5. Si films with structures tolerating the large volume changes on lithium alloying/dealloying. Porous Si (PS) anodes with one-dimensional channels [137], and Si pillar arrays [138] were investigated because they may tolerate the Si volume change on cycling. Porous Si anodes were prepared by electrochemical etching of Si substrates with acetonitrile solution [137]. As prepared PS was found to have interconnected Si pores perpendicular to the PS surface, with 1–1.5 μm diameter surface pores. When galvanostatically cycled between 2.0 and 0.1 V, their specific capacities were found to increase with increase in channel depth. On continuous cycling, PS anodes had reasonable cycling stability, and showed an unchanging porous structure explaining its cycling stability.

Pillar array anodes were fabricated by the "island lithography" method [138], also described in the US patent literature [139]. Si pillars used for testing were 580 nm diameter and 810 nm height. In spite of their reasonable capacity retention, they showed a low faradaic efficiency through 50 cycles, which would limit their practical use.

6.2. Binary Si alloy thin films

In this Subsection, the electrochemical performances of various Si binary alloy thin films prepared by different deposition processes are discussed. The elements and compounds used are lithium active materials such as Sn, Ag, Zn, Mg, V, and O, and lithium-inert materials such as Cr, Fe Mn, Ni, Co, Zr, and TiN.

6.2.1. Si–Sn alloy

The large specific capacities of Si and Sn, and Si–Sn alloys have made them attractive as thin film anodes. Ahn et al. [140] prepared $Si_{1-x}Sn_x$ nano-composite electrodes by depositing 230–244 nm thick Si–Sn films with an atomic Sn

content of 0.24–0.67 onto Cu foils. Cycled between 0.1 and 2.0 V, they had initial reversible capacities between 707 and 870 $\mu Ah\,cm^{-2}\,\mu m^{-1}$ depending on their composition. The low reversible capacity was due to the small operating voltage window used.

In contrast to these results, high reversible capacities were obtained for films with atomic Sn content between 0 and 0.45 prepared by magnetron sputtering by Hatchard and Dahn [141]. Film preparation used a combinatorial approach, in which 64 different compositions could be prepared simultaneously. Details of such work can be found elsewhere [142,143]. The thin $Si_{1-x}Sn_x$ deposits were amorphous throughout the selected composition range. At 10 cycles, stable capacities of 3500 and 2000 mAh g^{-1} were obtained for electrodes with the highest Si and Sn contents, respectively. Irreversible capacities of the 64 samples were between 15% and 30%. Low capacity fade rates of 1% per cycle and reasonable reversible capacities were obtained at a composition near $x = 0.3$. However, when the Sn content was above 0.4, their amorphous character disappeared and severe capacity fade was observed.

To understand why amorphous $Si_{1-x}Sn_x$ alloys cycled better than crystalline material, both *in-situ* AFM [144,145] and optical microscopy studies [144] were performed on 1 μm thick Si–Sn films deposited on stainless steel substrates. Optical images of Si–Sn film surfaces during cycling are shown in Fig. 25. From the start to the end of charge (Fig. 25a and b), no surface changes were observed. During charge, a 200% volume expansion should have occurred as the Si–Sn film was converted to $Li_{1.98}M$. However, no surface cracks were seen, which may have resulted from metal expansion in the out-of-plane direction. After 1 h discharge, the film started to shrink with cracking, which is not clearly visible in Fig. 25c. When discharging was complete, 100 nm cracks were observed (Fig. 25d). When the electrode was again charged, these became very small (Fig. 25e) and the image obtained was similar to that of a fresh electrode (Fig. 25a). On further cycling and after being left at full discharge, cracks were again observed (Fig. 25f and g). These results show the reversible volume change in thin SiSn alloy films. Similar observations were made from *in-situ* AFM analysis of thin SiSn alloy films during cycling [144]. These show that initial Li extraction results in crack formation, which in turn results in formation of separated flake-like particles. When the active particles centers are still connected to the substrate, they can reversibly expand and contract during further cycling. During charge, if enough Li is added, these particles will combine, and cracks will disappear. If more Li is added, expansion may cause their separation from the substrate collector. However, the latter was not observed. These results show that the reversible volume change in Si–Sn thin films is the major reason for their improved capacity retention. This was also confirmed by the volume change observed from *in-situ* AFM analysis [145]. Fig. 26 shows the change in area, height, and volume of an a-$Si_{0.64}Sn_{0.36}$ thin film during Li insertion/extraction, which shows a 250% reversible change in thickness and volume. Similar results were seen for a-Si thin film anode, which justifies the claims of better performance of a-Si thin film anodes by Maranchi et al. [129].

6.2.2. Si–Ag, Si–Zn, Si–Mg, and Si–V alloys and SiO compounds

Apart from Sn, Ag, Zn, Mg, and V also react with reversibly with Li. Binary Si alloys were prepared by replacing Sn in $Si_{1-x}Sn_x$ with elements allowing Li-insertion such as Ag and Zn. When Sn was replaced by Ag [146], capacity retention was less than with $Si_{1-x}Sn_x$. $Si_{1-x}Ag_x$ films prepared by combinatorial sputtering showed irreversible capacities between 6% and 10% of initial capacity and capacity fade between 3% and 8% per cycle. The reason for their high capacity fade was attributed to the crystalline films when Ag was used. Ag resulted in the formation of crystalline $Li_{15}Si_4$, which gave two-phase regions. A large aggregation of Ag particles was also found to give severe capacity fade. Apart from these problems, the high cost of Ag makes it unsuitable for practical applications.

As many as 64 different $Si_{1-x}Zn_x$ thin film compositions in the range $0 < x < 0.62$ were prepared by the combinatorial method [147]. At low Zn contents, anodes showed reversible capacities over 3000 mAh g^{-1}, but at high Zn, it was closer to 1000 mAh g^{-1}. Depending on the composition, their irreversible capacities varied from 6% to 12% of initial capacities, and their capacity fade was less than 4% per cycle. The electrochemical performance of these anodes was better than those of $Si_{1-x}Ag_x$ but lower than that of $Si_{1-x}Sn_x$, which was attributed to the lack of formation of crystalline $Li_{15}Si_4$. In anodes with lower Zn content, Li_2SiZn and $Li_{15}Si_4$ phases were formed during the first charge, which disappeared during subsequent cycles. Instead of these phases, $Li_4(SiZn_x)$ was formed in the second charge. In anodes with higher Zn content, $LiZn_9$, Li_2SiZn, and LiZn were formed during the first charge, and no $Li_{15}Si_4$ formation was observed. Irrespective of Zn content, after few cycles anodes were found to be amorphous during both charge and discharge. The amorphous nature of these anodes is the reason for their better performance compared to $Si_{1-x}Ag_x$.

Mg can be alloyed with Si to form Mg_2Si. Thin films were made by pulsed laser deposition (PLD) using Mg_2Si powder, and examined as anodes [148]. The deposited Mg_2Si films were found to be completely amorphous with thicknesses ranging from 30 to 380 nm. The Li insertion/extraction reaction mechanism for these films was found to be similar to that of Mg_2Si powder-based anodes, which was be discussed in Section 4. The increase in film thickness gave severe capacity fade and an increase in initial irreversibility. The higher reversibility and excellent cyclability observed for thinner films was due to shorter diffusion pathways for Li^+ ions, and to the stronger adherence of films to the substrate. As stressed earlier, the amorphous nature of the films was found to be another reason for excellent cycle life. However, these anodes showed high self-discharge during initial cycling. When discharged to 0.1 V and left at open circuit, their OCVs increased slowly to 1.0 V. This large increase in potential was observed during initial cycling and was attributed to a side reaction of Mg_2Si with the electrolyte. Their self-discharge and cycling voltage limits are not suitable for practical Li-ion cells.

Similarly, $Si_{0.7}V_{0.3}$ thin films deposited on Cu substrate by R.F. magnetron sputtering have been investigated as anodes [149]. Their voltage versus capacity curves were found to be

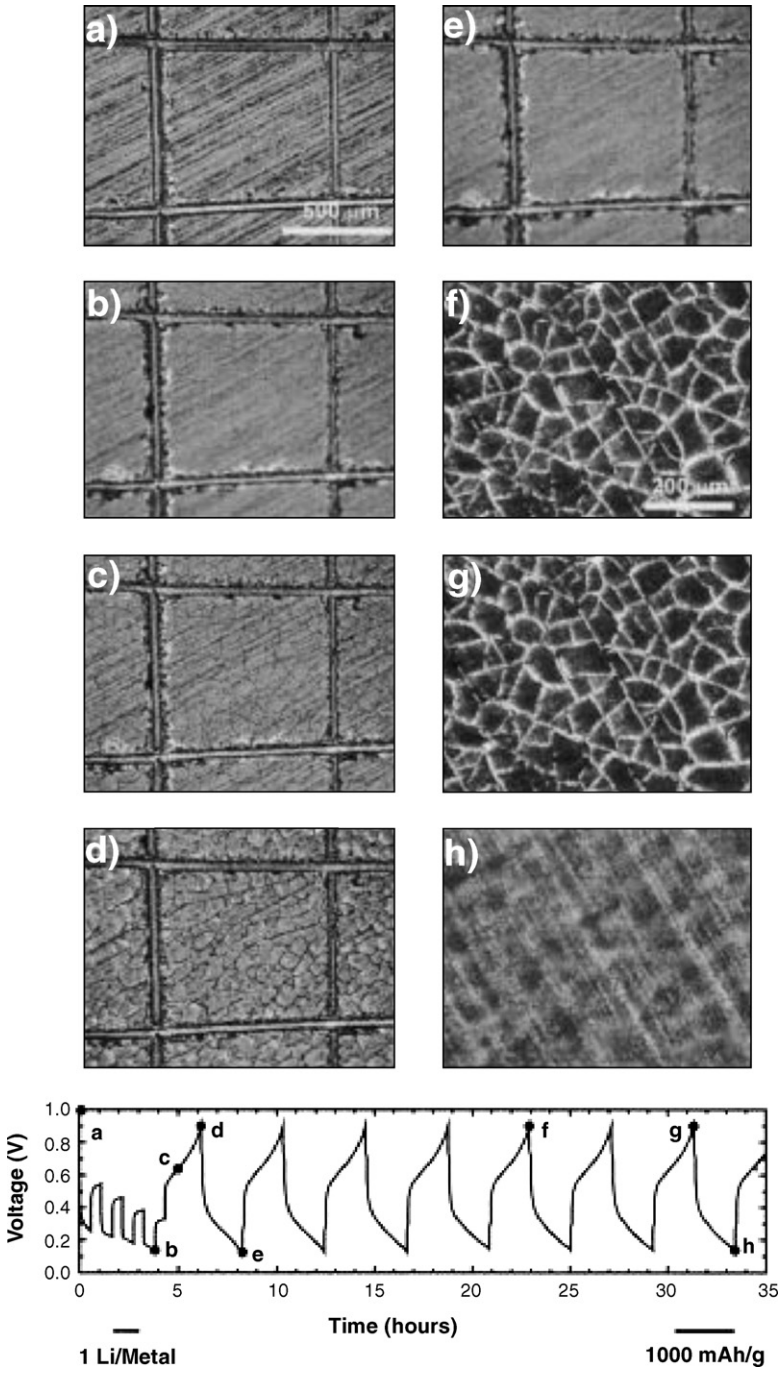

Fig. 25. Selected micrographs of surfaces of SiSn thin films corresponding to the points labeled in the voltage vs. capacity curve below. A scale bar displays the length of the time for charge transfer of 3.5 mol of lithium per mole of metal in the original film. Subparts (a)–(e) are at the same (lower) magnification and (f)–(h) are at higher magnification [144].

very smooth and plateau-free. Insertion profiles for the first and second cycle were similar, indicating potential cycling stability. When galvanostatically cycled between 3.9 and 2.0 V against a $LiCoO_2$ cathode in a cell with a LiSiPON solid electrolyte, a $Si_{0.7}V_{0.3}$ anode showed a reversible capacity of 50 $\mu Ah\,cm^{-2}\,\mu m^{-1}$ for 1500 cycles. However, when the upper charge voltage limit was increased to 4.2 V, severe capacity fade was observed. This was attributed to structural decay of the anode at total cell potentials above 3.9 V.

Due to the high capacity retention ability of tin oxide anodes, a 2 μm SiO thin film deposited on a Cu film by vapor deposition was investigated [150]. When cycled between 0.0 and 2.5 V, it showed an initial charge capacity of 2404 mAh g^{-1} and a coulombic efficiency of 25%. The initial charge of this anode was equivalent to adsorption ratio of 4 mol of Li per mole of Si and discharge was equivalent to a lithium de-alloying ratio of 1 mol of Li per mole of Si. The large irreversible capacity on the first cycle was due to irreversible Li trapping during charge.

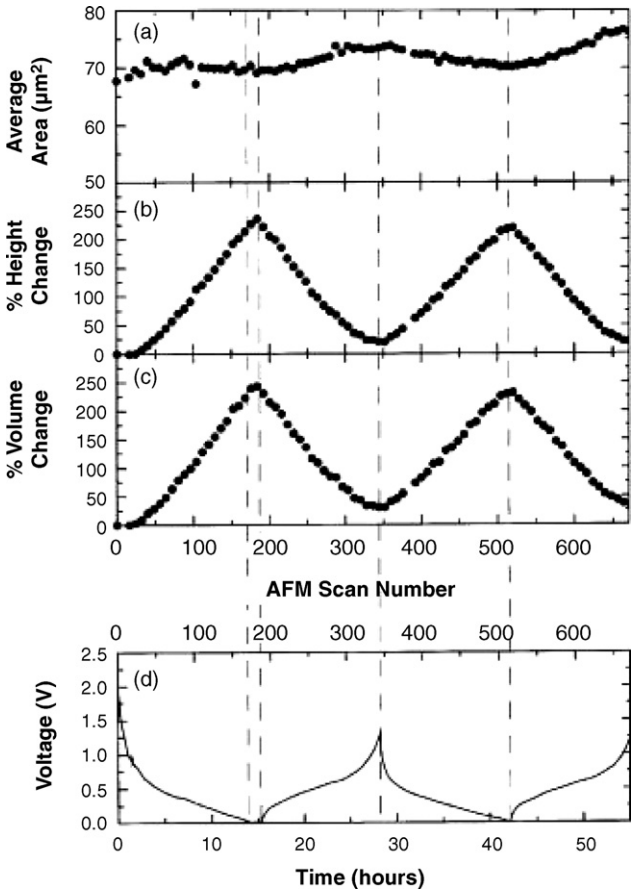

Fig. 26. *In-situ* experimental atomic force microscope (AFM) analysis of (a) the change in area; (b) percent change in height; and (c) percent change in volume observed for a patterned a-$Si_{0.64}Sn_{0.36}$ anode as a function of change in (d) voltage vs. time [145].

XPS showed that SiO was converted to lithium silicates during discharge and at the end of charge Si was observed to be in oxidized state. The high irreversible capacities observed during the initial cycle are not suitable for practical Li-ion cells.

6.2.3. *Si–M (M = Cr, Fe, Mn, Ni, Co, Zr) and Si–TiN alloy*

Transition metals (M = Cr, Fe, Mn, Ni, Co) and Zr and TiN are inert to Li insertion/extraction. The reason for examining Si-transition metal (Si–M) and Si–TiN alloys as anodes was to have an inert matrix in which active Si was dispersed, but whose electrochemical behavior might be independent of the matrix. Depending on the alloy composition, Si–M electrodes have shown specific capacities ranging from 60 to 1000 mAh g^{-1} [151]. No particular capacity phenomena were observed for these alloys. To investigate the effect of transition metal content on capacity, over 200 Si_xM_{1-x} (M = Cr + Ni, Fe, Mn) alloy compositions were prepared by combinatorial methods and tested for charge–discharge behavior. XRD analysis showed that the alloys showed nano-crystalline SiM and amorphous Si phases depending on their initial Si content. When this was increased from 70% to 100%, their capacity was found to increase linearly from 1000 to 3000 mAh g^{-1}, irrespective of the transition metal used. By comparing all the results, the capacity of Si_xM_{1-x} ($0 < x < 0.5$) anodes containing a $(2x - 1)$ mole fraction of a-Si and $(2–2x)$ mole faction of SiM phases was approximated by the following equation [151]:

$$\text{capacity (mAh g}^{-1}) = \frac{3.75\text{Li mol}^{-1} \times (2x-1)}{x \times \text{molar mass}_{\text{Si}} + (1-x) \times \text{molar mass}_{\text{M}}} \times \frac{96500\,\text{C mol}^{-1}}{3.6\,\text{C mAh}^{-1}}$$

Major differences in capacity were observed when the Si content was below 70%, which may be due to the different equilibrium phases for the various Si–M alloys. Co–Si_{2+x} thin films with different Si content (x) were prepared by co-sputtering of Co and Si targets [152]. When the Si content was low ($x = 2.2$), steep charge–discharge slopes were observed. With increasing Si content, the curves became flat, resulting in an increase in specific capacity. When the anode composition approached $CoSi_2$, the films were found to be completely amorphous, which was evident from differential capacity plots. When cycled between 0.0 and 1.5 V, films with a composition near $CoSi_2$, such as $CoSi_{2.06}$ and $CoSi_{2.2}$, showed very good capacity retention. This was attributed to strong bonding between Co and Si and to the amorphous nature of the films. When the Si content was increased to 2.7, an increase in reversible capacity was observed. This was attributed to the availability of a larger number of Si atoms for Li insertion. However, an increase in Si content resulted in poor capacity retention. From selected area diffraction pattern (SADP) experiments, $CoSi_{2.7}$ films were found to contain crystalline Si, which would have resulted in greater capacity fade. To improve capacity retention, Co–Si multilayer films were prepared. A thin film comprising of seven layers of each element with a total thickness of 150 nm was deposited on a Cu substrate. EDS showed the composition of this anode was close to $CoSi_{2.9}$. An as-deposited multilayer thin film was found to have better capacity retention than a single layer Co–Si thin film anode. Capacity retention was further improved by annealing the multilayer film, which resulted in a stable reversible capacity of 3000 mAh cm^{-3} for 100 cycles. However, annealing reduced the reversible capacity, which was attributed to formation of Co–Si alloy, which has a lower Li insertion capacity than Si. On the other hand, Co–Si alloy formation resulted in a more stable microstructure, giving improved capacity retention. Similar results were reported for Fe–Si multilayer thin films [153,154], Mo–Si multilayer thin films [155] and in the US patent literature, Ag–Si multilayer thin films [156]. With a 13-layered annealed Fe–Si thin film anode, a stable volumetric reversible capacity of 3000 mAh cm^{-3} for 300 cycles was obtained, which was better than that of an as-deposited Fe–Si multilayer thin film anode (Fig. 27). SEM of the as-deposited anode over 255 cycles showed surface cracking, whereas the annealed anode showed no evidence of cracks, indicating the high microstructural stability resulting from Fe–Si alloy formation. Apart from its microstructural stability, its cycling stability was attributed to the absence of $Li_{15}Si_4$ phase formation, which was confirmed by charge–discharge curves and differential capacity plots [154].

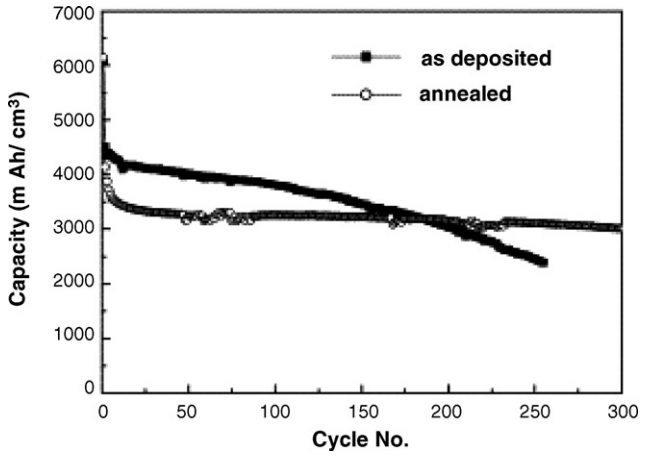

Fig. 27. Capacity vs. cycle number for Fe/Si multilayered thin film anode with stacking order Fe/Si/Fe (13 layers) [153].

It was also found that $Li_{15}Si_4$ phase formation in the Fe–Si multilayer thin film anode was dependant on film thickness and deposition conditions, in agreement with results of Hatchard and Dahn [121]. The electrochemical performance of the annealed Fe–Si multilayer thin film anode may be promising for micro-battery applications. With Mo–Si multilayer thin films prepared by R.F. magnetron sputtering, a capacity retention of 90% of initial (2653 mAh g^{-1}) for 100 cycles was obtained. These results show the importance of structure of the anode in improving cycling performance.

A strong affinity between components of silicon alloys seems to be essential for good cyclability of silicide electrodes because the strong bonding of metal atoms with Si may limit Li–Si alloying to form Li_xSi materials and prevent structural rearrangements of the electrode. The Zr–Si system has a large negative heat of mixing, and was chosen for investigation. Lee et al. [157] prepared Si–Zr thin films by co-sputtering from two separate Si and Zr targets, which were investigated as micro-battery anodes. As-deposited Si–Zr films with different compositions such as $Si_{0.8}Zr_{0.2}$, $Si_{0.7}Zr_{0.3}$, and $Si_{0.6}Zr_{0.4}$ were galvanostatically cycled in the range 1.5 and 0.0 V. Formation of two phases was observed in differential capacity plots for the first two anodes. At 50 cycles, the third had the highest capacity retention, which was attributed to strong bonding of Zr and Si, giving a stable microstructure on cycling.

TiN has also been also used as an inactive matrix, Si–TiN thin films being deposited by pulsed laser deposition (PLD) [158]. XRD showed that the as-deposited thin films were amorphous, while XPS and SEM–EDX showed that they contained uniformly dispersed nano-Si particles in a nano-TiN matrix. During the initial cycle, this anode showed an irreversible capacity close to 600 mAh g^{-1} and a charge capacity of 1800 mAh g^{-1}, equivalent to Li insertion of 1.8 atoms per Si atom. Upon cycling, it had a stable charge capacity of over 1000 mAh g^{-1} for 40 cycles. Compared to a-Si thin film anode prepared by the PLD process, Si-TiN has shown higher reversible capacity and better capacity retention due to its amorphous nature during both insertion and extraction. In contrast to an Si-TiN anode, the formation of crystalline Li–Si alloys was observed for a-Si anodes, which resulted in lower capacity retention. Conservation of an amorphous state in Si-TiN thin films was attributed to excellent dispersion of Si in the TiN matrix, which was considered to prevent the conversion of amorphous Li–Si alloy to crystalline Li–Si alloy at room temperature. Improved thin-film electronic conductivity was also thought to be another reason for the improved electrochemical performance of these anodes. Following the example of Si-TiN thin films, thin Si-metal oxide (TiO_2 or ZrO_2) films prepared by chemical vapor deposition were tested in the published US patent application literature as Li-ion secondary cell anodes [30]. In an operating voltage range of 0.0–1.2 V, anodes containing 7–8 wt% metal oxide showed reversible capacities close to 1000 mAh g^{-1}, which were stable for 100 cycles.

6.3. Ternary alloy thin films

Because of the superior cycling stability shown by amorphous anodes, ternary alloy films such as those containing SiAlSn [159,160] and SiAlMn [161] were investigated to determine their amorphous composition range, which XRD and electron microprobe studies showed to be wide [159]. $Si_{1-x-y}Al_xSn_y$ thin films with $0<x<0.23$ and $0<y<0.58$ were prepared by combinatorial magnetron sputtering and tested as anodes [160]. They included both amorphous and crystalline materials. The first charge capacity, reversible capacity, percent irreversible capacity and percent average capacity fade of anodes with different compositions are listed in Table 3. As shown in the table, films containing nano-crystalline tin (except film 23) showed poor capacity retention and films with only amorphous compositions had high capacity retention. It was therefore concluded that the presence of crystalline material in the anode is detrimental to capacity retention because of the non-homogeneous volume expansion–contraction during Li insertion and extraction. As with the SiAlSn films, 64 different SiAlMn film compositions were selected for electrochemical testing, of which 25 were completely amorphous [161]. The others were found to contain nano-crystalline Al. Of those tested, amorphous samples were found to exhibit reversible capacities close to 1000 mAh g^{-1} and good capacity retention for 18 cycles. Among the compositions tested, $Si_{0.42}Al_{0.44}Mn_{0.14}$ showed high capacity retention. Although capacity fade rate was less for amorphous $Si_{1-x-y}Al_xSn_y$ anodes and amorphous SiAlMn anodes, it is uncertain whether they can maintain their capacity retention ability for 500 cycles in the potential range 0.0–1.5 V.

In spite of the excellent cycling performance of the $Si_{0.6}Zi_{0.4}$ anode, its steeply sloping charge–discharge profiles are not suitable for Li-ion cells, which require only a small free energy change during the insertion reaction, i.e., a small potential change relative to lithium. The steep potential profiles for Si–Zr thin film electrodes indicate strong bonding between Zr atoms and Si atoms, which prevents Li from alloying with Si resulting in lower reversible capacities. To avoid this, Zr in Si–Zr thin films was partially replaced by Ag [162]. XPS showed the presence of Zr–Ag bonds in Si–Zr–Ag thin films, indicating the availability of more Si particles for Li insertion. This was evident from the high reversible capacity shown by Si–Zr–Ag film anodes with high Ag content. With increasing Ag content,

Table 3
Summary of electrochemical performance of $Si_{1-x-y}Al_xSn_y$ thin films

Cell	$Si_{1-x-y}Al_xSn_y$		Structure	First charge capacity (mAh g^{-1})	Reversible capacity (mAh g^{-1})	Irreversible capacity (%)	Avg. capacity fade (% $cycle^{-1}$)
	x	y					
1	0.02	0.20	a	1820	1530	16	0.12
2	0.01	0.35	a	1640	1410	14	0.25
3	0.01	0.45	a	1540	1440	6.7	1.6
4	0.008	0.52	a + nt	1280	1110	13	4.3
5	0.01	0.58	a + nt	1160	1030	11	5.4
6	0.08	0.17	a	1680	1380	18	0.14
7	0.07	0.32	a	1470	1270	14	0.07
8	0.06	0.43	a	1530	1350	12	4.9
9	0.05	0.50	a + nt	1370	1190	13	7.7
10	0.05	0.55	a + nt	1150	1030	11	6.4
11	0.14	0.17	a	1470	1200	18	0.26
12	0.12	0.30	a	1510	1260	17	1.8
13	0.10	0.39	a + nt	1640	1350	18	5.3
14	0.09	0.47	a + nt	1300	1120	14	6.4
15	0.08	0.53	a + nt	1180	1050	11	7.1
16	0.19	0.16	a	1600	1350	16	0.90
17	0.16	0.30	a	1510	1270	16	0.44
18	0.14	0.39	a + nt	1540	1350	13	6.3
19	0.12	0.46	a + nt	1310	1170	11	5.4
20	0.11	0.51	a + nt	1270	1110	12	7.9
21	0.24	0.16	a	1850	1530	17	0.75
22	0.20	0.28	a	1660	1400	16	1.0
23	0.17	0.38	a + nt	1640	1420	13	1.9
24	0.15	0.45	a + nt	1390	1220	12	8.4
25	0.14	0.51	a + nt	1230	1090	11	7.1

In the structure column, a: amorphous, nt: nanocrystalline tin [160].

charge and discharge plateaus became flat. The rate capability of Si–Zr–Ag film anodes was also higher than that of Si–Zr thin film anodes, which was attributed to a decrease in charge transfer resistance on addition of Ag, which also resulted in improved cycling stability. Improvements in rate capability, reversible capacity and cycling performance were observed for Si–Zr thin film anodes with added Ag, but its high cost will increase cell cost. While a-Si thin film anodes in general can offer capacities above 3000 mAh g^{-1}, cycle lives of 1500 cycles and high rate capability, the high cost of the deposition process makes them unsuitable for commercialization.

7. Summary

Since the types of materials and number of compositions tested are large, to facilitate comparisons and to determine material showing superior electrochemical performance, electrochemical data for different Si-based anodes were obtained from literature and tabulated. Tables 4–8 show the electrochemical properties of Si-based anodes prepared by the various methods discussed in Sections 1–6. In each case, important steps in anode preparation are given in the column Method of Preparation. Since capacity fade and reversible capacity depend on Li insertion and extraction voltages, the operating voltage of the half-cell was considered as an analytical parameter. For pure Si anodes and thin film anodes, particle size and film thickness were also considered. Based on the initial composition of each anode, the theoretical capacity was calculated. The reason for considering theoretical capacity as an analytical parameter is because if it is compared with the observed discharge capacity of an anode, the effect of operating voltage on cycle life can be determined. Based on the initial charge capacity and specific capacity reported in the literature, irreversible capacity and coulombic efficiencies were determined for each anode. In few cases, volumetric capacities are given instead of gravimetric capacities. In such cases, measurement units are listed in the table along with the parameter. From the initial discharge capacity and reversible capacity after certain number of cycles (N), the percentage capacity retention and average capacity loss per cycle were calculated and tabulated. For more detailed electrochemical data for any of these anodes, readers are referred to the corresponding articles cited in the tables. Since the voltage limitation or capacity limitation during galvanostatic cycling affects cycling performance, anodes which were cycled between 0.0 and 1.5 V were analyzed to determine the exact influence of material and method of preparation on cycling performance. From the comparison of the electrochemical properties of various anodes considered, the following materials were found to have superior electrochemical performance:

- Compared to powder-based anodes, irrespective of their compositions, thin film anodes always showed better reversible capacity, capacity retention and cycle life. Among the various thin film anodes tested, 50 nm amorphous n-type Si deposited by vacuum deposition on pristine Ni foil [132] showed a stable reversible capacity of 3600 mAh g^{-1} for 200 cycles (Table 4).

Table 4
Electrochemical properties of thin film Si anodes

No.	Anode composition	Si content (wt%)	Method of preparation	A_{th}	$Q_{theoretical}$ (mAh g^{-1})	Potential window (V)	Q_{C1} (mAh g^{-1})	Q_{d1} (mAh g^{-1})	Q_{irr} (%)	Q_f (%)	N	Q_{dN} (mAh g^{-1})	C.R.N.	Capacity loss per cycle (mAh g^{-1})	Ref.
1	Nano crystalline Si	100	PVD		4200	0.0–1.5	2400	1000	140	41.6	50	525	52.5	9.5	[126]
2	Amorphous Si	100	PVD	100 nm	4200	0.0–1.5	3500	2500	40	71.4	50	1800	72	14	[126]
3	Amorphous Si	100	CVD on porous Ni substrates at 650 °C	1.2 μm	4200	0.05–1.10		900			20	200	22.2	35	[136]
4	Amorphous Si	100	CVD at 450 °C	50 nm	4200	0.0–3.0	6000	3900	53.8	65	41	0	0	95.1	[127]
		100	CVD at 450 °C	50 nm	4200	CC	3500	2600	34.6	74.2	95	2500	96.1	1	[127]
5	Amorphous Si	100	Rf magnetron sputtering	1.2 μm	4200	0.02–1.2	3300	3000	10	90.9	30	1200	40	60	[130]
		100	Rf magnetron sputtering	250 nm	4200	0.02–1.2	5100	3900	30.7	76.4	40	1800	46.1	52.5	[130]
6	Amorphous Si	100	Vacuum deposition on pristine Ni foil	77 nm	4200	0.0–1.5		1250			1250	1000	80	0.2	[125]
		100	Vacuum deposition on pristine Ni foil	100 nm	4200	0.0–1.5	3200	2600	23	81.2	400	2000	76.9	1.5	[135]
		100	Vacuum deposition on pristine Ni foil	200 nm	4200	0.0–1.5	4000	3500	14.2	87.5	500	200	5.7	6.6	[135]
		100	Vacuum deposition on roughened Ni foil by filing with sandpaper	340 nm	4200	0.0–1.5	2750	2300	19.5	83.6	450	1500	65.2	1.7	[135]
		100	Vacuum deposition on roughened Ni foil by filing with sandpaper	520 nm	4200	0.0–1.5	3000	2500	20	83.3	400	1000	40	3.75	[135]
		100	Vacuum deposition on roughened Ni foil by etching	1.0 μm	4200	0.0–1.5	2700	2700	0	100	200	1750	64.8	4.75	[135]
		100	Vacuum deposition on electrolytically modified Cu foil	3.6 μm	4200	0.0–1.5	3100	2300	34.7	74.1	50	2000	86.9	6	[135]
7	Amorphous n-type Si	100	Vacuum deposition on pristine Ni foil	50 nm	4200	0.0–1.5	3700	3700	0	100	200	3600	97.2	0.5	[132]
		100	Vacuum deposition on pristine Ni foil	150 nm	4200	0.0–1.5	2900	2500	16	86.2	200	2200	88	1.5	[132]
		100	Vacuum deposition on roughened Ni foil by etching	440 nm	4200	0.0–1.5	2900	2500	16	86.2	200	1800	72	3.5	[133]
8	Amorphous Mg_2Si		Pulsed laser deposition at 250 °C	30 nm		0.1–1.0		1000			140	2200			[148]
			Pulsed laser deposition at 250 °C	137 nm		0.1–1.0		700			140	890			[148]
			Pulsed laser deposition at 250 °C	380 nm		0.1–1.0		700			140	400	57	2.14	[148]
9	Si–TiN	60	Pulsed laser deposition		2520	0.02–3.5	1850	1300	42.3	70.2	40	1000	76.9	7.5	[158]
10	Si–Zr	80	Sputtering		3360	0.0–1.5	120 μAh	85 μAh	41.1	70.8	40	50 μAh	58.8	0.875	[157]
	Si–Zr	70	Sputtering		2940	0.0–1.5	90 μAh	45 μAh	100	50	40	40 μAh	88.8	0.125	[157]
	Si–Zr	60	Sputtering		2520	0.0–1.5	50 μAh	20 μAh	150	40	50	15 μAh	75	0.1	[157]
	Si–Zr	80	Sputtering with under substrate bias voltage of −100 V		3360	0.0–1.5	120 μAh	90 μAh	33.3	75	60	78 μAh	86.6	0.2	[157]
11	Si–Zr–Ag	36.44	Sputtering	150 nm		0.0–1.5	3000 mAh cm^{-3}	1500 mAh cm^{-3}	10	100	50	1600 mAh cm^{-3} (charge)			[162]
	Si–Zr–Ag	37.2	Sputtering	150 nm		0.0–1.5	3500 mAh cm^{-3}	2000 mAh cm^{-3}	75	57.1	50	2000 mAh cm^{-3} (charge)			[162]
	Si–Zr–Ag	37.14	Sputtering	150 nm		0.0–1.5	5000 mAh cm^{-3}	3000 mAh cm^{-3}	66.6	60	50	2100 mAh cm^{-3} (charge)			[162]
12	Co–Si multilater films ($CoSi_{2.9}$)		Electron beam evaporation	150 nm		0.0–1.2	5700 mAh cm^{-3}				50	2300 mAh cm^{-3} (charge)			[152]
			Electron beam evaporation and annealing	150 nm		0.0–1.2	5500 mAh cm^{-3}				50	2900 mAh cm^{-3} (charge)			[152]
13	Fe–Si multilayer films		Electron beam evaporation	138 nm		0.0–1.2	6200 mAh cm^{-3}				250	2500 mAh cm^{-3} (charge)			[153]
			Electron beam evaporation and annealing	138 nm		0.0–1.2	6100 mAh cm^{-3}				300	3200 mAh cm^{-3} (charge)			[153]

A_{th}: Anode thickness; $Q_{theoretical}$: theoretical capacity; Q_{C1}: initial charge capacity; Q_{d1}: initial discharge capacity; Q_{irr}: irreversible capacity; N: number of cycles tested; Q_{dN}: discharge capacity in Nth cycle; C.R.N.: capacity retention in Nth cycle.

Table 5
Electrochemical properties of powder-based Si anodes with Si dispersed in inactive matrices

No.	Anode composition	Si content (wt%)	Method of preparation	$Q_{theoretical}$ (mAh g^{-1})	Potential window (V)	Q_{C1} (mAh g^{-1})	Q_{d1} (mAh g^{-1})	Q_{irr} (%)	Q_f (%)	N	Q_{dN} (mAh g^{-1})	C.R.N.	Capacity loss per cycle (mAh g^{-1})	Ref.
1	Si–TiN–AB (acetylene black)–PVDF	16	6 h milling	776	0.02–1.2	625	475	31.5	76	20	220	46.31	12.75	[23]
		16	12 h milling	776	0.02–1.2	425	290	46.5	68.2	20	290	100	0	[23]
		16	18 h milling	776	0.02–1.2	380	250	52	65.7	20	250	100	0	[23]
2	Si–TiB_2–AB–PVDF	20	10 h milling	891	0.02–1.2	726	600	21	82.6	15	310	51.66	19.33	[24]
		20	15 h milling	891	0.02–1.2	690	520	32.6	75.3	15	350	67.3	11.33	[24]
		20	20 h milling	891	0.02–1.2	500	400	25	80	15	350	87.5	3.33	[24]
		20	25 h milling	891	0.02–1.2	480	380	26.3	79.1	15	350	92.1	2	[24]
3	Si–SiC–AB–PVDF	25	20 h milling	1176	0.02–1.2	740	580	27.5	78.3	15	350	60.34	15.33	[25]
4	Si–TiC–AB–PVDF	23	6 h milling	999	0.02–1.2	475	330	43.9	69.4	30	260	78.78	2.33	[26]
5	Si–PVC–TiB_2/TiN–AB–PVDF		Pyrolysis at 900 °C followed by milling		0.05–1.5		800			36	500	62.5	8.33	[28]
6	Si–TiO_2/ZrO_2		Sol–gel		0.02–1.2 V	1000				16	950			[30]
7	Si_3N_4–PVDF		Milling		0.0–1.5	95	55	72.7	57.8	20	55	100	0	[33]
	$Si_{(3-x)}Fe_xN_4$		Milling and heat treating at 800 °C		0.0–1.5	470	240	95.8	51	50	220	91.66	0.4	[34]
8	$SiO_{1.1}$–AB–PVDF				0.02–1.4	1900	900	111.1	47.3	10	600 (charge)			[44]
9	Ni–Si–Carbon black–PVDF		Milling for 80–100 h	1297	0.0–2.5	1180	944	25	80	25	760 (charge)			[36]
	Fe–Si–Carbon black–PVDF		Milling for 80–100 h		0.0–2.5	620				25	320 (charge)			[36]
10	$Fe_{20}Si_{80}$–Graphite–AB–PVDF	30	Annealing at 1000 °C and 30 min milling		0.0–2.0	800	580	37.9	72.5	20	530 (charge)			[37]
11	Fe–Si alloy–graphite–AB–PTFE	33	Milling		0.02–1.5	1580	680	132.3	43	15	500	73.5	12	[38]
12	Ba–Fe–Si–graphite–AB–PVDF	20	Milling		0.02–1.0	1000	500	100	50	15	420	84	5.33	[39]
13	Si–Ni–graphite–AB–PVDF	25	Arc melting and milling		0.005–1.5	1160	830	39.7	71.5	40	730	87.95	2.5	[40]
14	$Ni_{20}Si_{80}$–graphite–pitch–PVDF	13	Milling followed by pyrolysis at 900 °C		0.0–1.2	630	530	18.8	84.1	30	500 (charge)			[41]

$Q_{theoretical}$: Theoretical capacity; Q_{C1}: initial charge capacity; Q_{d1}: initial discharge capacity; Q_{irr}: irreversible capacity; N: number of cycles tested; Q_{dN}: discharge capacity in Nth cycle; C.R.N.: capacity retention in Nth cycle (in anode composition column, AB: acetylene black).

Table 6
Electrochemical properties of pure Si anodes

No.	Anode composition	Si content (wt%)	Particle size of silicon	$Q_{theoretical}$ (mAh g^{-1})	Potential window (V)	Q_{C1} (mAh g^{-1})	Q_{d1} (mAh g^{-1})	Q_{irr} (%)	Q_f (%)	N	Q_{dN} (mAh g^{-1})	C.R.N.	Capacity loss per cycle (mAh g^{-1})	Ref.
1	Si, C black, PVDF	65	325 mesh	2730	0.0–2.0	3700	880	320.4	23.7	15	225	25.5	43.6	[12]
2	micro Si, C black, PVDF	80	10 μm	3360	0.0–2.0	3260	1170	178.6	35.8	10	200	17	97	[15]
3	nano Si, C black, PVDF	85	78 nm	3570	0.02–1.2	3500	2200	59	62.8	10	500	22.7	170	[21]
4	nano Si, C black, PVDF	40	78 nm	1680	0.0–0.8	2775	2100	32.1	75.6	22	1300	61.9	36.3	[22]
5	Si, CA, SBR, SCMC	62	5 μm	2604	800 mAh g^{-1} (designated Q_C)	800	720	11.1	90	60	200	27.7	8.6	[81]
	Si, CA, SBR, SCMC	62	5 μm	2604	1000 mAh g^{-1} (designated Q_C)	1000	850	17.6	85	20	100	11.7	37.5	[81]

$Q_{theoretical}$: Theoretical capacity; Q_{C1}: initial charge capacity; Q_{d1}: initial discharge capacity; Q_{irr}: irreversible capacity; N: number of cycles tested; Q_{dN}: discharge capacity in Nth cycle; C.R.N.: capacity retention in Nth cycle.

Table 7
Electrochemical properties of powder based Si anodes with Si dispersed in active matrices

No.	Anode composition	Method of preparation	$Q_{theoretical}$ (mAh g^{-1})	Potential window (V)	Q_{C1} (mAh g^{-1})	Q_{d1} (mAh g^{-1})	Q_{irr} (%)	Q_f (%)	N	Q_{dN} (mAh g^{-1})	C.R.N.	Capacity loss per cycle (mAh g^{-1})	Ref.
1	Mg_2Si–C black–PVDF			0.0–2.0	1200	850	41.1	70.83	10	100	11.7	75	[51]
2	Si–Ag–C black–PVDF	Milling for 2 h		0.0–2.0	920	800	15	86.95	10	450	56.2	35	[54]
		Milling for 2 h		0.07–2.0	825				50	100 (charge)			[54]
		Milling for 50 h		0.0–2.0	780	620	25.8	79.4	10	430	69.3	19	[54]
		Milling for 50 h		0.07–2.0	350				10	280 (charge)			[54]
3	Si–Sn–Ni	Melting		0.0–1.2		1850			30	1700	91.8	5	[58]
4	Cu–Si–C black–PVDF	Electroless depostion of Cu on Si followed by annealing		0.0–2.0	1700	1500	13.3	88.5	15	800	53.3	46.66	[12]
5	$Si_{0.64}Sn_{0.36}$–PVDF			0.2–2.0		800			40	400	50	10	[113]
6	$Si_{0.64}Sn_{0.36}$–Cross linked PVDF			0.2–2.0		850			40	750	88.2	2.5	[113]

$Q_{theoretical}$: Theoretical capacity of the anode, Q_{C1}: initial charge capacity, Q_{d1}: initial discharge capacity, Q_{irr}: irreversible capacity; N: number of cycles tested, Q_{dN}: discharge capacity in Nth cycle, C.R.N.: capacity retention in Nth cycle.

Table 8
Electrochemical properties of powder based Si anodes with Si dispersed in carbon matrix by different processes

No.	Anode composition	Method of preparation	Potential window (V)	Q_{C1} (mAh g^{-1})	Q_{d1} (mAh g^{-1})	Q_{irr} (%)	Q_f (%)	N	Q_{dN} (mAh g^{-1})	C.R.N.	Capacity loss per cycle (mAh g^{-1})	Ref.
1	Silane–MCMB–AB–PVDF	Si deposition by TVD at 450 °C	0.035–2.0	1000	462	116.4	46.2	30	301	65.1	5.3	[73]
		Si deposition by TVD at 500 °C	0.035–2.0	850	386	120.2	45.4	30	413			[73]
2	Silane–graphite–PVDF	Si deposition by TVD	0.0–2.0	1350	1000	35	74	100	900	90	1	[75]
3	Benzene–Si–CA–SBR–SCMC	C deposition by TVD at 900 °C	800 (designated Q_C)	800	750	6.6	93.7	70	580	77.3	2.4	[81]
		C deposition by TVD at 900 °C	1000 (designated Q_C)	1000	950	5.2	95	70	800	84.2	2.1	[81]
4	Si–pitch–graphite–PVDF	C deposition by pyrolysis at 900 °C	0.0–1.5	770	680	13.2	88.3	15	600 (charge)			[82]
5	Si–pitch–graphite–$CaCO_3$–C black–PVDF	C deposition by pyrolysis at 1000 °C	0.02–1.5	1000	840	19.4	84	23	600	71.4	10.4	[83]
6	Si–PVC–C black–PVDF	C deposition by pyrolysis at 900 °C	0.02–1.5	870	730	19.1	83.9	30	650	89	2.6	[84]
7	Si–Cu–Cu_3Si–PVA–C black–PVDF	Precipitation followed by pyrolysis at 900 °C	0.0–2.0	830	780	6.4	93.9	30	680	87.1	3.3	[85]
8	Si–acetylene–C black–PVDF	CNT deposition by decomposition at 1000 °C	0.0–1.5	1400	1120	25	80	20	940	83.9	9	[86]
9	Cr doped Si–methane–PVDF	CNT deposition by decomposition at 800 °C	0.0–1.5	1800	1400	28.5	77.7	10	1200	85.7	20	[87]
10	Si–graphite–PVDF	Milling for 150 h	0.005–1.5	2400	1050	128.5	43.75	20	794	75.6	12.8	[88]
11	Si–graphite–MWNTs–PVDF	Milling	0.01–3.0	2274	1450	56.8	63.7	20	584	40.0	43.3	[90]
12	Si–graphite–$Li_{2.6}Co_{0.4}N$–AB–PVDF	Milling twice	0.02–1.4	1050	925	13.5	88	19	600 (charge)			[91]
13	Si–MCMB–C black–PVDF	Milling	0.01–3.0	1175	1066	10.2	90.7	25	700 (charge)			[92]
14	Si–PVC–C black–PVDF	Milling followed by pyrolysis at 800 °C	0.05–1.2 V	1231	548	124.6	44.5	20	400	72.9	7.4	[95]
15	Si–PPP–C black–PVDF	Milling followed by pyrolysis at 800 °C	0.05–1.2 V	1625	560	190.1	34.4	18	310	55.3	13.8	[95]
16	Si–PVC–AB–PVDF	2 Pyrolysis (900 °C) and one intermittent milling	0.05–1.5	1042	854	22	81.9	30	750 (charge)			[96]
17	Si–PVC–PAni–AB–PVDF	2 Pyrolysis (900 °C) and one intermittent milling, followed by PAni coating	0.02–1.5	950	800	18.7	84.2	67	560	70	3.5	[98]
18	Si–PS resin–AB–PVDF	Milling followed by pyrolysis at 800 °C	0.02–1.2	1100	800	37.5	72.7	30	575	71.8	7.5	[99]
19	Si–Cu–pitch–graphite–PVDF	Milling twice and pyrolysis at 900 °C	0.0–1.5	800	700	14.2	87.5	15	630	90	4.6	[100]
20	Si–PVA–C black–PVDF (Si/PVA = 1:9)	Milling followed by pyrolysis at 600 °C	0.02–1.2	1165	935	24.5	80.2	20	754	80.6	9.05	[101]
21	Si–sucrose–C black–PVDF (Si/sucrose = 2:8)	Milling followed by pyrolysis at 600 °C	0.02–1.2	1254	841	49.1	67	20	600	71.3	12.05	[101]
22	SiO–Li_2O_2–Al–graphite–pitch–C black–PVDF	Milling followed by pyrolysis at 900 °C	0.0–1.2	650	525	23.8	80.7	40	510	97.1	0.375	[102]
23	SiO–graphite–furfuryl alcohol–ethanol–water	Milling followed by polymerization followed by heat treating	0.01–1.5	1000	700	42.8	70.0	200	620	88.5	0.4	[103]
24	Si–resorcinol–formaldehyde–PVDF	Sintering at 650 °C	0.02–2.0	2000	1475	35.5	73.7	50	1450	98.3	0.5	[104]
25	Si–SGG matrix–PVDF	Gelation followed by grinding	0.0–1.5	1033	832	24.1	80.5	25	740	88.9	3.68	[106]
26	Si–sucrose–PVDF	Dehydration with sulfuric acid	0.02–1.5	1360	1115	21.9	81.9	75	560	50.2	7.4	[108]
	Si–graphite–sucrose–PVDF	Dehydration with sulfuric acid	0.02–1.5	1750	1100	59.09	62.8	50	712.8	64.8	7.744	[109]

A_{th}: Anode thickness; $Q_{theoretical}$: theoretical capacity; Q_{C1}: initial charge capacity; Q_{d1}: initial discharge capacity; Q_{irr}: irreversible capacity; N: number of cycles tested; Q_{dN}: discharge capacity in Nth cycle; C.R.N.: capacity retention in Nth cycle (in anode composition column, AB: acetylene black).

The capacity retention of this anode after 200 cycles was 97% and average capacity loss was 0.5 mAh g^{-1} $cycle^{-1}$. This is so far the best cycling performance reported for Si anodes. Even for films with a thickness of 1.0 μm [135], a reversible capacity of 1750 mAh g^{-1} which is stable for 200 cycles can be obtained, showing the superior cycling stability of thin film anodes.

- Among Si powder-based anodes, those containing Si dispersed in a conductive metal matrix consisting of multiple metals/and intermetallic compounds showed better cycling stability. For example, in the US patent literature, anodes containing Si, an intermetallic compound, and synthetic graphite made by a fusion process showed a capacity retention greater than 80% over 300 cycles [57]. This is the highest cycle life so far reported for powder-based Si anodes. Their lifetime was due to the maintainance of the electronic pathways between the Si particles and the current collector on repeated cycling. Similarly, nano-Si cluster –SiO_x–C composite anodes prepared by milling, polymerization and heat treatment showed a reversible capacity of 620 mAh g^{-1} after 200 cycles [103]. Their capacity retention in the 200th cycle was 88%. The excellent cycling stability of this anode was due to its structural stability resulting from retention of nano-Si in SiO_x by the stable Si–O bond, along with carbon deposition. Si/C composite anodes prepared by Si deposition on graphite by chemical vapor deposition [72] showed high reversible capacity and capacity retention. The reversible capacities of this anode during the initial and 100th cycle were 1000 and 900 mAh g^{-1}, respectively. The capacity retention ability of this anode after 100 cycles was 90%. Its cycling was superior to that of Si/C composite anodes prepared by carbon deposition on Si. Since the particle size of the graphite used was larger than that of the deposited Si, a large number of nano-Si particles can be deposited on each graphite particle. This leads to better electronic contact between the Si particles during cycling. As with the Si/C composite anode discussed above, a Si/C composite prepared by the carbon aerogel method [104] showed higher reversible capacity and capacity retention. In the operating voltage range 0.02–2.0 V, a stable reversible capacity of 1450 mAh g^{-1} over 50 cycles was obtained. Since the lower cut-off voltage used for Li insertion (0.02 V) was less than 0.03 V, and two phases are possible within this voltage range, this anode may show high capacity retention when cycled between 0.0 and 1.5 V for a large number of cycles.

8. Conclusions

Since it has the highest known theoretical capacity (4200 mAh g^{-1}), silicon would seem to be a superior anode material for high-energy-density Li-ion secondary cells. However severe capacity fade during initial cycling has been found to be a limiting issue for Si anodes. During the last decade, intensive research has been conducted to understand the reasons for this poor capacity retention, and several methodologies have been proposed to overcome the problem. The primary goal of this work has been to review the available literature on Si-based anodes to assess the viability of silicon as a replacement for graphite or carbon in Li-ion cells. After analyzing the literature data, the following conclusions may be drawn regarding the electrochemical performance of Si anodes.

In powder-based Si anodes, the decrease in capacity during cycling results from the increasingly large volume changes in Si as Li insertion proceeds. Since Si undergoes 400% volume expansion at maximum Li insertion, it may not be possible to achieve a reversible volume change. Because of this expansion, stresses created in the anode may exceed the breaking stress of Si, resulting in particle cracking and the unavailability of progressive amounts of Si for further Li insertion and extraction due to loss of inter-particle electronic contact. In addition, when Si is charged to potentials less than 0.03 V versus Li/Li^+, formation of a two-phase system occurs, leading to higher internal stresses in the anode material. Several methods have been examined to attempt to improve the capacity retention of Si anodes. Among these, reduction of silicon particle size to nanometers has been somewhat helpful, but it has failed to completely prevent capacity fade. Since the stresses are very high, it may not be possible to accommodate them by dispersing Si in a brittle matrix, which usually has a very low plastic deformation region. When such brittle matrices are used, stress relief takes place via the new surfaces arising from particle cracking. However, this is not a desirable process, since it results in capacity fade. To prevent this and obtain improved cycle life, it is essential to disperse Si in a highly ductile matrix with a large plastic deformation region and a large fracture stress value. The matrix should also have a high electronic conductivity for effective charge transfer reactions to take place. Detailed studies of accommodation energies might be helpful in solving this problem.

Dispersed Si in an inactive host matrix [23–49] resulted in lower reversible capacity. Among the various materials tested, a Ni–Si alloy dispersed in a carbon matrix [40] showed higher capacity retention. During the initial cycle, a Ni–Si/graphite anode showed a reversible capacity of 830 mAh g^{-1}, which decreased to 730 mAh g^{-1} after 40 cycles. The improved capacity retention of this anode compared that of pure Si was due to better accommodation of volume change by NiSi and $NiSi_2$ phases and the disordered graphite matrix. When Si is dispersed in an *active* metal matrix such as Mg, Ag, Sn, and other metals, a further decrease in capacity retention was observed. This is due to increased pulverization of the anode resulting from Li insertion into the active metal matrix.

When the inactive metal matrix is replaced by soft carbon, a significant improvement in capacity retention has been observed. This is due to compliant nature of carbon, which maintained contact during the volume changes, at least to a certain extent. Carbon permits formation of a conductive network inside the anode, which resulted in improved electronic connection between the anode active particles. Among the Si/C composite anodes prepared by different methods [61–109], one prepared by Si deposition on graphite [75] was found to have a reversible capacity of 900 mAh g^{-1} after 100 cycles. However, the thermal vapor deposition process makes anode fabrication expensive, making it unsuitable for practical Li-ion cells. A nano-Si cluster/SiO_x–C composite anode prepared by milling

[103], polymerization and heat treatment showed a reversible capacity of 620 mAh g^{-1} after 200 cycles. Although the reported cycle life was the highest of all the powder-based Si anodes, its larger irreversible capacity observed during initial cycling is disadvantageous. A Si/C composite anode prepared from dispersion of Si in a carbon aerogel [104] showed a stable reversible capacity of 1450 mAh g^{-1} for 50 cycles. Its reported cycle life was still insufficient to meet commercial requirements.

Among the various powder based Si anodes reported in the published US patent application literature, systems prepared from Si dispersed in a matrix containing multiple metallic species or intermetallic compounds gave high reversible capacity and excellent cycling stability. One such anode was fusion-fabricated Si–Mg–graphite [57], which retained over 80% of its initial capacity after 300 cycles because of its excellent electronic conductivity. Several other similar Si alloy anodes prepared by a melting process have shown high capacity retention. The recently commercialized Sony Nexelion cell uses a tin-based amorphous alloy anode [49]. Although tin has a large volume change on Li insetion, tin-based amorphous alloy prepared by Sony was shown to exhibit 92% capacity retention after 100 cycles. This was attributed to the inclusion of multiple metallic elements into the anode, which minimized dimensional change. These results appear to indicate that alloy-based Si anodes may show potential for commercial Li-ion secondary cells. Future work might focus on identifying alloys which might suppress the large volume change on Li-insertion in Si.

When powder-free anodes were made by thin film deposition techniques, superior cycling stability was observed. For a 50 nm amorphous n-type Si anode [133], a reversible capacity of 3600 mAh g^{-1} was obtained which was stable for 200 cycles. The superior cycling stability shown by thin film Si anodes compared with that of powder-based anodes is due to their microstructural stability, greater adhesion to the current collector, and the shorter Li diffusion pathways in thin films. Structural studies of Si thin film anodes showed that films with thickness less than 2.5 μm did not show formation of two phases, which may be another reason for their improved capacity retention. Even for 3.6 μm thick films, a reversible capacity of 2000 mAh g^{-1} after 50 cycles was obtained by coating the anode material on roughened Cu foil [135]. These results signify the importance of the current collector surface in improving capacity retention. Although a reversible capacity 10 times higher than that of a graphite anode and high cycle life can be obtained for thin film Si anodes, the high cost of the deposition process limits their applicability in commercial Li-ion cells.

Two final points result from the completion of this review. The first is that secondary cells for given applications have figures of merit determined by their specific capacities or energy densities in Wh kg^{-1} or Wh l^{-1}. These depend on the application: For vehicles with battery-electric propulsion, the first has been generally more important. For portable electronics (or for submarine propulsion), the second counted for most. Because of the effect of cathode and other in-cell parameters, high-potential lithium-based anodes with a more than 1000 mAh g^{-1} (1.0 Ah g^{-1}) will not significantly improve the overall Ah kg^{-1} figure-of-merit in real cells. Similarly, in those systems whose important parameter is capacity per unit volume, values over 1.0 Ah cm^{-3} will not significantly improve capacity per unit volume if they are exceeded. These issues are addressed in some detail in Section 1. Hence, for silicon-based anodes, bearing in mind both their mass characteristics and the constraints associated with the volume increase in Si on charge, an anode composition limit of about $Li_{1.0}Si$ to $Li_{1.2}Si$ is acceptable for good energy density and specific energy performance at the cell level, given the type of cathodes available and the requirements for the other inert cell components, i.e., the electrolyte, separator, current collectors, case, and excess active material. Searching for satisfactory performance up to a degree of charge equal to $Li_{4.4}Si$ is counterproductive in practice, even though this has been a research goal in the past.

The last point is that the majority of studies conducted to date on Si-based anodes have shown serious performance degradation under the conditions of study, which may be characterized (for the most part) as resulting from anodic volume changes on cycling under constant pressure conditions. In practically all such cases, anode expansion occurred on charge, with loss of interparticle electronic contact and therefore anode capacity over time. Real Li-ion cells, however, are essentially constant volume devices constrained by a non-yielding outer container containing non-compressible components. Such environments may show quite different behavior, especially if cycling volume changes are minimized by the stoichiometrical constraints addressed in the previous paragraph. These considerations must be taken into account in future studies.

Acknowledgements

The authors acknowledge the NASA-Glenn Research Center, Cleveland OH, for partial financial support under Grant No. NAG3-2617. Tables 1 and 2 and Figs. 2, 3, 5, 10–14, 16, 18, 19, 21, 23, 25, and 26 are reproduced by permission of ECS – The Electrochemical Society, Inc., Pennington, NJ. Fig. 9 is reproduced by permission of the Royal Society of Chemistry, Cambridge, England. Figs. 6–8, 15, 17, 20, 22, 24, and 27, taken from Elsevier journals, are reproduced by permission of Elsevier.

References

[1] J.M. Tarascon, M. Armand, Nature 404 (2001) 359.
[2] P. Suresh, A.K. Shukla, N. Munichandraiah, J. Electrochem. Soc. 152 (2005) A2273.
[3] Z. Lu, D.D. Macneil, J.R. Dahn, Electrochem. Solid State Lett. 4 (2001) A200.
[4] M.R. Mancini, L. Petrucci, F. Ronci, P.P. Prosini, S. Passerini, J. Power Sources 76 (1998) 91.
[5] S.-H. Wu, K.-M. Hsiao, W.-R. Liu, J. Power Sources 146 (2005) 550.
[6] S.Y. Chung, J. Bloking, Y. Ching, Nat. Mater. 1 (2002) 123.
[7] M. Yoshio, T. Tsumura, N. Dimov, J. Power Sources 146 (2005) 10.
[8] A.N. Dey, J. Electrochem. Soc. 118 (1971) 1547.
[9] R.A. Sharma, R.N. Seefurth, J. Electrochem. Soc. 123 (1976) 1763.
[10] B.A. Boukamp, G.C. Lesh, R.A. Huggins, J. Electrochem. Soc. 128 (1981) 725.
[11] C.V.D. Marel, G.J.B. Vinke, W.V.D. Lugt, Solid State Commun. 54 (1985) 917.

[12] J.W. Kim, J.H. Ryu, K.T. Lee, S.M. Oh, J. Power Sources 147 (2005) 227.
[13] W.J. Weydanz, M. Wohlfahrt-Mehrens, R.A. Huggins, J. Power Sources 81 (1999) 237.
[14] B. Gao, S. Sinha, L. Fleming, O. Zhou, Adv. Mater. 13 (2001) 816.
[15] J.H. Ryu, J.W. Kim, Y.-E. Sung, S.M. Oh, Electrochem. Solid State Lett. 7 (2004) A306.
[16] Y. Jin, N. Li, C.H. Chen, S.Q. Wei, Electrochem. Solid State Lett. 9 (2006) A273.
[17] E. Antolini, E. Giorgi, M. Carewska, J. Mater. Sci. Lett. 18 (1999) 325.
[18] C. Wang, I. Kakwan, A.J. Appleby, F.E. Little, J. Electroanal. Chem. 489 (2000) 55.
[19] C. Wang, U.S. Kasavajjula, unpublished work.
[20] W.-R. Liu, Z.-Z. Guo, W.-S. Young, D.-Z. Sheih, H.-C. Wu, M.-H. Yang, N.-L. Wu, J. Power Sources 140 (2005) 139.
[21] Z.P. Guo, J.Z. Wang, H.K. Liu, S.X. Dou, J. Power Sources 146 (2005) 448.
[22] H. Li, X. Huang, L. Chen, Z. Wu, Y. Liang, Electrochem. Solid State Lett. 2 (1999) 547.
[23] I.-S. Kim, P.N. Kumta, G.E. Blomgren, Electrochem. Solid State Lett. 3 (2000) 493.
[24] I.-S. Kim, G.E. Blomgren, P.N. Kumta, Electrochem. Solid State Lett. 6 (2003) A157.
[25] I.-S. Kim, G.E. Blomgren, P.N. Kumta, J. Power Sources 130 (2004) 275.
[26] P. Patel, I.-S. Kim, P.N. Kumta, Mater. Sci. Eng. B-Solid 116 (2005) 347.
[27] Z.P. Guo, Z.W. Zhao, H.K. Liu, S.X. Dou, J. Power Sources 146 (2005) 190.
[28] Y. Liu, K. Hanai, T. Matsumura, N. Imanishi, A. Hirano, Y. Takeda, Electrochem. Solid State Lett. 7 (2004) A492.
[29] K. Hanai, Y. Liu, A. Hirano, M. Matsumura, T. Ichikawa, Y. Takeda, J. Power Sources 146 (2005) 156.
[30] H.-C. Wu, M.-H. Yang, N.-L. Wu, W.-R. Lu, published US. Pat. Applic. 2006/0147797 (July 2006) (to the Industrial Technology Research Institute of Taiwan).
[31] A. Netz, R.A. Huggins, W. Weppner, J. Power Sources 119–121 (2003) 95.
[32] J. Wolfenstine, J. Power Sources 124 (2003) 241.
[33] M. Gil, M.E. Rabanal, A. Varez, A. Kuhn, F. Alvarado, Mater. Lett. 57 (2003) 3063.
[34] C. Doh, N. Kalaiselvi, C. Park, B. Jin, S. Moon, M. Yun, Electrochem. Commun. 6 (2004) 965.
[35] G.X. Wang, L. Sun, D.H. Bradhurst, S. Zhong, S.X. Dou, H.K. Liu, J. Alloy Compd. 306 (2000) 249.
[36] G.X. Wang, L. Sun, D.H. Bradhurst, S. Zhong, S.X. Dou, H.K. Liu, J. Power Sources 88 (2000) 278.
[37] H.-Y. Lee, S.-M. Lee, J. Power Sources 112 (2002) 649.
[38] H. Dong, R.X. Feng, X.P. Ai, Y.L. Cao, H.X. Yang, Electrochim. Acta 49 (2004) 5217.
[39] H. Dong, X.P. Ai, H.X. Yang, Electrochem. Commun. 5 (2003) 952.
[40] M.S. Park, Y.J. Lee, S. Rajendran, M.S. Song, H.S. Kim, J.Y. Lee, Electrochim. Acta 50 (2005) 5561.
[41] H.Y. Lee, Y.L. Kim, M.K. Hong, S.M. Lee, J. Power Sources 141 (2005) 159.
[42] H. Huang, E.M. Kelder, J. Schoonman, J. Power Sources 94 (2001) 108.
[43] Y. Idota, T. Kubota, A. Matsufuji, Y. Maekawa, T. Miyasaka, Sci. J. 276 (1997) 1395.
[44] J. Yang, Y. Takeda, N. Imanishi, C. Capiglia, J.Y. Xie, O. Yamamoto, Solid State Ionics 152–153 (2002) 125.
[45] Y. Nagao, H. Sakaguchi, H. Honda, T. Fukunaga, T. Esaka, J. Electrochem. Soc. 151 (2004) A1572.
[46] T. Tabuchi, H. Yasuda, M. Yamachi, J. Power Sources 146 (2005) 507.
[47] J. Cabana, G. Rousse, A. Fuertes, M.R. Palacin, J. Mater. Chem. 13 (2003) 2402.
[48] Z. Wen, S. Li, J. Sun, K. Wang, J. Xie, Electrochem. Solid-State Lett. 9 (2006) A53.
[49] Y. Miyaki, published US. Pat. Applic. 2005/0181276 (August 2005) (to Sony Corp.).
[50] C.K. Huang, S. Surampudi, A.I. Attia, G. Halpert, U.S. Pat. 5,294,503 (March 1994) (to NASA).
[51] H. Kim, J. Choi, H. Sohn, T. Kang, J. Electrochem. Soc. 146 (1999) 4401.
[52] T. Moriga, K. Watanabe, D. Tsuji, S. Massaki, I. Nakabayashi, J. Solid State Chem. 153 (2000) 386.
[53] G.A. Roberts, E.J. Cairns, J.A. Reimer, J. Power Sources 110 (2002) 424.
[54] S.M. Hwang, H.Y. Lee, S.W. Jang, S.M. Lee, S.J. Lee, H.K. Baik, J.Y. Lee, Electrochem. Solid-State Lett. 4 (2001) A97.
[55] X. Wu, Z. Wang, L. Chen, X. Huang, Electrochem. Commun. 5 (2003) 935.
[56] L.Y. Beaulieu, K.C. Hewitt, R.L. Turner, A. Bonakdarpour, A.A. Abdo, L. Christensen, K.W. Eberman, L.J. Krause, J.R. Dahn, J. Electrochem. Soc. 150 (2003) A149.
[57] S. Kasamatsu, H. Shimamura, Y. Nitta, US Pat. 6,548,208 (April 2003) (to Matshushita Electrical Industrial Co.).
[58] M. Asao, S. Kawakami, T. Ogura, published US. Pat. Applic. 2004/0248011 (December 2004) (to Canon Kabushiki Kaisha).
[59] S. Kawakami, M. Asao, N. Suzuki, Y. Yamada, T. Ogura, published US. Pat. Applic. 2006/0040182 (February 2006) (to Canon Kabushiki Kaisha).
[60] S. Kawakami, A. Morita, T. Ogura, published US. Pat. Applic. 2006/0127773. (June 2006) (to Canon Kabushiki Kaisha).
[61] A.M. Wilson, J.N. Reimers, E.W. Fuller, J.R. Dahn, Solid State Ionics 74 (1994) 249.
[62] L.J. Ning, Y.P. Wu, L.Z. Wang, S.B. Fang, R. Holze, J. Solid State Electrochem. 9 (2005) 520.
[63] W. Xing, A.M. Wilson, G. Zank, K. Eguchi, J.R. Dahn, J. Electrochem. Soc. 144 (1997) 2410.
[64] J.S. Xue, K. Myrtle, J.R. Dahn, J. Electrochem. Soc. 142 (1995) 2927.
[65] A.M. Wilson, G. Zank, K. Eguchi, W. Xing, J.R. Dahn, J. Power Sources 68 (1997) 195.
[66] W. Xing, A.M. Wilson, G. Zank, J.R. Dahn, Solid State Ionics 93 (1997) 239.
[67] A.M. Wilson, W. Xing, G. Zank, B. Yates, J.R. Dahn, Solid State Ionics 100 (1997) 259.
[68] D. Larcher, C. Mudalige, A.E. George, V. Poter, M. Gharghouri, J.R. Dahn, Solid State Ionics 122 (1999) 71.
[69] H. Tamai, H. Sugahara, H. Yasuda, J. Mater. Sci. Lett. 19 (2000) 53.
[70] S.E. Hayes, H. Eckert, W.R. Even Jr., R. Guidotti, J. Electrochem. Soc. 146 (1999) 2435.
[71] A.M. Wilson, B.M. Way, J.R. Dahn, T.V. Buuren, J. Appl. Phys. 77 (1995) 2363.
[72] A.M. Wilson, J.R. Dahn, J. Electrochem. Soc. 142 (1995) 326.
[73] J. Xie, G.S. Cao, X.B. Zhao, Mater. Chem. Phys. 88 (2003) 295.
[74] M. Holzapfel, H. Buqa, F. Kruneich, P. Novak, F.-M. Petrat, C. Veit, Electrochem. Solid-State Lett. 8 (2005) A516.
[75] M. Holzapfel, H. Buqa, W. Scheifele, P. Novak, F.-M. Petrat, Chem. Commun. (2005) 1566.
[76] T. Umeno, K. Fukuda, H. Wang, N. Dimov, T. Iwao, M. Yoshio, Chem. Lett. 11 (2001) 1186.
[77] M. Yoshio, H. Wang, K. Fukuda, T. Umeno, N. Dimov, Z. Ogumi, J. Electrochem. Soc. 149 (2002) A1598.
[78] N. Dimov, K. Fukuda, T. Umeno, S. Kugino, M. Yoshio, J. Power Sources 114 (2003) 88.
[79] N. Dimov, S. Kugino, M. Yoshio, Electrochim. Acta 48 (2003) 1579.
[80] X. Yang, J. McBreen, W. Yoon, M. Yoshio, H. Wang, K. Fukuda, T. Umeno, Electrochem. Commun. 4 (2002) 893.
[81] W.R. Liu, J.-H. Wang, H.-C. Wu, D.-T. Shieh, M.-H. Yang, N.-L. Wu, J. Electrochem. Soc. 152 (2005) A1719.
[82] B.C. Kim, H. Uono, T. Sato, T. Fuse, T. Ishihara, M. Senna, Solid State Ionics 172 (2004) 33.
[83] Z.S. Wen, J. Yang, B.F. Wang, K. Wang, Y. Liu, Electrochem. Commun. 5 (2003) 165.
[84] J. Yang, B.F. Wang, K. Wang, Y. Liu, J.Y. Xie, Z.S. Wen, Electrochem. Solid-State Lett. 6 (2003) A154.
[85] J.-H. Kim, H. Kim, H.-J. Sohn, Electrochem. Commun. 7 (2005) 557.
[86] J. Shu, H. Li, R. Yang, Y. Shi, X. Huang, Electrochem. Commun. 8 (2005) 51.

[87] T. Ishihara, M. Nakasu, M. Yoshio, H. Nishiguchi, Y. Takita, J. Power Sources 146 (2005) 161.
[88] C.S. Wang, G.T. Wu, X.B. Zhang, Z.F. Qi, W.Z. Li, J. Electrochem. Soc. 145 (1998) 2751.
[89] N. Dimov, S. Kugino, M. Yoshio, J. Power Sources 136 (2004) 108.
[90] Y. Zhang, X.G. Zhang, H.L. Zhang, Z.G. Zhao, F. Li, C. Liu, H.M. Cheng, Electrochim. Acta 51 (2006) 4994.
[91] Y. Liu, K. Hanai, K. Horikawa, N. Imanishi, A. Hirano, Y. Takdea, Mater. Chem. Phys. 89 (2004) 80.
[92] G.X. Wang, J. Yao, H.K. Liu, Electrochem. Solid-State Lett. 7 (2004) A250.
[93] Y. NuLi, B. Wang, J. Yang, X. Yuan, Z. Ma, J. Power Sources 153 (2006) 371.
[94] M. Yoshio, S. Kugino, N. Dimov, J. Power Sources 153 (2006) 375.
[95] X. Zhang, P.K. Patil, C. Wang, A.J. Appleby, F.E. Little, D.L. Cocke, J. Power Sources 125 (2004) 206.
[96] Y. Liu, K. Hanai, J. Yang, N. Imanishi, A. Hirano, Y. Takeda, Solid State Ionics 168 (2004) 61.
[97] Y. Liu, K. Hanai, J. Yang, N. Imanishi, A. Hirano, Y. Takeda, Electrochem. Solid-State Lett. 7 (2004) A369.
[98] Y. Liu, T. Matsumura, N. Imanishi, A. Hirano, T. Ichiwaka, Y. Takeda, Electrochem. Solid-State Lett. 8 (2005) A599.
[99] I.-S. Kim, P.N. Kumta, J. Power Sources 136 (2004) 145.
[100] B.C. Kim, H. Uono, T. Sato, T. Fuse, T. Ishihara, M. Ue, M. Senna, J. Electrochem. Soc. 152 (2005) A523.
[101] Z.P. Guo, E. Milin, J.Z. Wang, J. Chen, H.K. Liu, J. Electrochem. Soc. 152 (2005) A2211.
[102] H.Y. Lee, S.M. Lee, Electrochem. Commun. 6 (2004) 465.
[103] T. Morita, N. Takami, J. Electrochem. Soc. 153 (2006) A425.
[104] G.X. Wang, J.H. Ahn, J. Yao, S. Bewlay, H.K. Liu, Electrochem. Commun. 6 (2004) 689.
[105] T. Hasegawa, S.R. Mukai, Y. Shirato, H. Tamon, Carbon 42 (2004) 2573.
[106] J. Niu, J.Y. Lee, Electrochem. Solid-State Lett. 5 (2002) A107.
[107] J. Niu, J.Y. Lee, Anal. Commun. 36 (1999) 81.
[108] X. Yang, Z. Wen, X. Zhu, S. Huang, Electrochem. Solid-State Lett. 8 (2005) A481.
[109] X. Yang, Z. Wen, X. Xu, B. Lin, Z. Lin, J. Electrochem. Soc. 153 (2006) A1341.
[110] U. Kasavajjula, C. Wang, Indian J. Chem., Sect. A 44 (2005) 975.
[111] C. Wang, U. Kasavajjula, J. Hong, unpublished work.
[112] Z. Chen, L. Christensen, J.R. Dahn, J. Electrochem. Soc. 150 (2003) A1073.
[113] Z. Chen, L. Christensen, J.R. Dahn, Electrochem. Commun. 5 (2003) 919.
[114] Z. Chen, V. Chevrier, L. Christensen, J.R. Dahn, Electrochem. Solid-State Lett. 7 (2004) A310.
[115] H.-S. La, K.-S. Park, K.-S. Nahm, K.-K. Jeong, Y.-S. Lee, Colloids Surf. A 272 (2006) 22.
[116] W.R. Liu, M. Yang, H. Wu, S.M. Chiao, N. Wu, Electrochem. Solid-State Lett. 8 (2005) A100.
[117] H. Li, X. Huang, L. Chen, G. Zhou, Z. Zhang, D. Yu, Y.J. Mo, N. Pei, Solid State Ionics 135 (2000) 181.
[118] P. Limthongkul, Y.-I. Jang, N.J. Dudney, Y.-M. Chiang, J. Power Sources 119–121 (2003) 604.
[119] P. Limthongkul, Y.-I. Jang, N.J. Dudney, Y.-M. Chiang, Acta Mater. 51 (2003) 1103.
[120] M.N. Obrovac, L. Christensen, Electrochem. Solid-State Lett. 7 (2004) A93.
[121] T.D. Hatchard, J.R. Dahn, J. Electrochem. Soc. 151 (2004) A838.
[122] I. Konishiike, T. Yamamoto, T. Takada, K. Kawase, Y. Miyaki, published US. Pat. Applic. 2005/0079421 (April 2005) (unassigned).
[123] S.-J. Lee, J.-K. Lee, S.-H. Chung, H.-Y. Lee, S.-M. Lee, H.-K. Baik, J. Power Sources 97–98 (2001) 191.
[124] K. Yoshimura, J. Suzuki, K. Sekine, T. Takamura, J. Power Sources 146 (2005) 445.
[125] S. Ohara, J. Suzuki, K. Sekine, T. Takamura, J. Power Sources 119–121 (2003) 591.
[126] J. Graetz, C.C. Ahn, R. Yazami, B. Fultz, Electrochem. Solid-State Lett. 6 (2003) A194.
[127] H. Jung, M. Park, Y. Yoon, G. Kim, S. Joo, J. Power Sources 115 (2003) 346.
[128] H. Jung, M. Park, S.H. Han, H. Lim, S. Joo, Solid State Commun. 125 (2003) 387.
[129] J.P. Maranchi, A.F. Hepp, P.N. Kumta, Electrochem. Solid-State Lett. 6 (2003) A198.
[130] J.P. Maranchi, A.F. Hepp, A.G. Evans, N.T. Nuhfer, P.N. Kumta, J. Electrochem. Soc. 153 (2006) A1246.
[131] S. Ohara, J. Suzuki, K. Sekine, T. Takamura, Electrochemistry 71 (2003) 1126.
[132] S. Ohara, J. Suzuki, K. Sekine, T. Takamura, J. Power Sources 136 (2004) 303.
[133] T. Takamura, S. Ohara, M. Uehara, J. Suzuki, K. Sekine, J. Power Sources 129 (2004) 96.
[134] K.-L. Lee, J.-Y. Jung, S.-W. Lee, H.-S. Moon, J.-W. Park, J. Power Sources 129 (2004) 270.
[135] M. Uehara, J. Suzuki, K. Tamura, K. Sekine, T. Takamura, J. Power Sources 146 (2005) 441.
[136] S. Bourderau, T. Brousse, D.M. Schleich, J. Power Sources 81 (1999) 233.
[137] H.-C. Shin, J.A. Corno, J.L. Gole, M. Liu, J. Power Sources 139 (2005) 314.
[138] M. Green, E. Fielder, B. Scrosati, M. Wachtler, J.S. Moreno, Electrochem. Solid-State Lett. 6 (2003) A75.
[139] M. Green, published US. Pat. Applic. 2006/0097691 (May 2006) (unassigned).
[140] H.-J. Ahn, Y.-S. Kim, K.-W. Park, T.-Y. Seong, Chem. Commun. (2005) 43.
[141] T.D. Hatchard, J.R. Dahn, J. Electrochem. Soc. 151 (2004) A1628.
[142] J.R. Dahn, S. Trussler, T.D. Hatchard, A. Bonakdarpour, J.R. Mueller-Neuhaus, K.C. Hewitt, M. Fleischauer, Chem. Mater. 14 (2002) 3519.
[143] M.D. Fleischauer, T.D. Hatchard, G.P. Rockwell, J.M. Topple, S. Trussler, S.K. Jericho, M.H. Jericho, J.R. Dahn, J. Electrochem. Soc. 150 (2003) A1465.
[144] L.Y. Beaulieu, K.W. Eberman, R.L. Turner, L.J. Krause, J.R. Dahn, Electrochem. Solid-State Lett. 4 (2001) A137.
[145] L.Y. Beaulieu, T.D. Hatchard, A. Bonakdarpour, M.D. Fleischauer, J.R. Dahn, J. Electrochem. Soc. 150 (2003) A1457.
[146] T.D. Hatchard, J.R. Dahn, J. Electrochem. Soc. 152 (2005) A1445.
[147] T.D. Hatchard, M.N. Obrovac, J.R. Dahn, J. Electrochem. Soc. 152 (2005) A2335.
[148] S.-W. Song, K.A. Striebel, R.P. Reade, G.A. Roberts, E.J. Cairns, J. Electrochem. Soc. 150 (2003) A121.
[149] S.-J. Lee, H.-K. Baik, S.-M. Lee, Electrochem. Commun. 5 (2003) 32.
[150] M. Miyachi, H. Yamamoto, H. Kawai, T. Ohta, M. Shirakata, J. Electrochem. Soc. 152 (2005) A2089.
[151] M.D. Fleischauer, J.M. Topple, J.R. Dahn, Electrochem. Solid-State Lett. 8 (2005) A137.
[152] Y.-L. Kim, H.-Y. Lee, S.-W. Jang, S.-H. Lim, S.-J. Lee, H.-K. Baik, Y.-S. Yoon, S.-M. Lee, Electrochim. Acta 48 (2003) 2593.
[153] J.-B. Kim, H.-Y. Lee, K.-S. Lee, S.-H. Lim, S.-M. Lee, Electrochem. Commun. 5 (2003) 544.
[154] J.-B. Kim, S.-H. Lim, S.-M. Lee, J. Electrochem. Soc. 153 (2006) A455.
[155] J.Y. Jung, M.H. Kim, H.S. Moon, J.W. Park, Mater. Sci. Forum 486 (2005) 558.
[156] Y.-S. Park, H.-K. Baik, S.-M. Lee, J.-Y. Oh, US Pat. 6,828,063 (December 2004) (to Samsung SDI Co.).
[157] S.-J. Lee, H.-Y. Lee, H.-K. Baik, S.-M. Lee, J. Power Sources 119–121 (2003) 113.
[158] Y. Zhang, Z.-W. Wu, Q.-Z. Qin, Electrochem. Commun. 6 (2004) 484.
[159] T.D. Hatchard, J.R. Dahn, S. Trussler, M. Fleischauer, A. Bonakdarpour, J.R. Mueller-Neuhaus, K.C. Hewitt, Thin Solid Films 443 (2003) 144.
[160] T.D. Hatchard, J.M. Topple, M.D. Fleischauer, J.R. Dahn, Electrochem. Solid-State Lett. 6 (2003) A129.
[161] M.D. Fleischauer, J.R. Dahn, J. Electrochem. Soc. 151 (2004) A1216.
[162] K.-S. Lee, Y.-L. Kim, S.-M. Lee, J. Power Sources 146 (2005) 464.